Institut für Nutzpflanzenwissenschaften und Ressourcenschutz (INRES)

Bodenwissenschaften

Real-time quantification of oxygen isotope exchange between carbon dioxide and leaf/soil water in terrestrial ecosystems with laser-based spectroscopy

Inaugural-Dissertation

zur

Erlangung des Grades

Doktor der Agrarwissenschaften

(Dr. agr.)

der

Landwirtschaftlichen Fakultät

der

Rheinischen Friedrich-Wilhelms-Universität Bonn

vorgelegt im Dezember 2014

von

Laura Gangi

aus

Mettmann

Referent: Prof. Dr. Nicolas Brüggemann

Korreferent: Prof. Dr. Wulf Amelung

Tag der mündlichen Prüfung: 9. April 2015

Erscheinungsjahr: 2015

Zusammenfassung

Das Verhältnis der stabilen Sauerstoffisotope $^{18}O/^{16}O$ im atmosphärischen Kohlenstoffdioxid ($\delta^{18}O\text{-}CO_2$) kann genutzt werden, um in terrestrischen Ökosystemen die Einzelflüsse des Spurengases (Photosynthese, Respiration) zu quantifizieren. Dies ist möglich, da bei Kontakt mit Wasseroberflächen im Blatt und in natürlichen Böden das sehr (orts-)spezifische Sauerstoffisotopenverhältnis des Wassers ($\delta^{18}O\text{-}H_2O$) auf die CO_2-Moleküle übertragen wird. Die Anwendung der Sauerstoffisotopenmethode erfordert jedoch ein detailliertes Verständnis der verschiedenen Prozesse und Faktoren, die den CO_2-H_2O-Sauerstoffisotopenaustausch auf verschiedenen Ebenen beeinflussen. Der Effekt von dynamischen Umweltbedingungen auf den ^{18}O-Austausch zwischen atmosphärischem CO_2 und Blattwasser wurde noch nicht ausreichend für verschiedene Pflanzenarten experimentell untersucht, und auch das Verständnis des aus Böden emittierten $\delta^{18}O$-Signals ist noch unzureichend, da die Einflüsse des Bodenfeuchtegehalts (*SWC*), der Bodentextur, der Tortuosität und der katalytischen Aktivität des Enzyms Carboanhydrase (*CA*) komplex sind. Daher war das Ziel dieser Arbeit, den ^{18}O-Austausch zwischen CO_2 und Blatt- bzw. Bodenwasser unter kontrollierten Laborbedingungen bei sehr hoher Zeitauflösung zu untersuchen. Dazu wurde $\delta^{18}O$ in CO_2 und Wasserdampf kontinuierlich mittels Laser-basierter Spektroskopie gemessen, zum einen in Pflanzenkammerexperimenten mit Fichte, Weizen, Pappel und Mais, und zum anderen in Sandsäulenexperimenten unter Anwendung von gasdurchlässigen Schläuchen. Des Weiteren wurde der ^{18}O-Austausch auf Ökosystemebene mithilfe des biophysikalischen Boden-Pflanze-Atmosphäre Modells MuSICA simuliert und getestet, ob der Einstellungsgrad des isotopischen Gleichgewichts zwischen CO_2 und Blattwasser (θ), der in den Pflanzenkammerexperimenten bestimmt wurde, zur Verbesserung der Parametrisierung des Modells genutzt werden kann.

Der Effekt von temporär veränderten Umweltbedingungen wurde sowohl für den ^{18}O-Austausch in Pflanzen untersucht, indem einzelne Pflanzen einer Erhöhung der Lufttemperatur (von 25 °C auf 35 °C) und Wassermangel ausgesetzt wurden, als auch für Böden, indem der Bodenwassergehalt in der Sandsäule variiert wurde. Der Einfluss der Pflanzen auf das $\delta^{18}O$-CO_2 in der Pflanzenkammer, das sogenannte $CO^{18}O$ isoforcing ($CO^{18}O$-*Iso*), wurde quantifiziert durch Multiplikation des Netto-CO_2-Flusses durch die Kammer und dem $\delta^{18}O$-Wert dieses Flusses, die durch differentielle Messungen der CO_2-Konzentration und des $\delta^{18}O$-Wertes am Kammereingang und -ausgang bestimmt wurden. $CO^{18}O$-*Iso* nahm sowohl in Reaktion auf die Temperaturerhöhung ab (bei allen Pflanzenarten außer Mais), einhergehend mit einer Verminderung der stomatären Leitfähigkeit (g_s), als auch mit zunehmender Wasserknappheit (bei allen Pflanzenarten), simultan mit einer Abnahme von θ, der Assimilationsrate (A_r) und g_s, während sich gleichzeitig das Blattwasser mit ^{18}O anreicherte. Die zeitlichen Veränderungen des $CO^{18}O$-*Iso* konnten fast vollständig durch die kombinierten Variationen von θ, g_s, A_r und $\delta^{18}O$ des Blattwassers ($\delta^{18}O_{ev}$) erklärt werden. Das experimentell bestimmte θ lag mit 0.51 und 0.53 für Mais bzw. Fichte, sowie 0.67 und 0.74 für Weizen bzw. Pappel unter den entsprechenden Literaturwerten für diese Pflanzenarten und zeigte eine Abhängigkeit von der angenommenen Mesophyllleitfähigkeit (g_m).

In der Sandsäule waren CO_2 und H_2O ebenfalls nicht im isotopischen Gleichgewicht, ein Zustand, der durch die geringe Bodenfeuchte und, wie in Modellsimulationen angedeutet, die damit verbundene Abnahme der Gleichgewichtsreaktionsrate (k_e) des Sauerstoffisotopenaustauschs zwischen CO_2 und H_2O hervorgerufen wurde. Die Bewässerung der Sandsäule mit Leitungswasser veränderte das Sauerstoffisotopenverhältnis im Bodenwasser ($\delta^{18}O_{sw}$), wirkte sich jedoch erst nach Zugabe von *CA* zum Bewässerungswasser auch auf das Sauerstoffisotopenverhältnis im CO_2 ($\delta^{18}O_{sc}$) aus. Zusätzlich erhöhte die Zugabe von *CA* auch den Einstellungsgrad des ^{18}O-Gleichgewichts zwischen CO_2 und Bodenwasser. Der

enzymatische Effekt der CA in Böden konnte somit erstmals experimentell nachgewiesen werden.

Simulationen des $\delta^{18}O\text{-}CO_2$ in einem Fichtenwald mit dem Ökosystem-Modell MuSICA zeigten, dass eine Parametrisierung mit θ = 0.53, dem für Fichten in den Pflanzenkammerexperimenten dieser Arbeit ermittelten Wert, zu einer Verbesserung der Simulationsergebnisse für $\delta^{18}O\text{-}CO_2$ im Fichtenbestand führte und dass die Implementierung eines zeitlich variabel anzupassenden θ sinnvoll wäre.

Die vorliegende Arbeit zeigt, dass der ^{18}O-Austausch zwischen CO_2 und H_2O sowie zwischen Boden, Vegetation und Atmosphäre, bedingt durch den Einfluss der Umweltbedingungen, ein dynamischer Prozess ist und dass θ tendenziell geringer sein könnte als bisher angenommen. Zudem wurde eine neue, vielversprechende Methode entwickelt, die zukünftig *in situ*-Messungen von $\delta^{18}O_{sw}$ und $\delta^{18}O_{sc}$ in hoher räumlicher und zeitlicher Auflösung ermöglicht. Die neu gewonnenen Kenntnisse und Methoden dieser Arbeit werden folglich zu einem erweiterten Verständnis des atmosphärischen $\delta^{18}O\text{-}CO_2$-Budgets beitragen.

Summary

The oxygen isotope ratio of atmospheric carbon dioxide ($\delta^{18}O\text{-}CO_2$) can be used to partition the gross fluxes of CO_2 in terrestrial ecosystems, such as soil respiration and plant assimilation, as a characteristic $\delta^{18}O$ value is transferred to CO_2 during isotopic equilibration with different water pools. However, the quantitative use of $\delta^{18}O\text{-}CO_2$ requires a detailed understanding of the different processes and factors that influence the CO_2–H_2O oxygen isotope exchange at different scales. The effect of varying environmental conditions on the ^{18}O-exchange between atmospheric CO_2 and the leaf water of different plant species has been insufficiently explored in experiments, and also the $\delta^{18}O$ of soil efflux is fraught with uncertainty due to the complex influence of soil water content (*SWC*), soil texture and tortuosity, as well as the catalytic activity of the enzyme carbonic anhydrase (*CA*). The aim of the present study was to elucidate the ^{18}O-exchange between CO_2 and leaf/soil water under controlled laboratory conditions and at a high temporal resolution. For this purpose, $\delta^{18}O$ of CO_2 and water vapor were measured *online* using infrared laser spectroscopy in plant chamber experiments with spruce, wheat, poplar and maize, as well as soil column experiments, which included the use of gas-permeable tubing. Finally, the biophysical soil–vegetation–atmosphere model MuSICA was applied to simulate the ^{18}O-exchange at the ecosystem level and to test whether a value for the degree of isotopic equilibrium (θ) obtained from plant chamber experiments was suitable for model parameterization.

The sensitivity of the ^{18}O-exchange to short-term changes in environmental conditions was studied by exposing the plants to increased air temperature (35°C vs. 25°C) and limited soil water availability, and the soil column to varying *SWC*. The $C^{18}O$ isoforcing ($CO^{18}O\text{-}Iso$) at the plant-chamber level, i.e., the product of the net CO_2 flux through the chamber and the $\delta^{18}O\text{-}CO_2$ of this flux obtained from differential measurements at the plant chamber inlet and outlet,

was used as a measure for the plants' impact on ambient $\delta^{18}O\text{-}CO_2$. $CO^{18}O\text{-}Iso$ decreased in response to elevated air temperature due to the reduction of stomatal conductance (g_s) in all plant species except for maize, and in response to water availability in all four plant species due to a reduction of θ, assimilation rate (A_r) and g_s, while leaf water became progressively ^{18}O-enriched. Almost 100% of the temporal variations in $CO^{18}O\text{-}Iso$ could be explained by the combination of θ, g_s, A_r and $\delta^{18}O$ of leaf water ($\delta^{18}O_{ev}$). The experimentally determined θ was considerably lower than reported in previous studies for the respective plant species, with values of 0.51 and 0.53 in maize and spruce, and 0.67 and 0.74 in wheat and poplar, respectively, and was highly sensitive to the parameterization of mesophyll conductance (g_m). In the soil column, an incomplete CO_2–H_2O isotopic equilibrium was observed, most likely due to the low soil water content (*SWC*), which yielded a low isotopic equilibration reaction rate (k_e) as indicated by model simulations. Irrigation of the soil column with tap water clearly influenced the $\delta^{18}O$ of soil water ($\delta^{18}O_{sw}$) in the drenched soil depths. However, the $\delta^{18}O$ of soil CO_2 ($\delta^{18}O_{sc}$) was only influenced at the top 3 cm, when *CA* was added to the irrigation water. This is an important finding, as, for the first time, the effect of *CA* activity in soils on the ^{18}O exchange between CO_2 and soil water was shown experimentally. Model simulations of $\delta^{18}O\text{-}CO_2$ in a Norway spruce forest with MuSICA revealed that $\theta = 0.53$, derived from isotopic gas exchange measurements, significantly improved simulations of canopy $\delta^{18}O\text{-}CO_2$ compared with $\theta = 1$ and indicated a temporally variable θ should be implemented in the model.

The present study highlights the need to i) consider the temporal variations in the oxygen isotope exchange between CO_2 and H_2O as well as between soil, plants and the atmosphere, which are induced by changes in environmental conditions, and ii) take into account potentially lower θ estimates. In addition, a promising method to measure $\delta^{18}O_{sc}$ and $\delta^{18}O_{sw}$ quasi simultaneously *in situ* with high temporal resolution was presented. The gained information

and novel tools presented in this study have the potential to improve our understanding of the atmospheric $\delta^{18}O$-CO_2 budget.

Contents

List of figures

List of tables

List of abbreviations

a	kinetic fractionation associated with CO_2 diffusion through stomata	
a_b	kinetic fractionation associated with CO_2 diffusion through leaf boundary layer	
a_d	total kinetic fractionation associated with CO_2 diffusion between leaf and atmosphere	
a_{eff}	kinetic isotopic fractionation related to soil surface	
a_{oc}	kinetic isotopic fractionation related to ocean surface	
A_r	plant assimilation rate	[µmol m^{-2} s^{-1}]
a_w	kinetic fractionation associated with CO_2 diffusion through intercellular space	
B	Bunsen solubility coefficient for CO_2	
b_c	boundary layer conductance	[mol m^{-2} s^{-1}]
C	molar density	[mol m^{-3}]
CA	carbonic anhydrase	
CA_{assay}	*in vitro CA* activity	[µmol m^{-2} s^{-1}]
CA_{leaf}	leaf-level *CA* activity	[µmol m^{-2} s^{-1}]
c_a	CO_2 mole fraction in the atmosphere	[ppmv]
c_i	CO_2 mole fraction in intercellular space	[ppmv]
c_c	CO_2 mole fraction inside the chloroplast	[ppmv]
$CO^{18}O_s$	soil $CO^{18}O$ isoflux	[µmol m^{-2} s^{-1} ‰]
$CO^{18}O$-*Iso*	plant $CO^{18}O$ isoforcing	[m s^{-1} ‰]

D	diffusivity	[m^2 s^{-1}]
D_{eq}	isotopic disequilibrium between F_r and F_a	
EC	eddy covariance	
Δ_A	^{18}O discrimination during plant assimilation	
Δ_{ca}	^{18}O-enrichment of chloroplast CO_2 relative to atmospheric CO_2	
Δ_{ea}	theoretical enrichment at full equilibrium between CO_2 and leaf water at evaporation sites	
$\delta^{18}O_A$	oxygen isotope ratio of photosynthetic CO_2	[‰ vs. VPDB-CO_2]
$\delta^{18}O_a$	oxygen isotope ratio of atmospheric CO_2	[‰ vs. VPDB-CO_2]
$\delta^{18}O_{av}$	oxygen isotope ratio of atmospheric water vapor	[‰ vs. VSMOW]
$\delta^{18}O_{bw}$	oxygen isotope ratio of bulk leaf water	[‰ vs. VSMOW]
$\delta^{18}O_{eql}$	oxygen isotope ratio of leaf CO_2 at full equilibrium with leaf H_2O	[‰ vs. VPDB-CO_2]
$\delta^{18}O_{eqs}$	oxygen isotope ratio of soil CO_2 at full equilibrium with soil H_2O	[‰ vs. VPDB-CO_2]
$\delta^{18}O_{ev}$	oxygen isotope ratio of leaf water at evaporation site	[‰ vs. VSMOW]
$\delta^{18}O_s$	oxygen isotope ratio of CO_2 emitted from soils	[‰ vs. VPDB-CO_2]
$\delta^{18}O_{sc}$	oxygen isotope ratio of soil CO_2	[‰ vs. VPDB-CO_2]
$\delta^{18}O_{sv}$	oxygen isotope ratio of soil water vapor	[‰ vs. VSMOW]
$\delta^{18}O_{sw}$	oxygen isotope ratio of liquid soil water/plant source water	[‰ vs. VSMOW]
$\delta^{18}O_t$	oxygen isotope ratio of CO_2 from total net exchange	[‰ vs. VPDB-CO_2]
$\delta^{18}O_{tr}$	oxygen isotope ratio of transpired water vapor	[‰ vs. VSMOW]

e_a	vapor pressure in the atmosphere	[Pa]
ε_{eq}	equilibrium fractionation factor	[-]
e_i	vapor pressure in the intercellular space	[Pa]
ε_k	kinetic fractionation factor	[-]
F_a	gross flux of CO_2 from plant assimilation	[mol m^{-2} s^{-1}]
F_{ao}	gross flux of CO_2 from atmosphere to ocean	[mol m^{-2} s^{-1}]
f_{CA}	soil *CA* activity factor	[-]
F_f	gross flux of CO_2 from anthropogenic sources	[mol m^{-2} s^{-1}]
F_I	gross flux of CO_2 from soil invasion	[mol m^{-2} s^{-1}]
F_{oa}	gross flux of CO_2 from ocean to atmosphere	[mol m^{-2} s^{-1}]
F_r	soil respiration rate	[mol m^{-2} s^{-1}]
F_t	total net CO_2 flux	[mol m^{-2} s^{-1}]
g_m	mesophyll conductance	[mmol m^{-2} s^{-1}]
GPP	gross primary productivity	[g C m^{-2} yr^{-1}]
g_s	stomatal conductance	[mmol m^{-2} s^{-1}]
g_t	total conductance	[mmol m^{-2} s^{-1}]
IAEA	International Atomic Energy Agency	
κ	tortuosity factor	[-]
k_e	effective rate constant of isotopic equilibration reaction in soils	[s^{-1}]
k_h	rate constant of hydration reaction	[s^{-1}]
K_m	Michaelis-Konstante	
k_s	rate constant of isotopic CO_2–H_2O equilibration reaction	[s^{-1}]

K_{sat}	soil hydraulic conductivity	[m d^{-1}]
L_A	Leaf area	[m^2]
L_{eff}	effective diffusion length	[m]
ρ	Péclet number	[-]
p	pressure	[Pa]
PAR	photosynthetically active radiation	[µmol photons m^{-2} s^{-1}]
Ψ	soil water potential	[hPa]
QCLAS	quantum cascade laser absorption spectrometer	
Q_{10}	temperature coefficient	
r_b	resistance of diffusion through leaf boundary layer	[m^2 s^{-1} $mmol^{-1}$]
R_g	Total incoming short-wave radiation	W m^{-2}
rh	air relative humidity	[-]
RMSE	root mean square error	
$RMSE_s$	systematic component of root mean square error	
$RMSE_u$	unsystematic component of root mean square error	
r_s	resistance of diffusion through stomata	[m^2 s^{-1} $mmol^{-1}$]
R_w	respiration from wood components	[µmol m^{-2} s^{-1}]
R_{25}	soil respiration rate at 25 °C	[µmol m^{-2} s^{-1}]
SWC	volumetric soil water content	[m^3 m^{-3}]
SWC_{res}	residual soil water content	[m^3 m^{-3}]
SWC_{sat}	saturation soil water content	[m^3 m^{-3}]
T_{air}	air temperature	[°C]
TDL	tunable diode laser	
T_{leaf}	leaf temperature	[°C]

T_r	plant transpiration rate	[mmol m^{-2} s^{-1}]
T_s	soil temperature	[°C]
θ	degree of CO_2−H_2O oxygen isotope equilibrium	[-]
θ_{kt}	degree of CO_2−H_2O oxygen isotope equilibrium determined from leaf *CA* activity	[-]
V_m	molar volume of air at standard conditions	[m^3 mol^{-1}]
VPD	vapor pressure deficit	[kPa]
VPDB	Vienna Pee Dee Belemnite	
VSMOW	Vienna Standard Mean Ocean Water	
WS-CRDS	wavelength-scanned cavity ring-down spectrometer	

I. General introduction

I.1 Theory

Stable isotopes are powerful tools for studying the global water and carbon cycle related to climate change, and the potential of stable isotope analysis has significantly increased because of the recent advances in measurement techniques (Werner et al., 2012). Stable isotopes of an element have the same number of protons but differ in their number of neutrons and consequently in their mass number. Different isotopes are usually denoted with their mass number in superscript, e.g. ^{12}C and ^{13}C. In contrast to radioactive isotopes, they do not decay and are therefore declared as "stable". Stable isotopes occur naturally and with distinct abundance for a wide range of elements. As an example, for oxygen the ^{16}O is the most abundant isotope (99.759 %), while ^{17}O (0.037 %) and ^{18}O (0.204 %) are the minor isotopes (Michener and Lajtha, 2008). Depending on whether the isotope contains more or less neutrons compared to the most abundant isotope it is termed "heavier" and "lighter", respectively. The term "isotopologue" refers to molecules that have the same chemical formula but contain different stable isotopes of an element. For this study, the following isotopologues of CO_2 and H_2O are relevant (with the bold letters referring to the naturally most abundant species): $\mathbf{^{12}C^{16}O^{16}O}$, $^{12}C^{16}O^{18}O$, $\mathbf{^{1}H^{1}H^{16}O}$, $^{1}H^{1}H^{18}O$. For simplicity, the term "isotope" is used in the following definitions, but can be substituted equivalently by the word "isotopologue". Usually the stable isotopic composition of an element or a compound is expressed in the delta notation (δ), which refers to the ratio between the heavy and light isotope rather than the absolute abundance and is given in per mil [‰] (Gonfiantini, 1978). For instance, $\delta^{18}O\text{-}CO_2$ refers to the $^{18}O/^{16}O$ ratio in CO_2. To obtain values, which are comparable between different laboratories, the isotopic ratio of a sample is referred to an international standard:

$$\delta_X = (R_{sample}/R_{standard} - 1) \quad \text{(I.1)}$$

where R_{sample} and $R_{standard}$ are the ratios of heavy to light isotope in sample and standard, respectively. For oxygen isotopes in water, the Vienna Standard Mean Ocean Water (VSMOW) is commonly used as a reference, whereas $\delta^{18}O\text{-}CO_2$ is normalized to the Vienna Pee Dee Belemnite (VPDB) scale (Werner and Brand, 2001).

Owing to the different masses of the stable isotopes, the $^{18}O/^{16}O$ ratio can change, a process referred to as "isotopic fractionation" or discrimination. In general, equilibrium (thermodynamic) and kinetic isotopic fractionation are distinguished. The former results from the different vibrational energy of the isotopes, which determines the strength of hydrogen or covalent bonds, and the latter is caused by the different diffusion velocities or reaction rates of different isotopes or isotopologues. An example for equilibrium isotopic fractionation is the hydration of CO_2 molecules in liquid water, as during this process the oxygen isotopes between CO_2 and water are exchanged. The evaporation of water, e.g., from the ocean to the atmosphere, is a common example for a kinetic isotopic fractionation process, which leads to the accumulation of heavier H_2O – referred to as "enrichment" – in the residual liquid water, as the lighter molecules evaporate more rapidly. The opposite of "enrichment" is "depletion", i.e., meaning that the $^{18}O/^{16}O$ ratio becomes smaller.

I.2 Rationale

The oxygen isotope ratio of carbon dioxide ($^{18}O/^{16}O$) is an important tool for understanding and predicting changes in the (global) carbon budget more precisely because it allows quantifying the gross fluxes of CO_2. During a simple hydration reaction, which usually occurs everywhere as soon as CO_2 dissolves in liquid water, the oxygen isotope composition of water is transferred to CO_2 molecules, plus a temperature-dependent thermodynamic fractionation, as the quantity of water is several magnitudes larger than that of CO_2 (Brenninkmeijer et al., 1983):

$$H_2{}^{18}O + CO_2 \rightleftarrows H^+ + [HCO_2{}^{18}O]^- \rightleftarrows H_2O + CO^{18}O \quad (I.2)$$

Each water pool in soils and leaves has a distinct isotopic signature, depending amongst others on the isotopic composition of the source water, evaporation rate and water pool size, as during evaporation processes the lighter molecules ($H_2{}^{16}O$) evaporate more easily than the heavier molecules ($H_2{}^{18}O$). As a result, CO_2 molecules differ in their isotopic composition, depending on whether they originate from soil respiration or have entered and back-diffused from plant leaves, thereby remaining unfixed by photosynthesis (Fig. I.1; Gillon and Yakir (2001)).

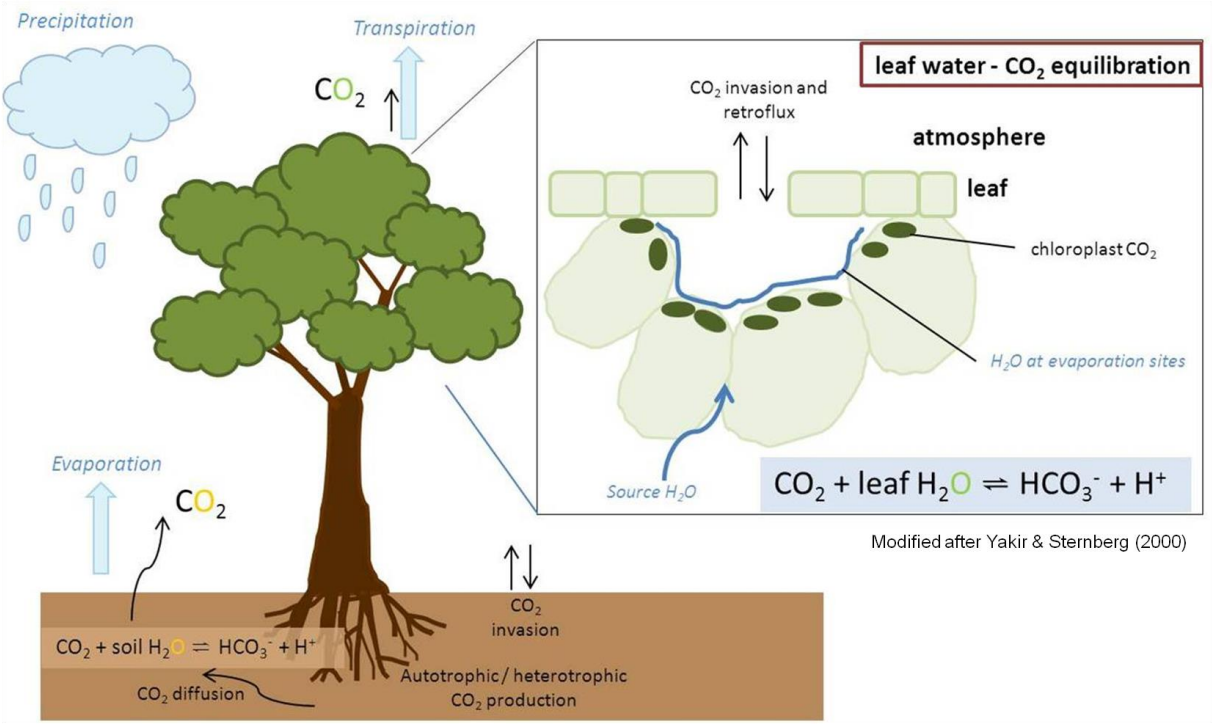

Figure I.1 Schematic overview of the oxygen isotope exchange in terrestrial ecosystems.

The influence of the terrestrial biosphere on the oxygen isotopic composition of atmospheric CO_2 was first recognized by Francey and Tans (1987) and Fiedli et al. (1987). Farquhar et al. (1993) established for the first time a global atmospheric $\delta^{18}O$-CO_2 budget (eq. I.3) and proposed a quantitative use of this isotopic information for the carbon budget, which was

adopted a few years later for the global scale on one hand (Ciais et al., 1997) and for the ecosystem scale on the other hand (Yakir and Wang, 1996):

$$c_a \frac{\mathrm{d}\delta^{18}O_a}{\mathrm{d}t} = F_f\,(\delta^{18}O_f - \delta^{18}O_a) + F_{oa}\,(\delta^{18}O_o - \delta^{18}O_a) + a_{oc}\,(F_{ao} - F_{oa}) + F_I\,(\delta^{18}O_s - \delta^{18}O_a) + F_r\,(\delta^{18}O_s - \delta^{18}O_a - a_{eff}) + F_a\,\Delta_A \quad \text{(I.3)}$$

where c_a is the concentration of atmospheric CO_2, $\delta^{18}O_a$ is the oxygen isotope composition of atmospheric CO_2, and F_f, F_{oa}, F_{ao}, F_I, F_r, and F_a are the gross fluxes of CO_2 from anthropogenic sources (e.g., burning of fossil fuels), from the ocean to the atmosphere and vice versa, from diffusion into and out of soils (CO_2 invasion), soil respiration, and plant assimilation (GPP, gross primary productivity), and their isotopic composition ($\delta^{18}O_x$), a_{oc} and a_{eff} are the kinetic isotopic fractionations related to the ocean and soil surface, and Δ_A is the ^{18}O discrimination during plant assimilation. If the magnitude and the isotopic composition of all the gross fluxes is known, eq. I.3 can be solved for F_a and thus provide independent estimates of GPP.

Since this potential was recognized for the first time, many studies have investigated the impact of vegetation and soils on $\delta^{18}O_a$, as these are the most uncertain budget components (Gillon and Yakir, 2001; Griffis et al., 2011; Seibt et al., 2006b; Sturm et al., 2012), but only very few studies conducted an ^{18}O-based gross flux partitioning (Langendörfer et al., 2002; Ogee et al., 2004; Yakir and Wang, 1996). The reason for the scarcity of such studies is that $\delta^{18}O_a$ is afflicted with high uncertainties due to isotopic effects occurring during CO_2 exchange with soil and leaf water at different scales. However, before the oxygen isotope signal of CO_2 can be used quantitatively, these uncertainties have to be reduced.

Past studies have addressed several aspects of the ^{18}O-exchange between CO_2 and H_2O in soils and leaves, but left behind some research gaps: The effect of soils on $\delta^{18}O_a$ has been examined in theoretical and model-based studies (Riley, 2005; Stern et al., 1999; Stern et al., 2001; Tans,

1998), but experimental data of the oxygen isotopic exchange in soils at varying soil water content are scarce (Hesterberg and Siegenthaler, 1991; Miller et al., 1999). The equilibrium between CO_2 and leaf water has been studied experimentally in more detail, but involves some critical assumptions, when scaled up from laboratory measurements to the canopy scale. Furthermore, the influence of dynamic environmental conditions on the oxygen isotope exchange remains an issue which has not been addressed properly up to now. The technical advances in laser-based spectroscopy over the last several years have the potential to bring research on the ^{18}O-exchange processes in terrestrial ecosystems to a new stage (Griffis, 2013) because the $^{18}O/^{16}O$ ratio in CO_2 and H_2O can be monitored in real-time and quasi-simultaneously.

I.3 State of the art

I.3.1 The degree of isotopic equilibrium in leaves

The impact of the vegetation on $\delta^{18}O_a$ is quantitatively described by the photosynthetic discrimination term (Gillon and Yakir, 2001):

$$\Delta_A = a_d + \xi\,[\theta\,(\delta^{18}O_{eql} - \delta^{18}O_a) - (1-\theta)\,a_d\,/(\xi+1)] \qquad \text{(I.4)}$$

where a_d is the mean diffusional isotopic fractionation of $CO^{18}O$ from atmosphere to leaf, and $\xi = c_c/(c_c - c_a)$ with c_c and c_a representing the CO_2 mixing ratio in the chloroplast and atmosphere, respectively. The variables $\delta^{18}O_a$ and $\delta^{18}O_{eql}$ are the $\delta^{18}O$ of atmospheric CO_2 and CO_2 in full equilibrium with leaf water, respectively, and θ is the actual degree of CO_2–H_2O isotopic equilibrium inside the leaf ranging between 0 (no exchange) and 1 (full equilibrium). Equation (I.4) shows that θ is one of the factors that determine the plants' influence on $\delta^{18}O_a$. Gillon and Yakir (2001) were the first to conduct a comprehensive study on θ at the leaf scale

over a wide range of plant species and found that θ differed considerably within and between C_3 and C_4 plant species, with values ranging between 0.7 and unity for C_3 plants, and θ = 0.4 for C_4 grasses, respectively (Barbour et al., 2007; Gillon and Yakir, 2000, 2001; Kodama et al., 2011). However, more recent studies reported much lower θ for C_3 and C_4 plants at the canopy scale (θ < 0.5) (Griffis et al., 2011; Xiao et al., 2010) and revealed that **up-scaling of θ from the leaf to the whole canopy, as done in big-leaf models, is challenging** (Santos et al., 2014). Estimates for θ are either derived as a function of the hydration rate constant (k) versus the residence time of CO_2 inside the chloroplast (τ), which is determined in biochemical enzyme assays with the responsible enzyme, carbonic anhydrase (*CA*):

$$\theta = 1 - e^{-k\tau/3} \quad \text{(I.5)}$$

or by gas exchange measurements and solving eq. I.4 for θ. The former method is based on *CA* activity measurements in leaf extracts prepared from the whole leaf, and therefore might not be representative of the actual extent of equilibrium found at the leaf sites relevant for the CO_2–H_2O exchange (Cousins et al., 2006). It also implies that θ is constant over time, an assumption which is challenged by the fact that several studies reported on the adaptation of plants' *CA* activity to changes in abiotic conditions (Durand et al., 2011; Kaul et al., 2011; Tiwari et al., 2006). **In fact, knowledge about the effects of temporal variations of *CA* activity on θ is scarce.**

I.3.2 The oxygen isotope signature of leaf water

The isotopic composition of leaf water at the evaporation site ($\delta^{18}O_{ev}$) is a major determinant for Δ_A, i.e., the $\delta^{18}O$-CO_2 signal transferred from plant leaves to the atmosphere (eq. I.4). Since $\delta^{18}O_{ev}$ cannot be measured directly, it is usually calculated using theoretical models. If isotopic

steady-state is prevailing, i.e., the $\delta^{18}O$ of transpired water vapor is equal to that of source water ($\delta^{18}O_{sw}$), the $\delta^{18}O_{ev}$ can be estimated by a Craig-Gordon-type model given by (Craig and Gordon, 1965; Farquhar and Lloyd, 1993):

$$\delta^{18}O_{ev} = \delta^{18}O_{sw} + \varepsilon_{eq} + \varepsilon_k + rh\,(\delta^{18}O_{av} - \delta^{18}O_{sw} - \varepsilon_k) \quad \text{(I.6)}$$

where ε_{eq} and ε_k are factors representing equilibrium isotopic fractionation during liquid–vapor phase transition of water and kinetic isotopic fractionation during diffusion of water vapor through stomata and boundary layer, respectively; *rh* is relative humidity, and $\delta^{18}O_{av}$ is the oxygen isotopic signature of atmospheric water vapor. However, frequently, i.e., when leaf water turnover is slow, isotopic non-steady state (NSS) prevails (Farquhar and Cernusak, 2005; Seibt et al., 2006a; Wang et al., 2012), and more complex models, which take into account intraleaf variations in $\delta^{18}O$ (Péclet effect), have to be used to adequately describe $\delta^{18}O_{ev}$ (Farquhar and Cernusak, 2005). Seibt et al. (2006a) emphasized the influence of diurnal variations in $\delta^{18}O_{ev}$ and (nighttime) isotopic NSS on Δ_A and postulated that these effects should be considered in global and ecosystem models of $\delta^{18}O$-CO_2. However, Xiao et al. (2012) showed that isotopic NSS, i.e., the Péclet effect, was negligible for $\delta^{18}O$-CO_2 simulations at the canopy-scale and indicated that the parameterization of a canopy kinetic fractionation factor is more relevant at the canopy scale. **These findings emphasized the need for studies that improve our process understanding of the CO_2–H_2O isotope exchange at different scales.** Advances in isotope-ratio infrared spectroscopy (Simonin et al., 2013; Wang et al., 2012) now allow obtaining data on $\delta^{18}O_{ev}$ at a high time resolution by calculation from continuously measured $\delta^{18}O$ of transpired water ($\delta^{18}O_{tr}$) in chamber experiments. **Despite of its great potential to monitor the influence of short-term variations of environmental conditions on**

isotopic (non) steady-state, this method has not yet been combined with simultaneous measurements of $\delta^{18}O$-CO_2 to study the effect of short-term variations in $\delta^{18}O_{ev}$ on Δ_A.

I.3.3 The oxygen isotope signature CO_2 emitted from soils

The oxygen isotopic signature of CO_2 emitted from soils ($\delta^{18}O_s$) can be described by the following equation (Wingate et al., 2009):

$$\delta^{18}O_s = \delta^{18}O_{eqs} + \varepsilon_d + (\delta^{18}O_{eqs} - \delta^{18}O_a)v_i\, c_a/F_r \quad \text{(I.7)}$$

where $\delta^{18}O_{eqs}$ is the oxygen isotopic signature of CO_2, derived from soil H_2O by taking into account temperature-dependent equilibrium isotopic fractionation, ε_d is the effective diffusional isotopic fractionation, c_a is the atmospheric CO_2 mixing ratio and F_r is the soil CO_2 flux. The exchange rate of CO_2 present in an air column above the soil with liquid soil water (v_i) is given by (Tans, 1998):

$$v_i = (B\, SWC\, k_h\, D_{18})^{1/2} \quad \text{(I.8)}$$

where B is the Bunsen solubility coefficient for CO_2, SWC is the volumetric soil water content, D_{18} is the effective diffusivity of $CO^{18}O$ in soil air, and k_h is the rate constant of the CO_2 hydration reaction (Skirrow, 1975).

Initially, $\delta^{18}O_s$ could be only derived by collecting flask air samples and subsequent analysis *via* isotope ratio mass spectrometry (Flanagan et al., 1999; Mortazavi et al., 2004; Seibt et al., 2006b). Although temporal resolution was limited, this methodology already allowed observing effects, e.g., of short-term changes in the oxygen isotope ratio of precipitation on $\delta^{18}O_s$. In the meantime, advances in optical isotope techniques have facilitated (near-) continuous

monitoring of $\delta^{18}O_s$, and laser spectroscopy has been combined with different experimental setups in the field. For example, a quantum cascade laser absorption spectrometer (QCLAS) was coupled to a closed soil-chamber system in a Swiss beech forest and allowed the observation of non-linearities in $\delta^{18}O_s$, which should be considered when $\delta^{18}O_s$ is derived from Keeling-plots (Kammer et al., 2011). Powers et al. (2010) connected a tunable diode laser (TDL) instrument to a dynamic soil chamber system in a semi-arid woodland and were able to detect the effect of irrigation on $\delta^{18}O_s$ at a temporal resolution of minutes. A TDL instrument was also used by Santos et al. (2012), who applied the isotope flux ratio (IFR) method to measure the isotope exchange of a deciduous forest floor. They reported strong diurnal variations in $\delta^{18}O_s$. Altogether, these studies pointed out that, in addition to high-frequency $\delta^{18}O_s$ measurements, sampling of $\delta^{18}O_{sw}$ at a high temporal and spatial resolution is required to adequately interpret temporal variations in $\delta^{18}O_s$. **Specific issues that remained unclear in this respect were the influence of varying soil water content on $\delta^{18}O_{sw}$ and $\delta^{18}O_s$, and the role of *CA* activity in soils**, which was indicated by the finding that soil CO_2 efflux was enriched compared with $\delta^{18}O_s$ values calculated from $\delta^{18}O_{sw}$ assuming an uncatalyzed equilibrium reaction (Seibt et al., 2006b; Wingate et al., 2008). More insight into the underlying processes governing $\delta^{18}O_s$ were gained from measurements or numerical simulations of the $\delta^{18}O$ of CO_2 ($\delta^{18}O_{sc}$) and H_2O ($\delta^{18}O_{sw}$) in the soil, but experimental data remains scarce and **no high resolution measurements of $\delta^{18}O_{sw}$ in combination with $\delta^{18}O_s$ have been reported yet** (Amundson et al., 1996; Amundson et al., 1998; Stern et al., 1999; Tans, 1998).

I.3.4 The oxygen isotope signature of soil water

As Stern et al. (1999) showed in a sensitivity analysis, the oxygen isotope ratio of soil water ($\delta^{18}O_{sw}$) is a major factor influencing $\delta^{18}O_{sc}$. The oxygen isotope ratio of soil water exhibits a strong vertical pattern, with ^{18}O-enriched water at the soil surface and ^{18}O-depleted water

deeper in the soil, approaching the $\delta^{18}O$ of input (precipitation) water (Barnes and Allison, 1983; Mathieu and Bariac, 1996). The logarithmic pattern of $\delta^{18}O_{sw}$ is not simply reflected in $\delta^{18}O_{sc}$, though, as in the near-surface soil CO_2 diffuses out of the soil at a rate which is faster than the reaction rate of the equilibrium reaction, leaving not enough time for complete CO_2–H_2O equilibrium. From this it becomes clear, that the soil depth at which $\delta^{18}O_{sc}$ is assumed to still be fully equilibrated with $\delta^{18}O_{sw}$ largely influences $\delta^{18}O_s$ in numerical simulations. According to this, Riley et al. (2005) pointed out that by not taking into account the $\delta^{18}O_{sw}$ gradients near the soil surface and by using a depth-averaged value for $\delta^{18}O_{sw}$, large errors were introduced in simulations of $\delta^{18}O_s$. Throughout the literature, estimates of the soil depth where CO_2 is in equilibrium with soil water vary from 2–8.5 cm, 5–15 cm, 10–12 cm, and 0–5 cm, respectively (Griffis et al., 2011; Kapiluto et al., 2007; Miller et al., 1999; Mortazavi et al., 2004; Riley, 2005), and **reveal the need for experiments that study the influence of environmental conditions and soil parameters on the CO_2–H_2O equilibration depth.**

Allison et al. (1987) and Hesterberg and Siegenthaler (1991) were the first to combine $\delta^{18}O_{sw}$ and $\delta^{18}O_{sc}$ measurements at different depths of the soil profile, which required a lot of effort at that time because of the flask sampling procedure, which was still hampered by methodological problems such as condensation inside the air flasks. Owing to the advent of microporous probes and gas-permeable tubing, soil air can now be sampled (near-) continuously and quasi non-destructively. **Combination of novel *in situ* sampling techniques with laser-based analyzers has been reported for measurements of $\delta^{18}O_{sw}$ (Rothfuss et al., 2013; Volkmann and Weiler, 2014), and $\delta^{13}C$ of soil CO_2 (Goffin et al., 2014; Parent et al., 2013), but so far not for combined monitoring of $\delta^{18}O_{sc}$ and $\delta^{18}O_{sw}$.**

I.3.5 Carbonic anhydrase activity and the effective rate constant of the oxygen isotope exchange in soils

The presence of carbonic anhydrase (*CA*) in plant leaves is unquestioned (Sültemeyer et al., 1993) and was also postulated for natural soils in modeling studies, where simulations and observations of $\delta^{18}O_s$ did only match, when the isotopic hydration rate constant (k_s) was enhanced by at least two orders of magnitude (Griffis et al., 2011; Seibt et al., 2006b; Wingate et al., 2009). In these studies, the enzyme activity of *CA* was mathematically expressed as a *CA* activity factor (f_{CA}), i.e., the relative increase in k_s caused by *CA* activity:

$$k_e = k_s f_{CA} \tag{I.9}$$

However, Santos et al. (2012) showed that, assuming a constant *CA* activity, i.e. f_{CA}, was inappropriate to simulate diurnal variations in $\delta^{18}O_s$ and highlighted the need for further research on the temporal variability of *CA* activity. According to simulations by Riley et al. (2002), the impact of *CA* activity is assumed to increase with decreasing soil water content and vice versa, and also influences the equilibrium depth of CO_2–H_2O exchange. Wingate et al. (2009) demonstrated the implications of accurate f_{CA} estimates for global isotope-based flux partitioning of CO_2, in that ignoring *CA* activity in soils resulted in values for global photosynthesis lower by 30 % than the current estimates. **Altogether, previous studies revealed that, although the theoretical knowledge and analytical equations related to *CA* activity in soils are well developed, experimental studies are scarce.**

Aside from its enzymatic enhancement by *CA*, the value of k_e itself has been questioned in previous studies. The uncatalyzed reaction rate for isotopic CO_2–H_2O exchange is usually set equal to one third the purely chemical hydration rate constant, i.e., $k_s = 0.037\ s^{-1}/3 = 0.012\ s^{-1}$ (Skirrow, 1975) because there are three oxygen atoms present in the bicarbonate intermediate

(eq. I.2). However, Stern et al. (1999) suggested that the rate constant of the oxygen isotope equilibrium reaction in unsaturated soils might be much smaller than k_s, depending on the soil type and soil water content, as physical processes interfere with the purely chemical oxygen isotope exchange reaction. Thus, they pointed out that an effective rate constant, k_e, rather than a true chemical rate constant in the narrow sense is more appropriate to describe the CO_2−H_2O oxygen isotope equilibrium reaction in soils and highlighted **the need for further experiments analyzing k_e in dependence of the soil type and soil water content.** Inspite of this, many studies still rely on the value of k_s = 0.012 s^{-1} (Seibt et al., 2006b; Wingate et al., 2008).

I.3.6 The atmosphere-soil invasion flux

Atmospheric CO_2 that invades the soil to a certain depth before diffusing back to the atmosphere is also influenced by $\delta^{18}O_{sw}$ to a considerable degree (Tans, 1998). Miller et al. (1999) were the first to show experimentally the existence of an abiotic CO_2 invasion flux (F_I). A sensitivity study revealed that the magnitude of F_I depended on the concentration of atmospheric CO_2, k_s, and also soil properties, e.g., water content, porosity, tortuosity and diffusivity (Stern et al., 1999). Kapiluto et al. (2007) conducted further experimental and numerical studies on the abiotic invasion of atmospheric CO_2 into soil and reported that F_I was highest at medium θ_w, long residence times, and high T_s, and higher in fine than coarse sand, where the structural effect was most pronounced at low θ_w. **However, most knowledge on F_I is based on modeling studies, and experimental data is scarce,** although the implication of F_I has been acknowledged even for the global ^{18}O budget of atmospheric CO_2 ($\delta^{18}O_a$), especially with regard to potential *CA* activity in soils which could greatly enhance the impact of F_I on $\delta^{18}O_a$ (Stern et al., 2001; Wingate et al., 2009). Furthermore, the discovery of this abiotic gross flux revealed the potentially high contribution of biologically inactive soils with low respiration rates to $\delta^{18}O_a$ (Stern et al., 2001).

I.3.7 $CO^{18}O$ isoforcing and isofluxes/ canopy-scale measurements of the oxygen isotope exchange

The advances in optical isotope techniques brought forward the examination of the oxygen isotope exchange also at the ecosystem scale. The first studies of isotopic flux measurements at the canopy scale were conducted by Griffis et al. (2008) and Lee et al. (2009). They applied TDL instruments for combined analysis of $\delta^{18}O\text{-}CO_2$, $\delta^{18}O\text{-}H_2O$, and $\delta^{13}C\text{-}CO_2$ fluxes with the eddy covariance (EC) technique at a soybean field and presented an isoforcing concept, where the $CO^{18}O$ isoforcing ($CO^{18}O\text{-}Iso$) was defined as the EC flux of $CO^{18}O$. They found that the use of leaf-scale instead of canopy-scale kinetic factors and the non-consideration of turbulent diffusion introduced large errors to the whole-ecosystem isoforcing, especially in ecosystems with low canopy resistance. Coupling of high-frequency measurements of CO_2 isotopologues with the EC method extended the measurement capacities to the measurement of isotopic fluxes in forests, whereas before they were limited to agricultural surfaces, as the flux-gradient method requires measurements above the roughness sublayer (Griffis et al., 2004). To conduct EC flux measurements of $CO^{18}O$ over a mixed deciduous forest, Sturm et al. (2012) used a QCLAS instead of a TDL analyzer, which requires cryogenic cooling. Their measurements revealed that EC isotopologue flux measurements at short time-scales of hours to a few days are unsuitable to capture whole-ecosystem isotope discrimination due to the high random errors associated with the EC isofluxes, especially in ecosystems where the individual component fluxes and the signal-to-noise ratio are low. However, they were able to capture a reducing effect of precipitation events on the ^{18}O-discrimination of the system, reflecting the equilibration of CO_2 with the respective water pools at the site. Long-term EC measurements of $CO^{18}O$ fluxes at a temperate deciduous forest using a QCLAS were conducted by Wehr et al. (2013), who drew similar conclusions as Sturm et al. (2012), in that precision was mainly limited by horizontal

heterogeneity at the measurement location. They observed a distinct diurnal pattern in $CO^{18}O$ isofluxes, which was assumed to reflect leaf water enrichment at daytime and the contribution of depleted soil water at nighttime. By combining the flux-gradient method for $\delta^{18}O\text{-}CO_2$ and EC measurements of the $\delta^{18}O$ of evapotranspiration, Griffis et al. (2011) found a hydration efficiency (θ) for a crop canopy that was considerably lower than the previously assumed θ for C_4 species derived from laboratory measurements (θ = 0.2 instead of θ = 0.7) and highlighted once more the challenge related to scaling from the leaf to the canopy level.

I.4 Objectives

The overall aim of the present study was to examine the processes and factors that influence the oxygen isotope exchange between atmospheric CO_2 and the water pools in leaves and soil in real-time using laser-based spectroscopy. The aim of the first study (chapter II) was to quantify the effect of short-term variations in environmental conditions on leaf water isotopic enrichment and on $\delta^{18}O\text{-}CO_2$. In the second study (chapter III), the ^{18}O-exchange between soil water and CO_2 at varying soil water content was examined in a laboratory experiment with a sand column. In both studies, a combination of two laser instruments was used for quasi-simultaneous measurements of $\delta^{18}O\text{-}CO_2$ and $\delta^{18}O\text{-}H_2O$ at high time resolution. While the first and second study were focused either on the aboveground or soil compartment of the soil–plant–atmosphere continuum, in a third study (chapter IV), the oxygen isotope exchange was examined at the ecosystem scale by means of model simulations and compared with time series of measured $\delta^{18}O\text{-}CO_2$ canopy profile data.

In the different studies, the following hypotheses were tested:

i) Short-term variations of environmental conditions significantly influence $CO^{18}O$ isoforcing, i.e., the plants' impact on atmospheric $\delta^{18}O\text{-}CO_2$, *via* induced changes in

the respective drivers (θ, g_s, A_r, $\delta^{18}O_{ev}$) of the oxygen isotope exchange, which vary between plant species.

Plant gas exchange measurements were combined with real-time measurements of the oxygen isotope ratios of CO_2 and water vapor inside a plant chamber. Air temperature and soil water availability were varied to quantify the impact on the oxygen isotope exchange between the plant and the chamber air. The experiments were conducted with Norway spruce, grey poplar, maize and wheat to study whether $CO^{18}O$ isoforcing and the underlying processes and factors vary between different plant functional types.

ii) The $\delta^{18}O_{sc}$ signal over the soil profile is influenced by variations in $\delta^{18}O_{sw}$, $\delta^{18}O_a$, soil water content, and *CA* activity.

A new methodology was developed in order to measure $\delta^{18}O_{sw}$ and $\delta^{18}O_{sc}$ quasi simultaneously in soil. Gas-permeable tubing was installed at different depths in a sand column allowing the depth-specific analysis of $\delta^{18}O_{sw}$ and $\delta^{18}O_{sc}$ in a high temporal resolution using two isotope-specific laser instruments for H_2O and CO_2. The effects of (abrupt) changes in soil water content, e.g., by irrigation of the column, and application of carbonic anhydrase were addressed in individual experiments.

iii) Estimates of θ obtained from gas exchange measurements with single Norway spruce plants can be up-scaled and help to improve simulations of canopy $\delta^{18}O$-CO_2.

The multilayer–multileaf model MuSICA was used to simulate the oxygen isotope signature of canopy CO_2 and soil efflux at a Norway spruce stand. Simulations were validated with isotope and EC data measured over one year at the Höglwald experimental site. Model runs with different parameterizations for θ, including θ = 0.53, that was determined in the plant chamber experiments with Norway spruce, were compared to

examine whether the laboratory-based estimates of θ yielded improved simulations of canopy $\delta^{18}O\text{-}CO_2$.

II. Effect of short-term variations of environmental conditions on atmospheric $CO^{18}O$ isoforcing of different plant species

Modified on the basis of

Laura Gangi, Wolfgang Tappe, Harry Vereecken, Nicolas Brüggemann, 2015. Agricultural and Forest Meteorology 201, 128-140

II.1 Introduction

The oxygen isotope signature of carbon dioxide ($\delta^{18}O\text{-}CO_2$) is a powerful tracer for CO_2 sources and sinks in terrestrial ecosystems (Yakir and Wang, 1996) and can help to improve calculations of the global carbon budget based on the atmospheric $\delta^{18}O\text{-}CO_2$ ($\delta^{18}O_a$) signal (Ciais et al., 1997; Gillon and Yakir, 2001). The $\delta^{18}O_a$ allows to disentangle CO_2 fluxes related to plant CO_2 exchange (F_a) and soil respiration (F_r) (Bowling et al., 1999; Langendörfer et al., 2002; Yakir and Wang, 1996), due to the ^{18}O-exchange between CO_2 and leaf or soil water pools, as long as the $\delta^{18}O$ values of these water pools differ enough from each other to generate a sufficient isotopic disequilibrium (D_{eq}) between F_a and F_r (Griffis et al., 2011; Santos et al., 2014; Wingate et al., 2010). In addition to D_{eq}, precise and frequent measurements of mixing ratios of CO_2 isotopologues and a comprehensive understanding of the isotopic fractionation processes during gas exchange within the soil-plant-atmosphere continuum are required. While the former has become feasible in recent years by technical progress of laser-based infrared absorption techniques (Griffis, 2013), the O isotope exchange between water pools and atmospheric CO_2 still lacks sufficient characterization and quantification. Furthermore, although global climate projections predict an increase in mean surface temperature and a greater risk of drought periods for specific areas (IPCC, 2007), there are few studies which examined the impact of environmental conditions on global $\delta^{18}O_a$ (Buenning et al., 2011; Buenning et al., 2014).

Various models for the simulation of $\delta^{18}O_a$ have been developed (Ciais et al., 1997; Cuntz et al., 2003; Ogee et al., 2004) and have been evaluated with the above mentioned high-frequency measurements (Lai et al., 2006; Lee et al., 2009; Riley et al., 2003; Xiao et al., 2010). Model simulations revealed that uncertainties related to the $\delta^{18}O_a$ signal are partly introduced by inaccurate estimations of the isotopic composition of leaf water at the evaporation site, $\delta^{18}O_{ev}$, which is transferred to CO_2 during isotopic equilibration (Farquhar et al., 1993). The isotopic

composition of leaf water at the evaporation site can be estimated by the Craig-Gordon model when the $\delta^{18}O$ signature of transpiration water is equal to source water ($\delta^{18}O_{sw}$), assuming an isotopic steady-state (Craig and Gordon, 1965). However, several studies have reported that isotopic non-steady state (NSS) is the rule rather than the exception in plant and soil water pools, especially at sub-diurnal time scales, e.g. during the night, and when stomatal conductance (g_s) or transpiration is low or specific leaf water content is high (Farquhar and Cernusak, 2005; Seibt et al., 2006a; Wang et al., 2012). Therefore, alternative models which account for NSS conditions and also the intraleaf variations in $\delta^{18}O$ (Péclet effect) have been established (Dongmann et al., 1974; Farquhar et al., 1993; Farquhar and Cernusak, 2005). In chamber experiments, $\delta^{18}O_{ev}$ can be calculated from measured $\delta^{18}O$ of transpired water ($\delta^{18}O_{tr}$). Also in this respect, the recent progress of laser-based isotope analyzers allowed the development of new methods to monitor $\delta^{18}O_{tr}$ at variable environmental conditions (Simonin et al., 2013; Wang et al., 2012). However, to which extent short-term variations of environmental conditions, such as leaf temperature and soil water supply, trigger isotopic NSS and how this influences $\delta^{18}O_a$, e.g., by affecting g_s, has been insufficiently characterized at present. In view of globally changing environmental conditions this will be highly relevant to understanding and predicting future changes in $\delta^{18}O_a$.

Several studies on the influence of plants on $\delta^{18}O_a$ also underpinned the need for quantification of the proportion of CO_2 in isotopic equilibrium with leaf water (θ) and found that θ differed considerably within and between C_3 and C_4 plant species, with values ranging from 0.7 to 1 for C_3, and 0 to 1 for C_4 plants, respectively (Barbour et al., 2007; Gillon and Yakir, 2000, 2001; Kodama et al., 2011). Due to its catalytic activity during the CO_2 hydration reaction, the enzyme carbonic anhydrase (*CA*) strongly influences θ. Leaf-level *CA* activities (CA_{leaf}) vary considerably among different plant species (Gillon and Yakir, 2001; Hatch and Burnell, 1990), but also along a single leaf (Affek et al., 2006; Kodama et al., 2011), and influence leaf $CO^{18}O$

discrimination (Cousins et al., 2006; Williams et al., 1996). Nevertheless, only little is known about the temporal regulation of CA_{leaf}, e.g., in response to changes in environmental conditions (Durand et al., 2011; Kaul et al., 2011; Lazova et al., 2012) and how that might affect θ.

The aim of the present study was to quantify the effect of short-term variations (from minutes to days) in air temperature and water availability on leaf water isotopic enrichment and on $\delta^{18}O$-CO_2 of four plant species representing four different plant functional types, i.e., Norway spruce as coniferous C_3 tree species, grey poplar as deciduous, dicotyledonous C_3 tree species, wheat as monocotyledonous C_3 crop, and maize as C_4 crop species. Isotopic signatures of CO_2 and H_2O were monitored *online* using a flow-through plant chamber and isotope-specific infrared laser absorption analyzers for CO_2 and H_2O. The following hypotheses were tested: i) short-term variations of environmental conditions significantly influence $\delta^{18}O$ of leaf water at the evaporation site and $CO^{18}O$ isoforcing, i.e., the impact on $\delta^{18}O_a$, *via* induced changes in g_s, assimilation rate (A_r) and θ; ii) ^{18}O discrimination and its drivers differ between the four plant species; and iii) CA_{leaf} varies with environmental conditions and directly affects the ^{18}O-exchange between H_2O and CO_2.

II.2 Material and Methods

II.2.1 Plant material

Rooted cuttings of grey poplar (*Populus x canescens*) were provided by Helmholtz Zentrum Munich, Germany, and grown in pots as described in Behnke et al. (2007). Three-year-old Norway spruce (*Picea abies*) seedlings, which had been purchased bare-root from a local nursery, were planted in pots and kept in a growth room with a 12 h light/12 h dark period at 22°C. The height of the poplar and spruce plants (from the soil surface to the top of the plant crown) varied between 0.6 and 0.7 m. Maize (*Zea mays* cv. Primus) seeds were provided by KWS Mais GmbH (Einbeck, Germany) and were grown in pots with a 12 h light/12 h dark

period at 25°C. Seeds for cultivation of wheat (*Triticum aestivum* cv. Ronaldinio) were provided by the local Chamber of Agriculture in Düren, Germany, and were grown under the same conditions as maize. At the time of measurement, maize plants were about three weeks (plant height: approx. 0.5 m) and wheat plants about two months old (plant height: approx. 0.4 m), respectively. To allow acclimatization, plants were transferred to the experimental plant chamber several days before the beginning of the measurements.

II.2.2 Gas exchange measurements

For photosynthetic and isotopic measurements, a single plant was inserted into a plant chamber (volume: 164 L, height: 0.6 m, diameter: 0.6 m, material: borosilicate glass), which was itself situated in a phytotron allowing for controlled environmental conditions. The glass chamber included only the upper part (stem, leaves) of the plant. A PTFE plate with a centrally arranged hole for the plant's stem separated the roots and the soil gas-tight from the photosynthetically active part of the plant. The taller the plant, the greater was the proportion of the stem which was excluded from the chamber, but no leaves were excluded from the chamber. The setup had to be slightly modified for wheat due to the different morphology of this species. Here, the soil part was sealed with plastic paraffin film (Parafilm®). Illumination was provided by six daylight lamps (Powerstar HQI-BT, 400 W/D, Osram, Germany) and was set to a diurnal cycle (10 h day/14 h night) with a maximum photosynthetically active radiation (PAR) of 600 µmol photons m^{-2} s^{-1} in the center of the plant chamber. The air temperature inside the chamber and the leaf temperature at the bottom side of at least two different leaves per plant were measured with thermocouples (GTF 300, Greisinger electronic GmbH, Regenstauf, Germany). Soil water potential was recorded with a tensiometer (T5, UMS, München, Germany). Details about the plant chamber can be found elsewhere (Wildt et al., 1997).

The CO_2 mixing ratio of re-moistened clean dry air flowing into the chamber was set around 400 ppmv, i.e. close to ambient conditions, with a mass flow controller. Prior to the addition of CO_2, dry air was directed through a temperature-controlled water bath to generate humid air at a distinct saturated vapor pressure. The temperature of the water bath was set to higher values during night and lower values during daytime to obtain higher and lower water vapor pressures at the chamber inlet, respectively. Additionally, the mixing ratio of dry and moistened inlet air was adjusted *via* two flow controllers. This allowed us to prevent a strong humidity drop due to low transpiration rates at night and to avoid condensation inside or outside the chamber. Unfortunately, we could not maintain water vapor levels close to physiological conditions within the chamber at nighttime during all experiments, as only the water bath temperature but not the mixing ratio of dry and moist air could be adjusted automatically on a diurnal scale which was sometimes insufficient to obtain sufficiently high humidity levels at nighttime.

Depending on the plant size and, thus, on the transpiring leaf area, the adjustment of the water vapor mixing ratio in the chamber required distinct flow rates for the individual plants between 15-35 L min^{-1}. A PTFE fan mounted at the top of the chamber ensured homogeneous mixing of the chamber air. We used ¼" polyethylene–aluminum composite tubing (Synflex 1300, Eaton Electric GmbH, Bonn, Germany) and PFA or PTFE tubing for gas lines leading to the chamber/measurement devices. Prior testing of the whole setup, including the plant chamber and the tubing, showed the absence of isotopic fractionation effects for CO_2 and H_2O at different flow rates, water vapor and CO_2 mixing ratios. Plants were exposed to two different treatments (elevated air temperature and limited water supply) to examine whether the oxygen isotopic exchange is influenced by these short-term changes in environmental conditions. Each type of experiment was replicated three times per plant species. To expose the plants to high temperature conditions, the chamber temperature was increased from 25 to 35°C for one day, while all other settings, for example the flow rate and water vapor mixing ratio of the chamber

inlet air, were not changed. During this time plants were well-watered to avoid water stress. Water shortage experiments were induced by omitting irrigation. Prior to and during the experiments, all plants were watered with local tap water. The tap water was analyzed regularly for its $\delta^{18}O$, which was relatively constant at around -8.2 ± 0.2 ‰. Except for the water shortage experiments, the plants were always kept well-watered to minimize ^{18}O enrichment of soil water and differences in source water isotopic composition for the different plants. Since our experiments were based on a non-destructive methodology, we could not sample xylem water or soil water.

II.2.3 Isotopic measurements

Isotopic compositions are expressed in the common delta notation (in ‰) and referenced to the Vienna Standard Mean Ocean Water (VSMOW):

$$\delta_X = (R_{sample}/R_{standard} - 1) \quad \text{(II.1)}$$

where R_{sample} and $R_{standard}$ are the ratios of heavy to light isotope in sample and standard, respectively. Against common use in atmospheric studies, also the $\delta^{18}O\text{-}CO_2$ values were related to the VSMOW scale to allow for direct use of equations from the literature for the calculation of the degree of oxygen isotopic exchange between CO_2 and leaf water (eqs. II.13-II.16). However, this did not affect the calculation of the $CO^{18}O$-isoforcing, as this is derived from differential terms (cf. eqs. II.19 and II.20). Water vapor and CO_2 mixing ratios and isotopic signatures were sampled alternately and pressureless from the excess air flow at the inlet and outlet of the chamber by a wavelength-scanned cavity ring-down spectrometer (WS-CRDS, L2120-i, Picarro, Inc., Santa Clara, CA, USA) and a tunable diode laser absorption spectrometer (TDLAS, TGA 200, Campbell Scientific, Inc., Logan, UT, USA), respectively. The WS-CRDS

and TDLAS sampled approximately 30 and 500 mL air min^{-1}, respectively. A datalogger (CR3000, Campbell Scientific) was used to control measurement cycles of both devices. Water vapor was measured alternately every 5 min at the inlet and at the outlet of the chamber by the WS-CRDS. Only the last minute (= 32 single data points) was used for averaging to account for the adaptation time of the analyzer to the respective mixing ratio and isotopic level. Measured $\delta^{18}O\text{-}H_2O$ was corrected for dependency on water vapor mixing ratios. The dependency was determined in advance by measuring $\delta^{18}O$ values at different mixing ratios generated by varying the ratio between synthetic dry and moist air which was produced by a dew point generator at a constant temperature. Measurements were tied to the VSMOW scale *via* two-point calibration using two laboratory standards which had been calibrated against the international standards VSMOW2, GISP and SLAP provided by the International Atomic Energy Agency (IAEA). For isotope analysis of irrigation (source) water, liquid water samples were injected into the vaporizer of the WS-CRDS using an autosampler (HTC-PAL, CTC Analytics, Zwingen, Switzerland). Each sample was measured at least six times, with the first two measurements being omitted to account for memory effects. Precision and accuracy of $\delta^{18}O\text{-}H_2O$ measurements was <0.1‰.

The TDLAS switched between inlet and outlet every 20 seconds (where only the last 10 s, corresponding to 100 single data points, were considered for averaging to account for instrument equilibration time between valve switching). Once every four minutes two reference gases (325 and 450 ppmv CO_2 in synthetic air; Air Liquide, Düsseldorf, Germany, and Linde AG, Pullach, Germany; $\delta^{18}O\text{-}CO_2$ vs. VPDB-CO_2: –33.17 to –30.65 ‰, ±0.2 ‰, and –15.53 to –14.03 ‰, ±0.2 ‰, respectively) were measured for one minute each. The two reference gases spanned the range of measured mixing ratios and were used to tie the isotopic measurements to the VPDB-CO_2 scale, then to correctly convert the values to the VSMOW scale, and finally to compensate for instrument drift. The actual isotope ratios of the reference gases were

determined by isotope ratio mass spectrometry (IsoPrime100, Isoprime Ltd., Cheadle Hulme, UK). The precision of TDLAS measurements was characterized by the Allan Variance (Sturm et al., 2012; Werle, 2011) and was 0.1 ‰ for an integration time of 10 s.

II.2.4 Calculation of gas exchange

Various gas exchange variables were calculated according to von Caemmerer and Farquhar (1981). The net transpiration rate (T_r) in mol m^{-2} s^{-1} was calculated with the following equation:

$$T_r = air_{in}/L_A \cdot (w_{out} - w_{in})/(1 - w_{out}) \quad \text{(II.2)}$$

where L_A stands for the leaf area in m^2, air_{in} is the molar air flow in mol s^{-1}, w_{in} and w_{out} are the mole fractions of water entering and leaving the chamber, respectively. The net assimilation (A_r) in mol m^{-2} s^{-1} was given by:

$$A_r = air_{in}/L_A \cdot (1 - w_{in})/(1 - w_{out}) \cdot (c_{in} - c_{out}) - T_r \cdot c_{in} \quad \text{(II.3)}$$

Here, c_{in} and c_{out} represent the CO_2 mole fractions measured at inlet and outlet of the chamber, respectively. Total conductance to water ($g_{t\text{-}H2O}$) in mol m^{-2} s^{-1} was used to calculate the respective stomatal conductance to water ($g_{s\text{-}H2O}$) and was estimated based on the following equation:

$$g_{t\text{-}H2O} = T_r \cdot [1 - (w_{leaf} - w_{out})/2]/(w_{leaf} - w_{out}) \quad \text{(II.4)}$$

with w_{leaf} as the mole fraction of water in the intercellular space, calculated based on the assumption that relative humidity inside the leaf is 100%. Taking into account the good

ventilation of the chamber air, a constantly high boundary layer conductance (b_c) of 1.5 mol m^{-2} s^{-1} was assumed (Wingate et al., 2007) to calculate stomatal conductance to water vapor in mol m^{-2} s^{-1}.

$$g_{s\text{-}H2O}=1/(1/g_{t\text{-}H2O}-1/b_c) \quad \text{(II.5)}$$

To assess whether our assumptions about b_c significantly influenced the results of our calculations, we conducted a sensitivity analysis by increasing and decreasing the value for b_c by 50 %, respectively (Table II.1). The stomatal conductance to CO_2 ($g_{s\text{-}CO2}$) was calculated from $g_{s\text{-}H2O}$ by considering a factor of 1.6 (Von Caemmerer and Farquhar, 1981):

$$g_{s\text{-}CO2}=g_{s\text{-}H2O}/1.6 \quad \text{(II.6)}$$

Table II.1 Values for input parameters of the sensitivity analysis, where zero refers to default settings for the parameters and g_m − and g_m + refer to the minimum and maximum values, respectively, found for the four plant species in the literature.

	b_c 0 [mol m^{-2} s^{-1}]	g_m 0 [mol m^{-2} s^{-1}]	b_c –50% [mol m^{-2} s^{-1}]	b_c +50% [mol m^{-2} s^{-1}]	g_m − [mol m^{-2} s^{-1}]	g_m + [mol m^{-2} s^{-1}]
Poplar	1.5	0.2	0.75	2.25	0.1	0.5
Maize	1.5	0.82	0.75	2.25	0.26	1.37
Spruce	1.5	0.1	0.75	2.25	0.02	0.16
Wheat	1.5	0.3	0.75	2.25	0.15	0.64

II.2.5 Calculations of isotopic exchange

The oxygen isotopic signature of leaf water at the evaporation site ($\delta^{18}O_{ev}$) was calculated from the $\delta^{18}O$ of ambient (chamber) water vapor ($\delta^{18}O\text{-}H_2O_{out}$), independent of the $\delta^{18}O$ of source water ($\delta^{18}O_{sw}$) and without assuming isotopic steady state. Therefore, kinetic fractionation (ε_k) during diffusion of water vapor through stomata and boundary layer, temperature-dependent

equilibrium fractionation (ε_{eq}), and vapor pressure deficit between leaf and chamber were taken into account (Farquhar and Lloyd, 1993):

$$\delta^{18}O_{ev} = \delta^{18}O_{tr} + \varepsilon_{eq} + \varepsilon_k + e_a/e_i \cdot (\delta^{18}O\text{-}H_2O_{out} - \varepsilon_k - \delta^{18}O_{tr}) \quad \text{(II.7)}$$

where e_a and e_i represent the vapor pressure in the atmosphere and intercellular space, respectively, and $\delta^{18}O_{tr}$ is the oxygen isotopic signature of transpiration, which was calculated directly from the mass balance of (isotopic) chamber gas exchange measurements (Simonin et al., 2013):

$$\delta^{18}O_{tr} = (\delta^{18}O\text{-}H_2O_{out} \cdot (1 - w_{in}) - \delta^{18}O\text{-}H_2O_{in} \cdot w_{in}/w_{out} (1 - w_{out})) \cdot w_{out}/(w_{out} - w_{in}) \quad \text{(II.8)}$$

ε_{eq} and ε_k were calculated according to Farquhar and Lloyd (1993) and Cernusak et al. (2004), respectively:

$$\varepsilon_{eq} = 2.644 - 3.206 \cdot 10^3 / T_{leaf} + 1.534 \cdot 10^6 / T_{leaf}^2 \quad \text{(II.9)}$$

$$\varepsilon_k = (28\, r_s + 21\, r_b)/(r_s + r_b) \quad \text{(II.10)}$$

where T_{leaf} is the leaf temperature in Kelvin, and r_s and r_b are the respective resistances during water vapor diffusion through stomata and leaf boundary layer in $m^2\ s^{-1}\ mmol^{-1}$ (Bottinga and Craig, 1968). To examine the sensitivity of the isotopic calculations to the leaf water isotopic signature, we compared the calculations based on $\delta^{18}O_{ev}$ with those based on the oxygen isotopic signature of bulk leaf water ($\delta^{18}O_{bw}$). Therefore, we calculated $\delta^{18}O_{bw}$ according to Farquhar and Lloyd (1993):

$$\delta^{18}O_{bw} = (\delta^{18}O_{ev} - \delta^{18}O_{sw}) \cdot (1-exp^{-\rho})/\rho + \delta^{18}O_{sw} \quad \text{(II.11)}$$

$$\rho = (T_r \cdot L_{eff})/(C \cdot D) \quad \text{(II.12)}$$

where ρ is the non-dimensional Péclet number, L_{eff} is the effective diffusion length (m), C is the molar density of water ($55.6 \cdot 10^3$ mol m^{-3}), and D is the temperature-dependent diffusivity of the $H_2{}^{18}O$ in water (Cuntz et al., 2007). Since we did not measure L_{eff} independently, we used a value of 150 mm for spruce (Song et al., 2013), 8 mm for wheat (Barbour et al., 2000), 19 mm for maize, and 34 mm for poplar (Ferrio et al., 2012). The degree of isotopic equilibration between CO_2 and H_2O molecules (θ) was calculated according to Gillon and Yakir (2000) (eq. II.13). This method allowed us to detect temporal variations in θ, while the determination of θ based on the regression of $\delta^{18}O\text{-}CO_2$ inside the chloroplast vs. $\delta^{18}O_{ev}$ as used in Cernusak et al. (2004), includes the assumption that θ is invariant. Since the regression approach was not applied and the variables used to calculate θ were mainly derived from direct measurements of mixing ratios and $\delta^{18}O$ at the chamber inlet and outlet, ternary effects, which have been introduced recently by Farquhar and Cernusak (2012), were not taken into account. Nighttime values of θ were discarded as they showed too large fluctuations resulting from the low CO_2 concentration difference between chloroplast and atmosphere.

$$\theta = [\Delta_{ca} + a_d \cdot (1-c_c/c_a)]/[\Delta_{ea} + a_d \cdot (1-c_c/c_a)] \quad \text{(II.13)}$$

Here, a_d is the diffusional fractionation, c_c stands for the partial pressure of CO_2 in the chloroplast (C_3 plants) or cytosol (maize), and c_a for the CO_2 partial pressure of the atmosphere (here $c_a = c_{out}$), respectively. Δ_{ca} (eq. II.14) represents the ^{18}O-enrichment of chloroplast CO_2 relative to atmospheric CO_2, whereas Δ_{ea} (eq. II.16) is the theoretical enrichment at full equilibrium between CO_2 and leaf water at evaporation sites (Cernusak et al., 2004; Farquhar et al., 1993). We assumed that the evaporation sites are the relevant place for the oxygen isotope

exchange rather than bulk leaf water, as this is supposedly where CO_2 exiting the leaf has the last contact to a water surface, and therefore eq. II.16 includes $\delta^{18}O_{ev}$ rather than $\delta^{18}O_{bw}$. Nevertheless, we conducted a sensitivity analysis to estimate the influence of this choice on our results.

$$\Delta_{ca} = (\Delta_A - a_d)/[(1 + \Delta_A)\cdot c_c/(c_a - c_c)] \quad \text{(II.14)}$$

where Δ_A is the discrimination against ^{18}O during photosynthesis (Cernusak et al., 2004), with $\xi = c_{in}/(c_{in} - c_{out})$.

$$\Delta_A = [\xi\cdot(\delta^{18}O\text{-}CO_{2\_out} - \delta^{18}O\text{-}CO_{2\_in})]/[1 + \delta^{18}O\text{-}CO_{2\_out} - \xi\cdot(\delta^{18}O\text{-}CO_{2\_out} - \delta^{18}O\text{-}CO_{2\_in})] \quad \text{(II.15)}$$

$$\Delta_{ea} = [\delta^{18}O_{ev}(1 + \varepsilon_{eq\text{-}CO2}) + \varepsilon_{eq\text{-}CO2} - \delta^{18}O\text{-}CO_{2\_out}]/(1 + \delta^{18}O\text{-}CO_{2\_out}) \quad \text{(II.16)}$$

Here, $\delta^{18}O\text{-}CO_{2\_out}$ is the oxygen isotopic signature measured at the outlet of the chamber, and $\varepsilon_{eq\text{-}CO2}$ is the temperature-dependent equilibrium fractionation of CO_2, calculated according to eq. II.17 (Brenninkmeijer et al., 1983):

$$\varepsilon_{eq\text{-}CO2} = (17604/T - 17.93) \quad \text{(II.17)}$$

The diffusional fractionation used in eqs. II.13 and II.14 was calculated as follows:

$$a_d = [(c_a - c_s)\cdot a_b + (c_s - c_i)\cdot a + (c_i - cc)\cdot a_w]/(c_a - c_c) \quad \text{(II.18)}$$

with a_b, a and a_w being the kinetic fractionation associated with diffusion of CO_2 through boundary layer, stomata and intercellular space, respectively, and c_i the CO_2 mole fraction in the intercellular space which was calculated according to von Caemmerer and Farquhar(1981). CO_2 partial pressure inside the chloroplast (C_3) or cytosol (C_4), here specified as c_c, was determined based on the assimilation rate and mesophyll conductance (g_m) by applying Fick's first law of diffusion. Estimates had to be made for mesophyll conductance because direct measurements of g_m, e.g., *via* $\delta^{13}C$-CO_2, could not be conducted. For wheat, g_m was set to 0.3 mol m^{-2} s^{-1} according to values that had been determined for wheat leaves older than 14 days under laboratory conditions (Loreto et al., 1994). For Norway spruce, g_m of 0.10 mol m^{-2} s^{-1} was chosen, which represents an average value for evergreen gymnosperms (Flexas et al., 2008). For poplar, a value for g_m of 0.2 mol m^{-2} s^{-1} was chosen according to the value assigned by Flexas et al. (2008) to the group of woody deciduous angiosperms. For maize, g_m was assumed to be 0.82 mol m^{-2} s^{-1}, which is the average of literature values ranging from 0.26 to 1.37 mol m^{-2} s^{-1} (Pfeffer and Peisker, 1995). To assess the sensitivity of relevant output variables to different g_m values, we performed recalculations with g_m values varying between the maximum and minimum values, found for the four plant species in the literature (Table II.1).

To quantify the plants' influence on the isotopic signature of ambient (chamber) CO_2 and to allow for comparison with canopy scale isoflux measurements, chamber level $CO^{18}O$-isoforcing ($CO^{18}O$-*Iso*) in m s^{-1} ‰ was calculated based on the isoforcing concept presented by Lee et al.(2009). For this purpose, the oxygen isotopic signature of the net CO_2 flux through the chamber ($\delta^{18}O$-CO_{2net}) and the $\delta^{18}O$ and CO_2 mixing ratio at the chamber outlet were considered as equivalent to the isotopic composition of the ecosystem flux and the $\delta^{18}O$ and CO_2 mixing ratio in ambient air, respectively.

$$CO^{18}O\text{-}Iso = -A_r \cdot (\delta^{18}O\text{-}CO_{2net} - \delta^{18}O\text{-}CO_{2out})/c_{out} \quad \text{(II.19)}$$

$$\delta^{18}O\text{-}CO_{2net} = (\delta^{18}O\text{-}CO_{2out} \cdot c_{out} - \delta^{18}O\text{-}CO_{2in} \cdot c_{in})/(c_{out} - c_{in}) \quad \text{(II.20)}$$

The $CO^{18}O$-isoforcing was also calculated according to the mechanistic model provided by eq. 21 in Lee et al. (2009):

$$CO^{18}O\text{-}Iso_{sim} = -A_r / c_{out} \cdot (c_c/(c_c - c_a) \cdot (\delta^{18}O_{eql} - \delta^{18}O\text{-}CO_{2out}) \cdot \theta + (1-\theta) \cdot a_d \cdot c_c / c_a - a_d) \quad \text{(II.21)}$$

where $\delta^{18}O_{eql}$ is the $\delta^{18}O$ for CO_2 in full equilibrium with $\delta^{18}O_{ev}$, given by $\delta^{18}O_{eql} = \delta^{18}O_{ev} + \varepsilon_{eq\text{-}CO2}$. Only daytime $CO^{18}O\text{-}Iso_{sim}$ could be calculated as no nighttime values of θ were available for the above-mentioned reasons.

II.2.6 Carbonic anhydrase assay

The carbonic anhydrase (*CA*) assay was modified from Hatch (1991). For *CA* analysis a composite sample of at least three leaves per plant was sampled, frozen in liquid nitrogen immediately afterwards and stored at -80°C until analysis. Leaves were ground in liquid nitrogen using mortar and pestle. Extracts of poplar, maize and wheat were prepared by dissolving 200 mg of the obtained leaf powder in 2 mL of ice-cold extraction buffer (50 mM Hepes-NaOH at pH 8.3, 10 mM dithiothreitol, 0.5 mM EDTA, 10% v/v glycerol and 1% Triton X-100). For Norway spruce, a different extraction buffer was used (50 mM Hepes-KOH at pH 7.3, 10% v/v glycerol, 2 % (w/v) polyvinylpyrrolidone K-25, 5 mM Na-ascorbic acid, 5 mM dithiothreitol), as protein extraction was hampered by phenolic substances when using the other

extraction buffer. Extracts were centrifuged at 5,200 *g* for 10 min, and the supernatant was used for subsequent analysis of *in vitro CA* enzyme activity (CA_{assay}). Protein concentration of fresh leaf extracts was determined *via* the Bradford protein assay at a wavelength of 593 nm. For this purpose, 420 µL of Coomassie solution (0.01 % (w/v) Coomassie Brilliant Blue G-250 in 5 % (v/v) ethanol, 10 % (v/v) 85 % o-phosphoric acid, 85 % ultrapure water, double filtered) were added to 20 µL of leaf extract (previously diluted 1:10 with bidistilled water). Calibration curves for each measurement were based on simultaneous measurements of Albumin Fraction V protein with concentrations of 10, 25, 50, 75, and 100 µg mL^{-1}. For measurements of enzymatic activity, 100 µL of leaf extract were added to 7 mL of assay buffer (30 mM barbital buffer at pH 8.3). The time needed for a change from pH 8.3 to pH 7.8 after addition of ultrapure water containing 10 mM CO_2 was measured using a pH microelectrode (A 157, SI Analytics, Mainz, Germany). The reaction mixture was continuously stirred on ice with a magnetic stirrer, and the reaction tube was sealed during the reaction to reduce the influence of external atmospheric CO_2. To determine the molar rate of CO_2 that had been converted during this pH change (1 mole H^+ formed for every mole of CO_2 hydrated; Hatch and Burnell (1990)), the same pH change was titrated with 0.005 M H_2SO_4. The net molar rate of CO_2 conversion was obtained by subtracting the maximum molar rate of CO_2 conversion of a blank assay (without leaf extract) from the enzymatic rate, and was normalized to leaf area.

The calculation of the *in vivo CA* activity based on *in vitro* measurements required further information on substrate concentration and temperature dependency of the enzymatic rates (K_m and Q_{10} value, respectively). To determine the K_m value of the leaf enzyme, the enzymatic activity was measured at different CO_2 concentrations (2, 3.5, 5, 10, 20 mM). The Q_{10} value was determined by measuring the enzymatic activity at different temperatures (2, 12, 22, 32 °C). *In vivo CA* activity (CA_{leaf}) was then calculated using the following equation as proposed by Gillon and Yakir (2000):

$$CA_{leaf} = CO_{2assay} \cdot [(T_{leaf} - T_{assay})/10]^{Q10} \cdot CA_{assay} \cdot CO_{2\_liq} / [(CO_{2assay} + K_m) \cdot (CO_{2\_liq} + K_m)] \quad \text{(II.22)}$$

where CO_{2assay} is the CO_2 concentration during *in vitro* reaction, T_{leaf} and T_{assay} refer to measured leaf temperature and temperature during *CA* assay, respectively; CO_{2_liq} is the CO_2 concentration at the catalytic site inside the chloroplast (calculated under consideration of Henry's law ($CO_{2\_liq} = 3.4 \cdot 10^{-2} \cdot (c_c/10^6)$). Based on CA_{leaf}, the degree of equilibrium (θ_{kt}) was calculated according to eq. II.23 (Mills and Urey, 1940) and was compared to θ derived from isotopic gas exchange measurements:

$$\theta_{kt} = 1 - exp^{(-k\tau/3)} \quad \text{(II.23)}$$

where k_τ is the number of hydrations per CO_2 molecule ($k_\tau = CA_{leaf}/F_{in} \cdot$) and F_{in} is to the gross flux of CO_2 into the leaf.

II.3 Results

II.3.1 CO_2–H_2O isotopic exchange before treatment

Leaf water at evaporation sites was on average more ^{18}O-enriched in poplar and maize (16.6 and 17.4 ‰, respectively) and less enriched in spruce (12.7 ‰) and wheat (8.7 ‰), and the enrichment was positively correlated with vapor pressure deficit (*VPD*) (Table II.2). The $\delta^{18}O$ of transpired water vapor ($\delta^{18}O_{tr}$) was always heavier than the $\delta^{18}O$ of source (irrigation) water ($\delta^{18}O_{sw}$), indicating isotopic non-steady state (data not shown). As for A_r and T_r, midday averages of $CO^{18}O$-*Iso* differed between the four plant species, but consistently showed diurnal variations corresponding to the respective light and dark periods during all of the experiments (Table II.2; Fig. II.1).

Table II.2 Pre-treatment values of transpiration and assimilation rate (T_r, A_r), stomatal conductance to CO_2 (g_{s_CO2}), vapor pressure deficit (*VPD*), $CO^{18}O$ isoforcing (*$CO^{18}O$-Iso*), simulated $CO^{18}O$ isoforcing (*$CO^{18}O$-Iso$_{sim}$*), $\delta^{18}O$-H_2O at evaporation site within the leaf ($\delta^{18}O_{ev}$), and degree of leaf isotopic CO_2–H_2O equilibrium (θ) inside the plant chamber at midday, averaged over all measured plants (n = 3, ± s.d.).

	Poplar		**Maize**		**Spruce**		**Wheat**	
T_r [mmol m^{-2} s^{-1}]	1.4	± 0.1	2.1	± 0.3	0.4	± 0.1	2.1	± 0.3
A_r [µmol m^{-2} s^{-1}]	4.3	± 0.4	11.2	± 2.1	1.0	± 0.2	4.1	± 0.7
$g_{s\_CO_2}$ [mmol m^{-2} s^{-1}]	60.4	± 6.2	85.4	± 15.5	23.5	± 8.5	348.5	± 82.9
VPD [kPa]	1.6	± 0.2	1.7	± 0.2	1.2	± 0.3	0.7	± 0.1
$CO^{18}O$-Iso [m s^{-1} ‰]	0.021	± 0.004	0.020	± 0.002	0.005	± 0.001	0.035	± 0.005
$CO^{18}O$-Iso$_{sim}$ [m s^{-1} ‰]	0.019	± 0.003	0.020	± 0.002	0.005	± 0.001	0.034	± 0.004
$\delta^{18}O_{ev}$ [‰]	16.6	± 2.4	17.4	± 2.5	12.7	± 3.0	8.7	± 0.8
θ [-]	0.74	± 0.15	0.51	± 0.02	0.53	± 0.05	0.67	± 0.04

Daytime *$CO^{18}O$-Iso* was on average highest in wheat (0.035 m s^{-1} ‰), around 0.02 m s^{-1} ‰ for poplar and maize, and lowest in spruce (0.005 m s^{-1} ‰) (Table II.2). The diurnal pattern of *$CO^{18}O$-Iso* varied among the plant species and was most pronounced for wheat and maize (Fig. II.1). To get an independent estimate of *$CO^{18}O$-Iso* and validate our chamber-based measurements of *$CO^{18}O$-Iso*, we compared measured *$CO^{18}O$-Iso* with simulated $CO^{18}O$ isoforcing (*$CO^{18}O$-Iso$_{sim}$*) based on A_r and θ (eq. II.21). The midday averages and temporal variations of directly measured *$CO^{18}O$-Iso* and *$CO^{18}O$-Iso$_{sim}$* agreed considerably well for all species during the daytime (Fig. II.1, Table II.2). For the nighttime, *$CO^{18}O$-Iso$_{sim}$* could not be reliably calculated, as nighttime values of θ exhibited too large fluctuations due to the low CO_2 concentration difference between chloroplast and atmosphere. The degree of isotopic CO_2–H_2O equilibrium was less than 100% in all species during daytime (day zero in Fig. II.1 and Table II.2). Highest θ values of up to 0.74 and 0.67 were found for poplar and wheat, respectively, while average values for spruce and maize were 0.53 and 0.51, respectively (Table II.2).

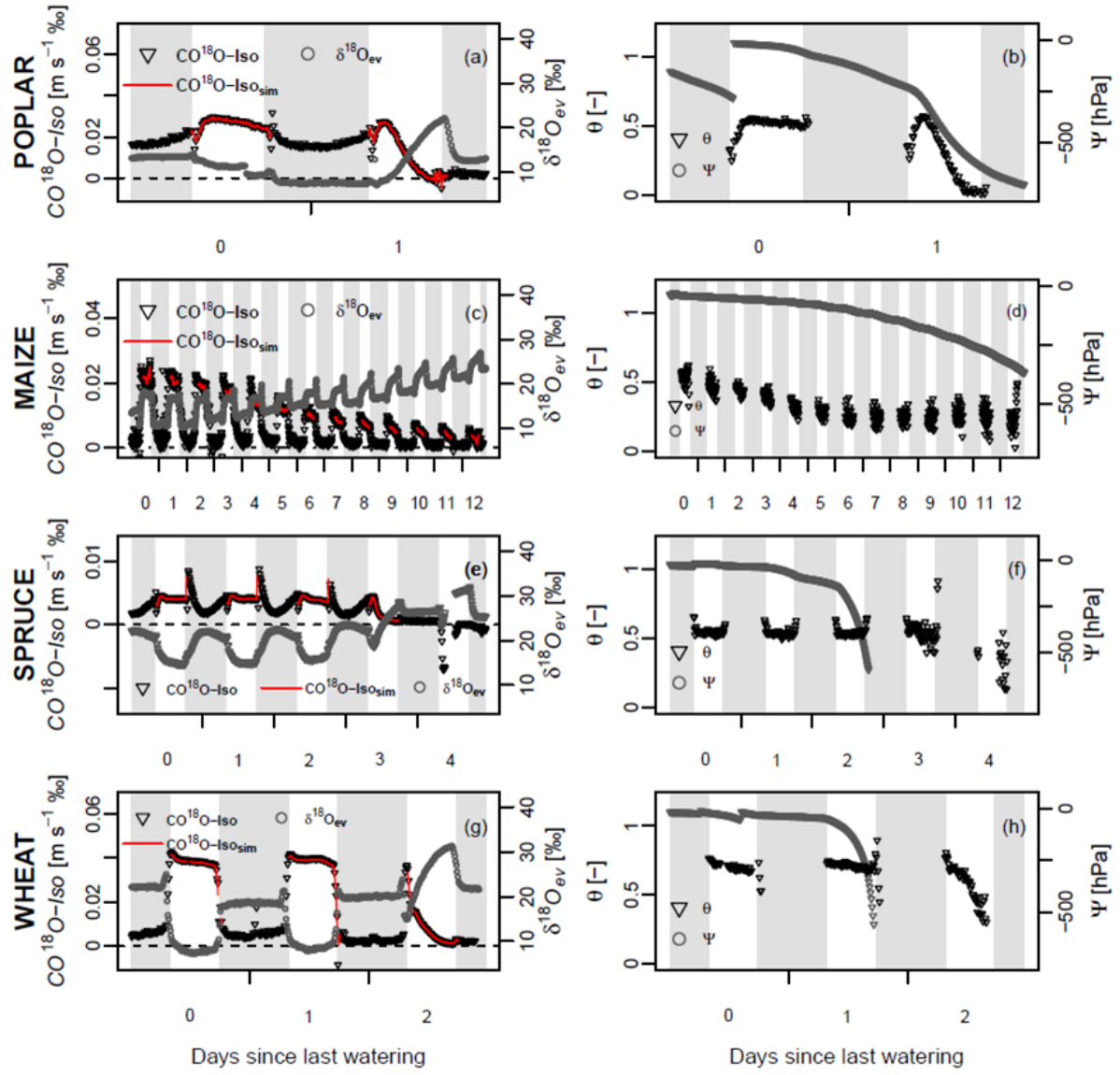

Figure II.1 Chamber-based $CO^{18}O$ isoforcing ($CO^{18}O$-*Iso*), simulated $CO^{18}O$-Iso ($CO^{18}O$-Iso_{sim}), and $\delta^{18}O$-H_2O at evaporation site ($\delta^{18}O_{ev}$) (a, c, e, g), degree of leaf isotopic CO_2–H_2O exchange (θ) and soil water potential (Ψ) (b, d, f, h) in response to decreasing water availability for the different plant species. Grey shaded areas refer to dark periods. Soil water potential measurements in (d) and (h) terminated around Ψ = –500 hPa after the tensiometer had run dry.

II.3.2 Impact of short-term variations of environmental conditions

II.3.2.1 Elevated air temperature

To test whether the plant-mediated isotopic exchange was sensitive to changes in air temperature (T_{air}), well-watered plants were exposed to an elevated T_{air} of 35°C for one day as compared to 25°C as normal condition. Associated with the increase in T_{air}, the *VPD* inside the

plant chamber also increased by a factor of 1.7 for maize, spruce and wheat experiments, and by a factor of 2.3 for poplar experiments (data not shown). The combination of elevated T_{air} and increased *VPD* affected the photosynthetic gas exchange of all plants in that the transpiration rates of all four plant species were higher at 35°C than at 25°C (Fig. II.2 a). For maize, T_r was more than 1.75-fold higher at 35°C than at 25°C, while for poplar, spruce, and wheat the increase was between 1.15 and 1.4-fold. In contrast, the assimilation rate was reduced at 35°C in all four species, with poplar and spruce showing the strongest reduction of about 25% (Fig. II.2 b). Similar to changes in A_r, but contrary to changes in T_r, stomatal conductance was reduced at 35°C in all species except for maize, where g_{s_CO2} did not significantly change (Fig. II.2 e). In all four plant species, leaf water at evaporation sites was about 1 ‰ (maize) to 4 ‰ (poplar) heavier at 35°C (Fig. II.2 c). The $CO^{18}O$-*Iso* decreased in response to increased T_{air}, except for the C_4 species maize, where $CO^{18}O$-*Iso* was about 1.2-fold higher at elevated T_{air} (Fig. II.2 d). The degree of isotopic CO_2–H_2O equilibrium was slightly higher (1.1-fold) in spruce and wheat, and 1.5-fold higher in poplar at 35°C as compared to 25°C, although here the variability within the same plant species was relatively high (Fig. II.2 f). However, θ did not change significantly in maize.

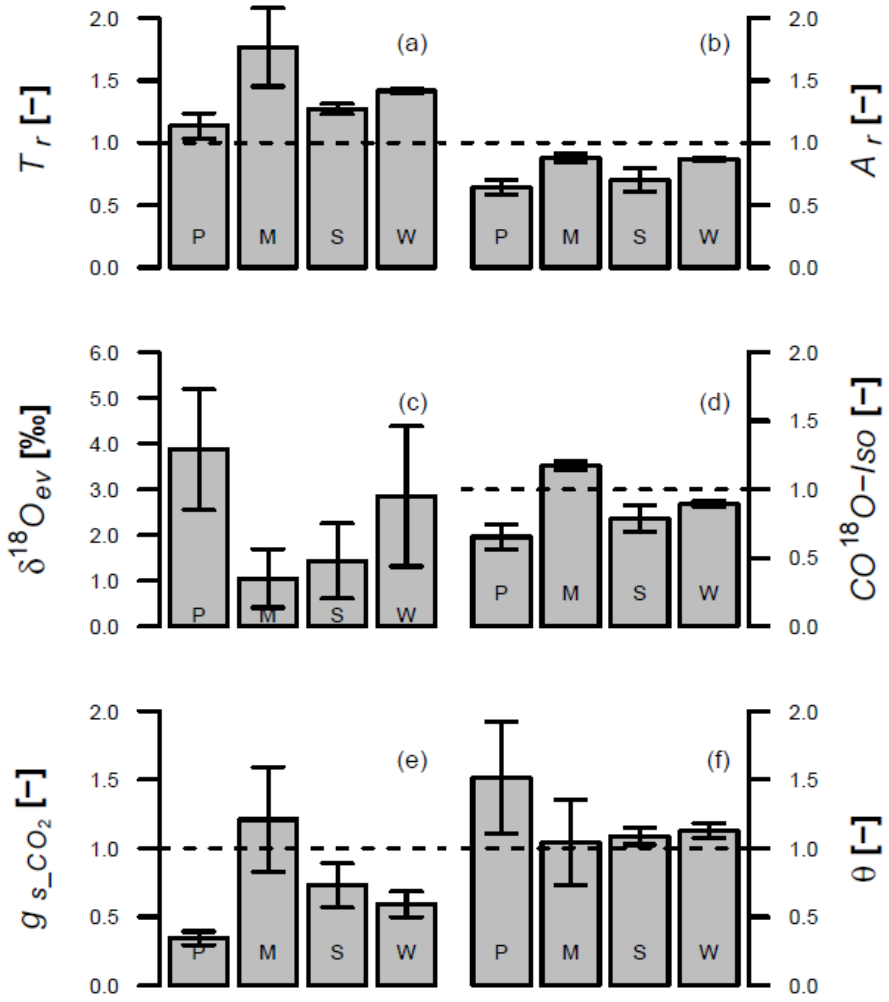

Figure II.2 Changes (± s.d.) in transpiration and assimilation rate (T_r, A_r) (a, b), $\delta^{18}O$-H_2O at evaporation site ($\delta^{18}O_{ev}$) (c), $CO^{18}O$ isoforcing ($CO^{18}O$-Iso) (d), stomatal conductance to CO_2 ($g_{s\_CO_2}$) (e), and degree of leaf isotopic CO_2–H_2O equilibrium (θ) (f) during midday steady-state in response to elevated air temperature (35°C compared to 25°C) in poplar (P), maize (M), spruce (S), and wheat (W). Note that for all variables except $\delta^{18}O_{ev}$ relative changes are shown (T_{35}/T_{25}), where a T_{35}/T_{25} ratio of 1 means no change, while values >1 (<1) refer to a temperature-related relative increase (decrease) in the variables, respectively. For $\delta^{18}O_{ev}$ absolute changes ($T_{35}-T_{25}$) in ‰ are shown (c).

II.3.2.2 Limited water availability

To examine the impact of limited water availability on oxygen isotope exchange between leaf water and atmospheric CO_2, irrigation of plants was terminated, while the soil water potential was measured to follow the desiccation of the soil. In all four plant species, θ and $CO^{18}O$-Iso decreased, while $\delta^{18}O_{ev}$ increased in response to decreasing water availability (Fig. II.1). At the same time also T_r, A_r, and g_{s_CO2} decreased (data not shown). The rate of decrease/increase

varied between the individual variables and between the plant species in that $\delta^{18}O_{ev}$ increased and θ decreased linearly, except for maize, whereas the decrease in T_r, A_r, g_{s_CO2}, and *$CO^{18}O$-Iso* was exponential for most plant species (Table A 1). The simulated $CO^{18}O$ isoforcing showed the same decrease as *$CO^{18}O$-Iso* for all experiments (Fig. II.1).

To identify the relative importance of the different determinants of plant-related ^{18}O-isoforcing, *$CO^{18}O$-Iso* was plotted against g_{s_CO2}, θ, $\delta^{18}O_{ev}$, and A_r, considering pre-treatment data as well as data from the limited water supply treatment (Fig. II.3). For *$CO^{18}O$-Iso* vs. $g_{s\_CO_2}$, a linear relationship was found for poplar and maize, while a logarithmic regression yielded the best fit for wheat. For spruce no significant relationship was found. A positive linear and logistic correlation between *$CO^{18}O$-Iso* and θ was found for poplar (r^2=0.88) and wheat (r^2=0.70), respectively, but not for spruce and maize. For the relationship *$CO^{18}O$-Iso* vs. $\delta^{18}O_{ev}$, only for spruce and wheat an exponential decay function (r^2=0.63 and 0.68, respectively) was obtained, whereas for the other species no clear relationship was observed (Fig. II.3). The *$CO^{18}O$-Iso* vs. A_r plots show a u-shape for maize, an ellipse-like shape for wheat, and a v-shape pattern for poplar and spruce (although not visible for one of the spruce replicates in this resolution of the plot). Common for all plant species is the positive relationship between *$CO^{18}O$-Iso* and A_r for positive values of A_r (Fig. II.3, regression line not shown). Stepwise linear regression of *$CO^{18}O$-Iso* vs. g_{s_CO2}, θ, $\delta^{18}O_{ev}$, and A_r revealed that the linear model was best when all four variables were included (poplar: r^2=0.97, spruce: r^2=0.86, wheat: r^2=0.95, maize: r^2=0.98, data not shown).

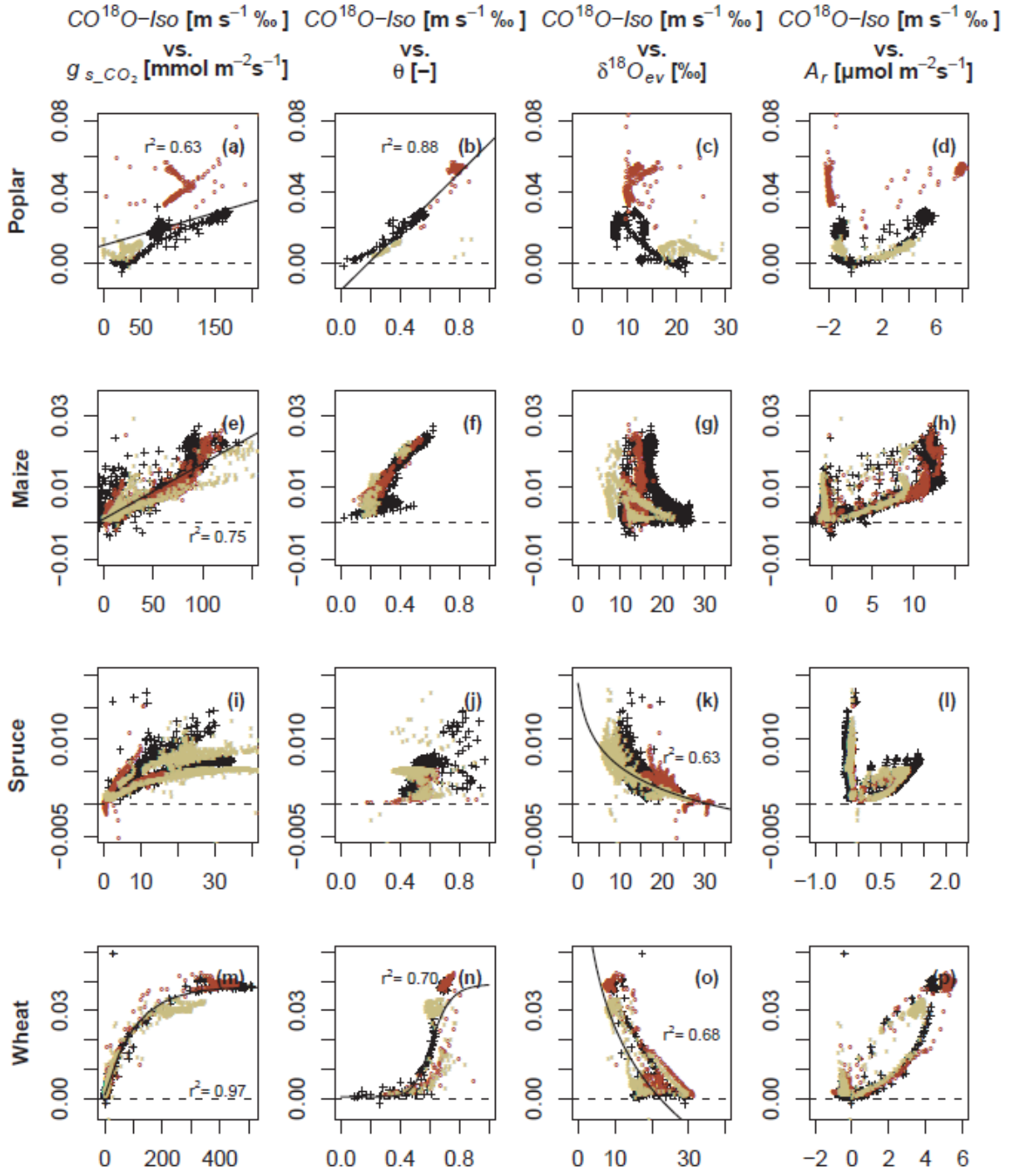

Figure II.3 $CO^{18}O$ isoforcing ($CO^{18}O$-*Iso*) vs. stomatal conductance to CO_2 (g_{s_CO2}) (a, e, i, m), and degree of leaf isotopic CO_2–H_2O equilibrium (θ) (b, f, j, n), $\delta^{18}O$-H_2O at evaporation site ($\delta^{18}O_{ev}$) (c, g, k, o), and assimilation rate (A_r) (d, h, l, p) for poplar, maize, spruce, and wheat, respectively. The lines show results from least squares regression (only for $r^2 > 0.5$ and $p < 0.001$). The three different colors in each plot refer to the three replicates of every plant species.

II.3.3 Variations in *CA* activity

In vitro activities of carbonic anhydrase ($CA_{in\ vitro}$) were between 6 and 8 mmol m^{-2} s^{-1} in leaf extracts of wheat, poplar and maize, whereas they were only around 4 mmol m^{-2} s^{-1} in spruce extracts (Fig. II.4 a). *In vivo* activities (CA_{leaf}), which were calculated based on measured leaf temperature, CO_2 concentration inside the leaf, and $CA_{in\ vitro}$, were considerably different between the four species (Fig. II.4 b). CA_{leaf} was higher in poplar and wheat (>150 µmol m^{-2} s^{-1}) as compared to maize and especially spruce (<50 µmol m^{-2} s^{-1}). To test whether $CA_{in\ vitro}$ determined in the laboratory can be used as a proxy for the isotopic CO_2–H_2O exchange inside the leaf, θ was calculated based on CA_{leaf} (θ_{kt}) and compared with the θ obtained from the isotopic gas exchange measurements. Both θ derived from gas exchange measurements and θ_{kt} were of the same order of magnitude (Fig. II.5). However, the linear fit was poor and an r^2 of 0.81 for poplar was the highest coefficient of determination that could be found.

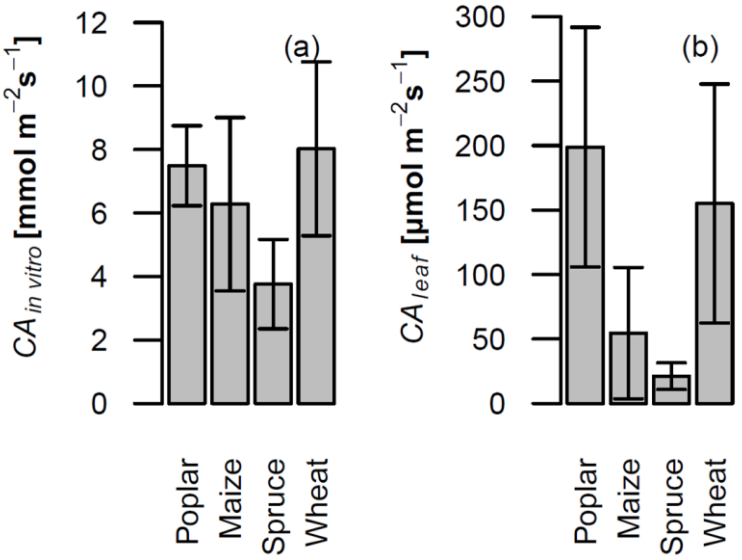

Figure II.4 *In vitro* (a) and *in vivo* (b) activity of carbonic anhydrase (*CA*) (± s.d.) for the four different plant species. *In vivo CA* activity was calculated based on measured *in vitro CA* activity, leaf temperature and CO_2 concentration inside the chloroplast during plant chamber measurements considering the experimentally determined temperature and substrate dependency of the enzyme.

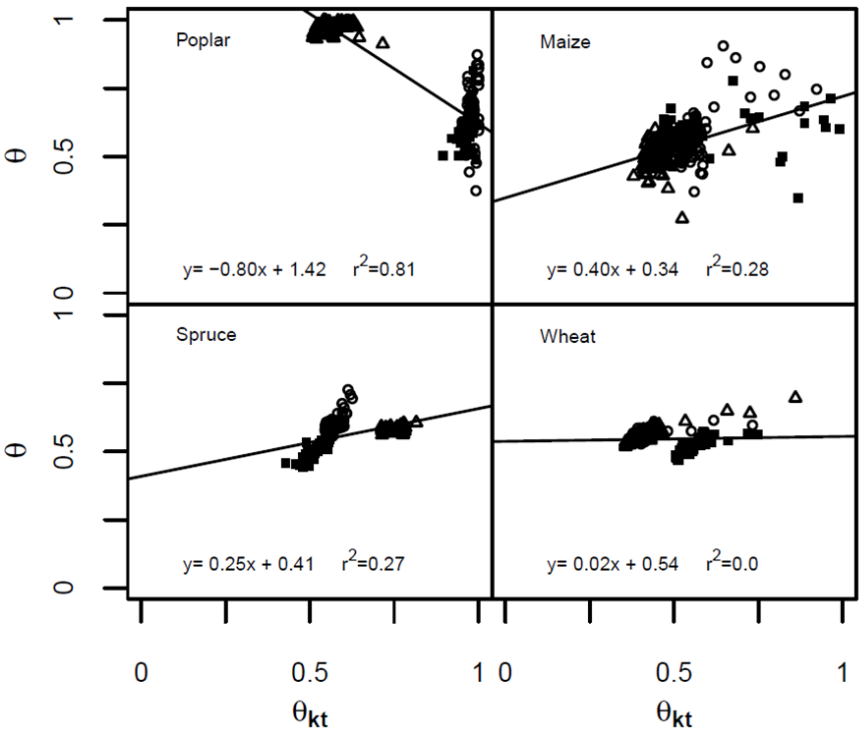

Figure II.5 Degree of CO_2–H_2O isotopic equilibrium (θ) determined from isotopic gas exchange measurements vs. θ_{kt}, calculated from *in vivo* carbonic anhydrase activity, and the respective regression lines and equations ($p < 0.001$).

II.3.4 Sensitivity analysis

We examined the impact of our assumptions about boundary layer conductance, mesophyll conductance, and the exact location of the CO_2–H_2O isotopic exchange within the leaf ($\delta^{18}O_{ev}$ and $\delta^{18}O_{bw}$) in a sensitivity analysis (Table II.1). The recalculated variables θ, $CO^{18}O$-*Iso*, and $\delta^{18}O_{ev}$ (cf. eqs. II.7, II.13, and II.19) were not significantly sensitive to a 50 % increase or decrease of b_c in any of the plant experiments (Table II.3). However, we found that g_m influenced the calculated θ for all plant experiments. The absolute value of the degree of isotopic CO_2–H_2O equilibrium was approximately 0.2 higher for poplar and maize, when recalculated with the minimum g_m found for the respective species in literature and up to 0.1 lower when recalculated with the species-specific maximum g_m. The strongest effect, however, was observed for spruce and wheat where θ exceeded and was equal to unity, respectively, when recalculated with the minimum g_m found for these species in the literature (Table II.3).

The absolute value of the degree of CO_2–H_2O isotopic equilibrium also increased by 0.05 to 0.08 when recalculated with $\delta^{18}O_{bw}$ instead of $\delta^{18}O_{ev}$, as $\delta^{18}O_{bw}$ was on average about 3 to 4 ‰ lighter than $\delta^{18}O_{ev}$, except for wheat where it was only approximately 1 ‰ lighter (Table II.3). In contrast to θ, any recalculated $CO^{18}O\text{-}Iso_{sim}$ was not significantly different from $CO^{18}O\text{-}Iso_{sim}$ calculated with default settings, as values only differed in the fifth decimal place (Table II.3).

Table II.3 Recalculated values for θ and $CO^{18}O\text{-}Iso$ at midday, averaged over all measured plants (n = 3 ± s.d.), changing either g_m to the minimum/maximum values found for the respective plant species in the literature, or b_c values by -50 % and +50 %, respectively, or replacing $\delta^{18}O_{ev}$ by $\delta^{18}O_{bw}$. First column (0) refers to results for default settings as shown in Table II.1.

		0	**g_m −**	**g_m +**	**b_c −50 %**	**b_c +50 %**	**$\delta^{18}O_{bw}$**
Poplar	θ [-]	0.74 ±0.15	0.97 ±0.20	0.62 ±0.12	0.74 ±0.15	0.74 ±0.15	0.82 ±0.17
	$CO^{18}O\text{-}Iso_{sim}$ [m s^{-1} ‰]	0.019 ±0.003	0.019 ±0.003	0.019 ±0.003	0.019 ±0.003	0.019 ±0.003	0.020 ±0.003
	$\delta^{18}O_{ev}$ [‰]	16.6 ±2.4	16.6 ±2.4	16.6 ±2.4	16.6 ±2.4	16.5 ±2.4	13.0 ±2.2
Maize	θ [-]	0.51 ±0.02	0.71 ±0.05	0.48 ±0.02	0.51 ±0.02	0.51 ±0.02	0.56 ±0.03
	$CO^{18}O\text{-}Iso_{sim}$ [m s^{-1} ‰]	0.020 ±0.002	0.020 ±0.002	0.020 ±0.002	0.020 ±0.002	0.020 ±0.002	0.020 ±0.002
	$\delta^{18}O_{ev}$ [‰]	17.4 ±2.5	17.4 ±2.5	17.4 ±2.5	17.4 ±2.5	17.2 ±2.5	14.0 ±2.0
Spruce	θ [-]	0.53 ±0.05	1.01 ±0.13	0.49 ±0.05	0.53 ±0.05	0.53 ±0.05	0.61 ±0.06
	$CO^{18}O\text{-}Iso_{sim}$ [m s^{-1} ‰]	0.005 ±0.001	0.005 ±0.001	0.005 ±0.001	0.005 ±0.001	0.005 ±0.001	0.005 ±0.001
	$\delta^{18}O_{ev}$ [‰]	12.7 ±3.0	12.7 ±3.0	12.7 ±3.0	12.7 ±3.1	12.6 ±2.9	8.7 ±2.9
Wheat	θ [-]	0.67 ±0.04	1.00 ±0.11	0.51 ±0.02	0.67 ±0.05	0.67 ±0.05	0.72 ±0.06
	$CO^{18}O\text{-}Iso_{sim}$ [m s^{-1} ‰]	0.034 ±0.004	0.034 ±0.004	0.034 ±0.004	0.034 ±0.004	0.034 ±0.004	0.034 ±0.004
	$\delta^{18}O_{ev}$ [‰]	8.7 ±0.8	8.7 ±0.8	8.7 ±0.8	8.8 ±0.8	8.3 ±0.8	7.6 ±0.8

II.4 Discussion

II.4.1 General patterns of the oxygen isotopic exchange in different plant types

The degree of isotopic equilibration between leaf water and CO_2 molecules, which was derived empirically from isotopic gas exchange measurements, was always incomplete and varied between the different plant types (Table II.2). The plant-specific differences in average θ corresponded to the magnitude of leaf *CA* activity (Fig. II.4) in that the latter was higher in poplar and wheat and lower in maize and spruce. This indicated that, as suggested by Gillon and Yakir (2000), CA_{leaf} was a limiting factor for θ in these four plant species. The degree of isotopic CO_2–H_2O equilibration for wheat was only slightly lower than the range reported for monocots (0.77–0.87), whereas values for poplar and spruce were substantially lower than average values reported for deciduous trees (0.99) and conifers (0.97), respectively (Gillon and Yakir, 2001). For maize, the observed θ was also lower than the range reported for this species by other studies (0.7–0.8) (Affek et al., 2006; Gillon and Yakir, 2000; Griffis et al., 2011), but was higher than the average value reported for C_4 grasses (0.38) (Gillon and Yakir, 2001). The lower θ values for C_3 plants and maize might indeed be closer to physiological conditions as suggested by measurements and model simulations for both C_3 and C_4 canopies, where estimates for θ were in part substantially lower than 0.5 (Griffis et al., 2011; Xiao et al., 2010). In contrast to most other studies, where θ was derived from *in vitro CA* activity, in the present study θ was determined empirically by isotopic gas exchange measurements which allowed us to monitor temporal variations in θ. Although the degree of isotopic CO_2–H_2O equilibration which we calculated from *in vitro CA* activity and leaf internal CO_2 concentration (θ_{kt}) was in the same order of magnitude as θ, it failed to represent the actual degree of equilibration inside the plant leaf which was indicated by the low r^2 obtained for the θ vs. θ_{kt} regression. This is presumably because *CA* activity is leaf-site specific and masked by the use of whole-leaf extracts (Cousins et al., 2006).

The average midday *$CO^{18}O$-Iso* was highest in wheat, similar in poplar and maize and lowest in spruce, whereas the average A_r was highest in maize, around a factor of 0.5 lower in poplar and wheat and by a factor of 10 lower in spruce. This demonstrates that the species-specific differences in *$CO^{18}O$-Iso* could not be simply explained by differences in A_r. We could show that the combined daytime variations in θ, g_{s_CO2}, $\delta^{18}O_{ev}$, and A_r accounted for up to 98% of the observed pattern in *$CO^{18}O$-Iso* in poplar, maize, and wheat, confirming the importance of these four variables for the impact of plants on atmospheric $\delta^{18}O$-CO_2. However, for spruce other factors seemed to play a role as well, since here only 86% of the variations in *$CO^{18}O$-Iso* were explained by the interaction between θ, g_{s_CO2}, $\delta^{18}O_{ev}$, and A_r. Sensitivity of *$CO^{18}O$-Iso* to θ, g_{s_CO2}, $\delta^{18}O_{ev}$, and A_r individually was much lower or lacking, except for *$CO^{18}O$-Iso* vs. g_{s_CO2} in wheat and *$CO^{18}O$-Iso* vs. θ in poplar.

Higher sensitivity of $CO^{18}O$ isofluxes to changes in θ in C_3 species compared to C_4 has been reported before by Gillon and Yakir (2000), and has been explained by higher c_c and retro-flux in C_3 than in C_4 plants. This could also explain the lower sensitivity of *$CO^{18}O$-Iso* to θ which we observed for maize. Since the $\delta^{18}O$ of retro-diffusing CO_2 is generally assumed to depend, among others, on leaf water ^{18}O enrichment (Peylin et al., 1999), and since previous studies observed a dependency between canopy $\delta^{18}O$-CO_2 and $\delta^{18}O_{ev}$ (Griffis et al., 2011; Xiao et al., 2010), $\delta^{18}O_{ev}$ was expected to considerably influence *$CO^{18}O$-Iso*. Only in spruce and wheat a clear relationship between *$CO^{18}O$-Iso* and $\delta^{18}O_{ev}$ was observed in that $\delta^{18}O_{ev}$ was negatively correlated with *$CO^{18}O$-Iso*, mainly reflecting the simultaneous reduction of *$CO^{18}O$-Iso* and increase in $\delta^{18}O_{ev}$ under water limitation. However, for poplar and maize the relationship was less pronounced, resulting most likely from the opposing relationship between *$CO^{18}O$-Iso* and $\delta^{18}O_{ev}$ at normal conditions (positive) and under water limitation (negative). The rather low contribution of $\delta^{18}O_{ev}$ to *$CO^{18}O$-Iso* dynamics is consistent with the relatively low θ and low *in vivo CA* activity which we found in our study. Griffis et al. (2011) also found only a weak

correlation of $H_2{}^{18}O$ and $CO^{18}O$ isofluxes at the canopy scale together with a low CO_2 hydration efficiency and emphasized the implications for gross primary productivity (GPP) estimates that are inversely calculated from atmospheric $\delta^{18}O\text{-}CO_2$.

The relationship of $CO^{18}O\text{-}Iso$ vs. A_r was positive during daytime as can be seen from the increasing $CO^{18}O\text{-}Iso$ with increasing A_r. This is not surprising, as the plant chamber $CO^{18}O\text{-}Iso$ is the product of the isotopic discrimination and the assimilation rate. The $CO^{18}O$ isoforcing which was calculated *via* a mechanistic model ($CO^{18}O\text{-}Iso_{sim}$), including θ and $\delta^{18}O_{eql}$, was highly consistent with $CO^{18}O\text{-}Iso$ which was determined from gas exchange measurements. On the one hand, the good fit between $CO^{18}O\text{-}Iso_{sim}$ and $CO^{18}O\text{-}Iso$ proved that the model, which was originally applied at the canopy scale by Lee et al. (2009), was also valid at the single plant scale. On the other hand, it confirmed that $CO^{18}O\text{-}Iso$ could be simply calculated from a mass balance over the plant chamber even without additional measurements of $\delta^{18}O\text{-}H_2O$ which are essential when $CO^{18}O$ isoforcing would be estimated *via* a mechanistic model. Hence, our experiments revealed that plant chamber measurements provide a convenient method to examine $CO^{18}O\text{-}Iso$ for a wide range of plant species in a cost-effective and time-saving way as compared to field measurements.

II.4.2 Sensitivity of the main drivers of $CO^{18}O\text{-}Iso$ to short-term variations in environmental conditions

II.4.2.1 Elevated T_{air}

The ^{18}O enrichment of leaf water at evaporation sites was higher at 35°C in all plant species as compared to 25°C due to the higher *VPD* under these conditions, overcompensating the reduced equilibrium fractionation of $H_2{}^{18}O$ during liquid–vapor phase transition at higher temperature (Bottinga and Craig, 1968; Majoube, 1971). Also θ was enhanced at 35°C in spruce, wheat, and poplar, while it remained stable for maize, indicating that *CA* activity in the C_3 plant species

followed typical enzyme temperature kinetics, with 35°C being still below the critical temperature at which enzyme activity starts to decline again (e.g., 40°C in potato leaves; Demir et al. (2009)). Furthermore, the higher CO_2 concentration inside the chloroplast at high T_{air}, associated with reduced A_r, could explain the increase in θ. Given the higher values for $\delta^{18}O_{ev}$ in all four species and for θ in the C_3 species, an increase in $CO^{18}O\text{-}Iso$ could have been expected at 35°C as compared to 25°C. However, only for maize a 20% increase of $CO^{18}O\text{-}Iso$ was observed, as only in this species g_{s_CO2} did not decrease at elevated T_{air}, allowing an enhanced retro-diffusion of ^{18}O-enriched CO_2 from leaf to air. In contrast, $CO^{18}O\text{-}Iso$ for poplar, wheat, and spruce was reduced at 35°C despite increased values for $\delta^{18}O_{ev}$ and θ, as these were overcompensated by reduced g_{s_CO2} and therefore reduced CO_2 retro-flux at increased air and leaf temperature.

To the authors' knowledge, no experimental studies on the temperature dependence of oxygen isotope fractionation in plants are available at present, as up to now the focus has rather been on the temperature dependence of carbon isotopic discrimination (Evans and Von Caemmerer, 2013) or simulated temperature effects on global $\delta^{18}O\text{-}CO_2$ (Buenning et al., 2014). The results presented in our study suggest that $CO^{18}O\text{-}Iso$ will most likely be reduced when both T_{air} and VPD increase, as most plant species react with reduced g_{s_CO2} to elevated T_{air} beyond 30°C (Wilson, 1948) and equilibrium fractionation is reduced. However, a direct comparison with the sensitivity analysis conducted by Buenning et al. (2014) is difficult because they increased global surface air temperature by only 1 °C without altering atmospheric relative humidity whereas we changed the chamber temperature by 10 °C and did not keep relative humidity constant. Nevertheless, the general trend was similar in that $\delta^{18}O\text{-}CO_2$ decreased with elevated T_{air}. Given widely predicted increasing mean surface temperatures, this will be highly relevant to interpreting the atmospheric $CO^{18}O$ signal in the future.

II.4.2.2 Limited water availability

Since limited water availability generally leads to a reduction of stomatal conductance (Flexas et al., 2004; Reddy et al., 2004), the plant $CO^{18}O$ signal is also likely to be influenced. Furthermore, previous studies found an increase of *CA* protein abundance in poplar and wheat in response to water limitation (Bazargani et al., 2011; Durand et al., 2011), but a decrease in *in vitro CA* enzyme activity for maize (Prakash and Rao, 1996), which could have a considerable impact on the CO_2–H_2O oxygen isotopic exchange under drought conditions. Our experiments demonstrated that towards the end of the water limitation treatment $CO^{18}O\text{-}Iso$ decreased nearly to zero in all four plant species. In contrast, $\delta^{18}O_{ev}$ increased with ongoing drought due to enhanced kinetic fractionation associated with reduced g_s which is consistent with findings from laboratory experiments on *Citrus* and tobacco plants conducted recently by Simonin et al. (2013). However, the ^{18}O-enriched leaf water did not result in higher $CO^{18}O\text{-}Iso$, as θ and especially A_r and g_{s_CO2} declined with decreasing water availability. A mathematical explanation for the decreasing θ values is the proportionally high increase in the theoretical enrichment of CO_2 at full equilibrium between CO_2 and the progressively more enriched leaf water, thereby increasing the denominator for the calculation of θ (eq. II.13). Reduced *in vivo CA* activity due to declining CO_2 substrate under drought conditions provides a mechanistic explanation for decreasing θ. However, *in vitro CA* activity in leaf extracts from drought-stressed plants was not significantly reduced as compared to non-stressed plants (data not shown), as *in vitro CA* activity was always measured at unlimited substrate availability.

II.4.3 Effect of experimental setup and assumptions made on results

The sensitivity analysis showed that assuming a constant boundary layer conductance of 1.5 mol m^{-2} s^{-1} did not affect the major output variables of the isotopic or gas exchange calculations. This is consistent with our expectations as the air inside the plant chamber was kept

homogenous and well-mixed during all experiments by a fan which was mounted at the top of the chamber. Due to technical limitations we could not measure g_m, e.g. *via* combined measurements of gas exchange and chlorophyll fluorescence or ^{13}C isotope discrimination (Pons et al., 2009). Hence, we had to assume a constant value for g_m for each plant species based on findings from literature, even though studies have shown that g_m can vary with environmental conditions and plant traits (Flexas et al., 2012; Oliver et al., 2012; Tazoe et al., 2011). The $CO^{18}O$ isoforcing which was calculated according to the mechanistic model by Lee et al. (2009) was insensitive to the parameterization of g_m and to the choice of either $\delta^{18}O_{ev}$ or $\delta^{18}O_{bw}$, which shows that the isoforcing parameterization by Lee et al. (2009) provides robust estimates for $CO^{18}O\text{-}Iso$ which are independent of the g_m parameterization. The insensitivity of $CO^{18}O\text{-}Iso_{sim}$ to variations in g_m can be explained by an opposing and counterbalancing effect of the g_m parameterization on θ and c_c (eq. II.21). However, the assumptions made about g_m clearly influenced θ, in that a higher g_m reduced the recalculated θ up to 0.1, while a lower g_m increased the recalculated θ up to 0.2. This is consistent when taking into account that θ was determined from gas exchange variables including c_c which was calculated in dependence of g_m. According to this, a decrease of g_m resulted in a reduced c_c and had to be compensated by a higher θ to result in the measured Δ_A. Overall, these findings emphasize that independent measurements of g_m are crucial for obtaining precise estimates of θ from gas exchange measurements.

The degree of isotopic CO_2–H_2O equilibrium was also sensitive to the calculation of the $\delta^{18}O$ of leaf water depending on whether it was calculated for water at the evaporation site or bulk leaf water. However, the sensitivity was less pronounced compared to changes in g_m. Absolute values of recalculated θ using $\delta^{18}O_{bw}$ instead of $\delta^{18}O_{ev}$ were 0.05 to 0.1 higher. This was expectable, as the values for $\delta^{18}O_{bw}$ were 1 and 3 ‰ lower than $\delta^{18}O_{ev}$ in wheat and maize, and 4 ‰ lower in poplar and spruce, respectively, due to the counterflow of enriched water from

the evaporation sites and unenriched water from the xylem known as Péclet effect (Farquhar and Lloyd, 1993). This finally resulted in a decrease in the value of the denominator for the calculation of θ (eq. II.13). For wheat, the impact on θ was not significant due to the relatively small difference between $\delta^{18}O_{bw}$ and $\delta^{18}O_{ev}$. As for g_m, $CO^{18}O\text{-}Iso_{sim}$ was also insensitive to the replacement of $\delta^{18}O_{ev}$ by $\delta^{18}O_{bw}$ because the increase in θ was cancelled out by a decrease in $\delta^{18}O_{eql}$.

Since we conducted our experiments in plant chambers under laboratory conditions, we created some artificial conditions which differed from those expected for the field. The most important deviation from physiological conditions was undoubtedly a higher vapor pressure deficit during nighttime compared with daytime during some of the plant chamber experiments, which occurred when the lack of transpired water vapor during nighttime could not be sufficiently compensated for by increasing the water vapor concentration at the chamber inlet. This was most obvious for the spruce and the wheat experiments. Consequently, under these conditions also the diurnal pattern of $\delta^{18}O_{ev}$ was different than expected for natural conditions, resulting in lower values of $\delta^{18}O_{ev}$ during daytime as compared to nighttime. Since θ is a relative quantity, it should be insensitive to changes in the absolute values of $\delta^{18}O_{ev}$. In contrast to this, absolute values of $CO^{18}O\text{-}Iso$ are expected to be sensitive to changes in absolute values of $\delta^{18}O_{ev}$, as $CO^{18}O\text{-}Iso$ is the product of the net CO_2 flux through the chamber and the $\delta^{18}O\text{-}CO_2$ of this flux, which is determined by the isotopic exchange with leaf water and therefore by $\delta^{18}O_{ev}$. Hence, unnatural *VPD* conditions introduced by the plant chamber setup could partly explain the absence of a clear relationship between $CO^{18}O\text{-}Iso$ and $\delta^{18}O_{ev}$. For future experiments, the use of a vaporization module as described in Simonin et al. (2013) provides a method to generate water vapor with a constant $\delta^{18}O\text{-}H_2O$ at the chamber inlet and to avoid unusual diurnal patterns of $\delta^{18}O_{ev}$.

Transpired leaf water was enriched compared to source water and, therefore, in an isotopic non-steady state during all the experiments (data not shown), which has been found previously also for other plant species (Harwood et al., 1999; Simonin et al., 2013; Wang and Yakir, 1995). Isotopic NSS was likely caused by the variable $\delta^{18}O$ of water vapor at the inlet of the chamber, which originated from the method of producing distinct water vapor concentrations by evaporation of water from a reservoir at distinct (variable) temperatures of a water bath. The changes in temperature caused changes in equilibrium fractionation during the generation of water vapor. In addition, the residual water reservoir for the water vapor production became gradually enriched in ^{18}O, resulting in a non-constant $\delta^{18}O\text{-}H_2O_{in}$ and leading to isotopic NSS. This is consistent with findings reported by Simonin et al. (2013), where variations in background water vapor isotopic signature also influenced isotopic steady state. Another explanation for isotopic NSS of leaf water during our experiments could be a high leaf water residence time, which we could not verify, though, since we did not measure leaf water content. Although the origin of isotopic NSS was most likely related to the setup in this study, the occurrence of isotopic NSS is realistic under field conditions where plants are exposed to even more variable environmental conditions.

We conducted our experiments in a glass chamber rather than leaf cuvettes. Consequently, (isotopic) gas exchange measurements included also parts of the stem and branches of poplar and spruce trees, and we cannot exclude that the respiratory flux from these parts influenced the $\delta^{18}O\text{-}CO_2$ inside the chamber. However, the contribution of respiration from wood components (R_w), especially in young trees (< 4 years) is rather small (Khomik et al., 2010; Vose and Ryan, 2002) and expected to be even smaller during daytime and under water stress due to the positive relationship between R_w and stem turgor pressure (Saveyn et al., 2007).

II.5 Conclusions

The large uncertainties in the simulation of global $\delta^{18}O\text{-}CO_2$ and inversely calculated biosphere–atmosphere gross CO_2 fluxes are associated with uncertainties in leaf oxygen isotope exchange between CO_2 and H_2O, in particular with the degree of isotopic CO_2–H_2O equilibrium and with isotopic non-steady state of leaf water ^{18}O enrichment. In this study, we show that θ, g_{s_CO2}, A_r and $\delta^{18}O_{ev}$ together accounted for up to 98 % of the variations in $CO^{18}O$ isoforcing in poplar, wheat and maize, and for at least 86 % in spruce. The degree of oxygen isotope exchange between CO_2 and leaf water, θ, was significantly below unity in all four measured plant species and varied over time in response to environmental conditions. Together with earlier findings from canopy-scale studies, our results suggest that θ could be significantly lower than previously reported especially for C_3 plants. Former estimates of θ were often determined from *in vitro CA* activity, which might have led to wrong estimates of *in vivo* θ. Based on our findings we do not recommend to derive θ from *in vitro CA* activity but rather from gas exchange measurements which, in addition, allow for monitoring temporal variations in θ. However, these measurements should be accompanied by measurements of g_m to obtain precise estimates of θ, as θ calculated by this method was highly sensitive to g_m. Assuming our estimates for g_m were realistic and θ is in fact lower than previously anticipated, a lower θ would have to be compensated for by an increase of leaf water $\delta^{18}O$ or an increase in GPP with regard to the global atmospheric $\delta^{18}O\text{-}CO_2$ budget. The latter is in agreement with a previous study of Welp et al. (2011) where, based on correlations between $\delta^{18}O_a$ and precipitation $\delta^{18}O$, the GPP was found to be about 50 Pg of carbon per year higher than the current estimates.

Furthermore, we found that, due to low θ, $CO^{18}O\text{-}Iso$ was not necessarily coupled to $\delta^{18}O_{ev}$, which varied diurnally in all plant species. The experiments related to limited water availability demonstrated that reduced stomatal conductance and CO_2 flux together with reduced θ might lead to substantially reduced $CO^{18}O\text{-}Iso$ of plants under mild water stress, while at the same

time $\delta^{18}O_{ev}$ becomes more ^{18}O-enriched. Especially the effect of stomatal conductance on $CO^{18}O\text{-}Iso$ could become increasingly relevant in a future climate as rising atmospheric CO_2 concentrations are supposed to lead to a general reduction in g_s (Ainsworth and Rogers, 2007) and, therefore, will further decrease $CO^{18}O\text{-}Iso$. Finally, our experiments demonstrated that the $CO^{18}O$ isoforcing of different plant species can be determined efficiently by combining gas exchange and isotopic measurements with mass balance calculations, making the calculation of $CO^{18}O$ isoforcing with mechanistic models, as for example presented by Lee et al. (2009), dispensable.

III. A new method for quasi-simultaneous measurements of $\delta^{18}O$ of soil water and CO_2 with high time resolution

Modified on the basis of

Laura Gangi, Youri Rothfuss, Jerôme Ogée, Lisa Wingate, Harry Vereecken, Nicolas Brüggemann

manuscript accepted for publication in Vadose Zone Journal

III.1 Introduction

The oxygen isotope ratio ($^{18}O/^{16}O$) of CO_2 enables partitioning of soil respiration and plant assimilation, as CO_2 attains a distinct $\delta^{18}O$ composition ($\delta^{18}O$) during equilibration with isotopically different soil and leaf water pools during soil respiration and leaf photosynthesis, respectively (Yakir, 2003). The equilibration process between CO_2 and soil water is determined by the residence time of soil CO_2, which itself is influenced by soil water content (*SWC*) and temperature (Amundson et al., 1998; Cernusak et al., 2004), and the effective equilibrium reaction rate constant (k_e). Stern et al. (1999) showed that oxygen isotope ratio of soil CO_2 ($\delta^{18}O_{sc}$) was highly sensitive to k_e, and they suggested that k_e in unsaturated soils might be much smaller than the rate constant in pure water due to the additional contribution of physical processes, such as transport of CO_2 across the water/air interface. On the other hand, there has been evidence that k_e could be much higher than the uncatalyzed rate constant of the oxygen isotope exchange because of the catalytic activity of the enzyme carbonic anhydrase (*CA*). Wingate et al. (2009) and Seibt et al. (2006b) showed that modeled and observed $\delta^{18}O$-CO_2 of the soil CO_2 efflux ($\delta^{18}O_s$) could only be matched by consideration of *CA* activity.

The $\delta^{18}O$ of the soil CO_2 efflux is influenced by several parameters: the $\delta^{18}O$ of liquid soil water ($\delta^{18}O_{sw}$), the CO_2–H_2O equilibration rate, kinetic effects, and CO_2 invasion from the atmosphere into the soil (Miller et al., 1999; Tans, 1998). The magnitude of the CO_2 invasion flux depends on the concentration of atmospheric CO_2, k_e, and also on soil properties, e.g., water content, porosity, tortuosity and diffusivity (Stern et al., 2001). Wingate et al. (2009) demonstrated that taking into account the effect of *CA* activity in soils significantly increases the relevance of CO_2 invasion for the global ^{18}O budget of atmospheric CO_2 ($\delta^{18}O_a$) and highlights the need to consider one-way (gross) fluxes rather than net fluxes for constraining the influence of soils on $\delta^{18}O_a$. For instance, soils with low respiration activity and a net efflux = 0 μmol m^{-2} s^{-1} still

influence $\delta^{18}O_a$ to a large extent *via* the interaction of abiotic gross (atmospheric invasion and back-diffusion) fluxes of $CO^{18}O$ exchanging with water pools.

Since $\delta^{18}O_{sw}$ is imprinted on soil CO_2 in a temperature-dependent equilibrium reaction, using wrong or bulk estimates of $\delta^{18}O_{sw}$ can introduce considerable uncertainties in the modeling of $\delta^{18}O_{sc}$ (Riley, 2005). However, experimental data on $\delta^{18}O_{sw}$ variations within the soil profile at high temporal resolution, and in particular at the location of the evaporation front, are scarce (Barnes and Allison, 1988; Lai et al., 2006; Yepez et al., 2005), as most studies rely on laborious destructive sampling or model simulations. Furthermore, our understanding of how soil *CA* activity affects the $\delta^{18}O$ of the CO_2 soil efflux remains thin (Wingate et al., 2009), despite the evident importance of *CA* for CO_2–H_2O isotopic exchange. Previous studies on soil H_2O and CO_2 isotopic exchange were rather theoretical and model-based (Riley, 2005; Stern et al., 1999; Stern et al., 2001; Tans, 1998), and experimental data of soil H_2O and CO_2 isotopic exchange at changing *SWC* are scarce (Hesterberg and Siegenthaler, 1991; Miller et al., 1999). Continuous and simultaneous monitoring of $\delta^{18}O_{sw}$ and $\delta^{18}O_{sc}$, that would be the prerequisite for validation and improvements of models simulating soil–atmosphere exchange of $CO^{18}O$, are non-existent at present.

The aim of the present study was to quantify the ^{18}O-exchange between soil water and CO_2 by *on-line* determination of $\delta^{18}O_{sw}$ and $\delta^{18}O_{sc}$ with high time-resolution. For this purpose we developed a new method for simultaneous determination of $\delta^{18}O_{sw}$ and $\delta^{18}O_{sc}$ in soil profiles based on isotope-specific infrared laser spectroscopy and gas-permeable microporous polypropylene tubing installed at different depths in a sand column. Using this setup we measured the oxygen isotope exchange within a sand column over nine days at relatively low soil water content (experiment 1, dry column), after irrigation of the sand column (experiment 2, irrigation) and after irrigation of the sand column with addition of *CA* (experiment 3, irrigation+*CA*). The measurements were confronted with simulations based on the soil sub-

module of the process-based biosphere–atmosphere gas exchange model MuSICA (Ogee et al., 2003a). Within this framework we tested whether spatiotemporal variations in $\delta^{18}O_{sw}$ and $\delta^{18}O_{sc}$ could be reliably monitored with this novel methodology and reproduced by the model. We also investigated whether the $\delta^{18}O_{sc}$ signal over the soil profile was influenced by variations in $\delta^{18}O_{sw}$, $\delta^{18}O_a$, and *SWC*, and if the degree of isotopic CO_2−H_2O equilibrium in the sand column increased after *CA* addition and could be reproduced with a higher k_e parameterization in the model.

III.2 Materials and Methods

III.2.1 Experimental setup

Measurements were conducted in the laboratory using a custom-built PVC sand column (volume: 133 L, inner diameter: 0.5 m, height: 0.7 m). The column was coated with insulation material (Armaflex 25 mm, Armacell GmbH, Münster, Germany). The bottom of the column was sealed with a perforated PTFE plate (hole diameter: 2 mm; thickness: 8 mm), which was covered by a polyamide membrane filter (pore diameter 0.45µm, Ecotech, Bonn, Germany). Below the perforated plate, the column had a single outlet that could be used to saturate the column from the bottom to the top with deionized tap water or to actively drain the column using a diaphragm vacuum pump (Laboport N820.3FTP, KNF Neuberger, Freiburg, Germany). The column had three different connection ports at each of six different depths (–1 cm, –3 cm, –7 cm, –15 cm, –30 cm, –55 cm; distance from the surface of the column, Fig. III.1 a), where the synthetic dry air inlet and outlet as well as a sensor for volumetric water content (*SWC*, in $m^3\ m^{-3}$, precision: 0.03 $m^3\ m^{-3}$) and soil temperature (T_s, in °C, precision: 0.5 °C) (Sceme Spade, Sceme.de GmbH, Horn-Bad Meinberg, Germany) were connected.

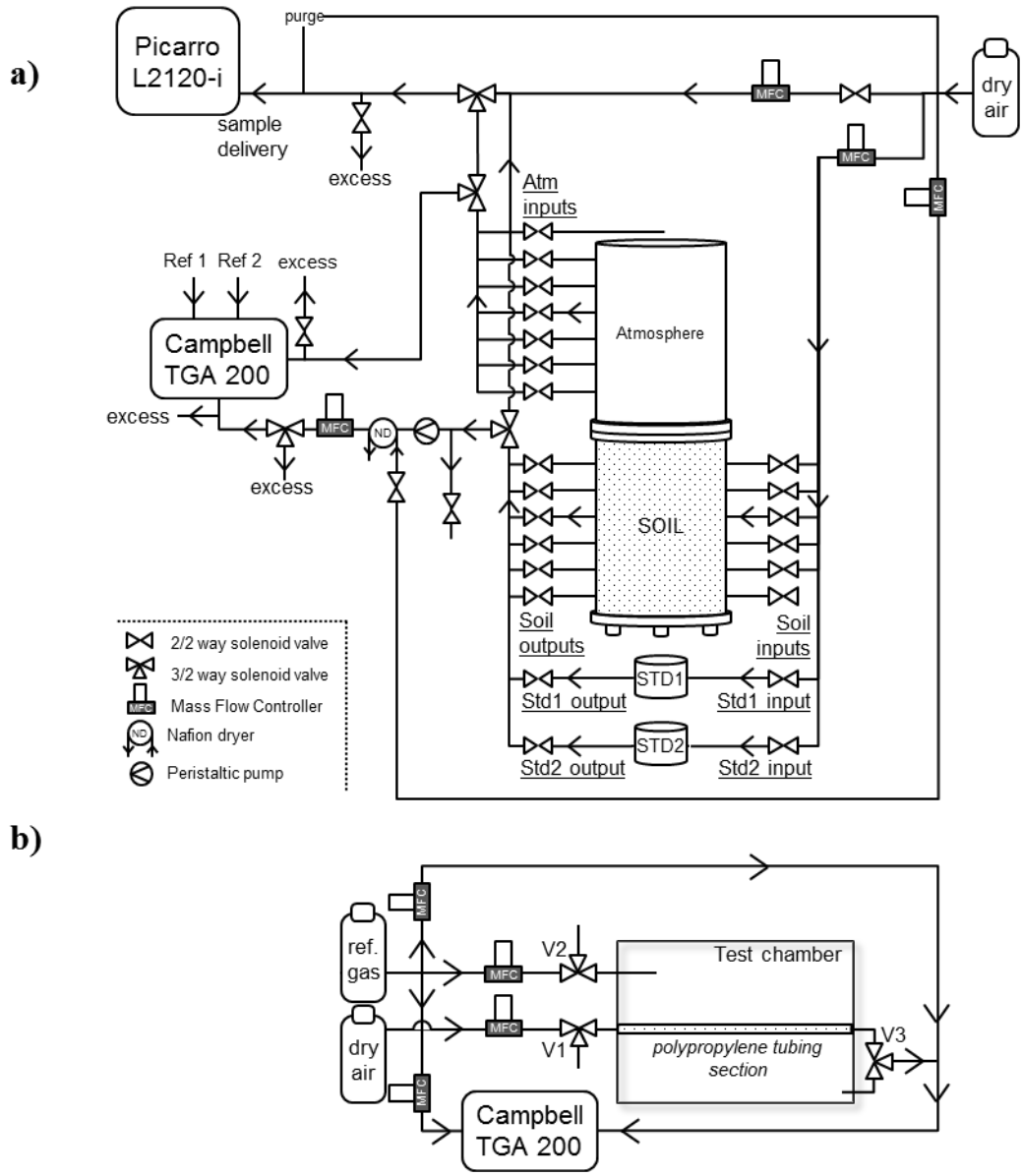

Figure III.1 Measurement setup for experiments 1 to 3 (a) and preliminary tests (b).

We used ¼" polyethylene–aluminum composite tubing (Synflex 1300, Eaton Electric GmbH, Bonn, Germany) for gas lines outside of the column. The column was filled with medium, inorganic sand ('FH31', Quarzwerke Frechen GmbH, Frechen, Germany). For detailed information on this sand see Stingaciu et al. (2009). A 2 m long piece of gas-permeable polypropylene tubing (Accurel® PP V8/2HF, Membrana GmbH, Germany; 0.2 µm porosity, 0.155 cm wall thickness, 0.55 cm i.d., 0.86 cm o.d.), coiled up to form a loose spiral, was

installed horizontally at each depth. The properties of this tubing and its suitability for soil trace gas analysis, $\delta^{13}C\text{-}CO_2$, and $\delta^{18}O_{sw}$ measurements have been described previously (Gut et al., 1998; Parent et al., 2013; Rothfuss et al., 2013).

III.2.2 Isotopic measurements

Prior to measurements of $\delta^{18}O_{sc}$ and soil water vapor isotopic signature ($\delta^{18}O_{sv}$) at a given depth in the soil profile, the two 2-way magnetic valves (MV 1326 G, Riegler und Co. KG, Bad Urach, Germany) located at both inlet and outlet of the sand column were kept in a closed position. The $\delta^{18}O_{sc}$ and $\delta^{18}O_{sv}$ were then analyzed at each available depth in the following manner: i) the magnetic valves were activated by an automated switching unit based on a relay system (ICP DAS I-7061, Omtec GmbH, Varel, Germany) and a custom-made software on Labview® (National Instruments, Austin, Texas, USA) basis; ii) synthetic dry air (20.5 % O_2 in N_2, with approx. 20–30 ppmv water vapor, Air Liquide, Germany) was run into the microporous tubing (at a flow rate of 85 mL min^{-1} set by a mass flow controller – MFC; GF40, Brooks Instrument, Hatfield, USA) for exactly 34 min; iii) the sand column outlet air was directed during the first 4 min to a tunable diode laser absorption spectrometer (TDLAS, TGA 200, Campbell Scientific, Inc., Logan, UT, USA) for determination of CO_2 mixing ratios and $\delta^{18}O_{sc}$, and the last 30 min to a wavelength-scanned cavity ring-down spectrometer (WS-CRDS, L2120-*i*, Picarro, Inc., Santa Clara, CA, USA) for water vapor mixing ratios and $\delta^{18}O_{sw}$ measurements. The low flow rate minimized disturbance of the sand and allowed for equilibration of the air inside the tubing with the surrounding air.

To account for air flow across the microporous tubing caused by the pressure gradient between tubing and air-filled sand pore space, and to ensure a constant flow of 85 mL min^{-1}, a peristaltic pump (Minipuls 3 Abimed, Gilson, Villiers-le-Bel, France) was installed downstream of the outlet prior to a second MFC, which was also adjusted to 85 mL min^{-1}. This MFC was protected

from moist air using a Nafion dryer (MD-050-24-F-2, Perma Pure, Toms River, NJ, USA) purged with a counter flow of 200 mL min^{-1} dry synthetic air. To keep the water vapor mixing ratio between 10,000 and 17,000 ppmv, that had proven to be the ideal measurement range of the particular water isotope analyzer used in this experiment, the air flow was diluted with synthetic dry air before entering the water isotope analyzer. The oxygen isotopic signature of CO_2 was measured three times per day at each depth. Since measurement times for $\delta^{18}O_{sv}$ lasted much longer than for $\delta^{18}O_{sc}$ because of the much slower stabilization of isotope values in the water isotope analyzer, $\delta^{18}O_{sv}$ was measured only once a day at each depth to minimize the inevitable removal of CO_2 from the sand column with the synthetic air stream through the gas-permeable tubing during water isotope measurements. Another PVC column, that had the same dimensions as the sand column and that was open at the top to allow exchange with ambient air, was installed above the sand column. Air from above the sand column was sampled at heights +1 cm, +3 cm, +7 cm, +15 cm, +30 cm, +55 cm (within the air-filled PVC column) and +100 cm above the surface (free laboratory air). Each height was sampled five times per day for 12 min at approximately 35 mL min^{-1} and for 6 min at 550 mL min^{-1} by the WS-CRDS and TDLAS, respectively, to measure H_2O and CO_2 mixing ratios as well as $\delta^{18}O_{av}$ and $\delta^{18}O_a$. Air relative humidity (*rh*) and temperature (T_a) were monitored at 100 cm above the sand surface with a combined *rh* and T_a sensor (RFT-2 UMS GmbH, Munich, Germany).

Isotopic compositions are reported on the international "delta" scale:

$$\delta_{sample} = (R_{sample}/R_{standard} - 1) \quad \text{(III.1)}$$

where R_{sample} and $R_{standard}$ are the ratios of heavy to light isotope in sample and standard (i.e., Vienna Standard Mean Ocean Water (VSMOW) for H_2O and Vienna Pee Dee Belemnite (VPDB-CO_2) for CO_2, respectively.

III.2.2.1 H_2O

In order to account for the adaptation time of the WS-CRDS analyzer to the different mixing ratio levels and isotopic signature values observed at the different available depths, only the last minute (= 32 single data points) of the 30-min measurement period was kept to compute $\delta^{18}O_{sv}$ values.

The isotopic signature of liquid water ($\delta^{18}O_{sw}$) in the sand was calculated from $\delta^{18}O_{sv}$ using a temperature-dependent empirical equation established by Rothfuss et al. (2013), that showed soil water around the gas-permeable tubing was in isotopic equilibrium with soil water vapor inside the tubing:

$$\delta^{18}O_{sw} = A - B \cdot T_s + C \cdot \delta^{18}O_{sv} \quad \text{(III.2)}$$

where $\delta^{18}O_{sw}$ and $\delta^{18}O_{sv}$ are expressed in permil, T_s (K) represents the soil temperature and A, B, C are constants equal to 33.17 ‰, –0.0795 ‰ K^{-1}, and 1.0012, respectively.

Equation (III.2) accounts for the specific conditions by which soil water vapor was sampled from the soil using our specific methodology, i.e., vapor removal occurred at thermodynamic equilibrium and was, as reported by Gat et al. (1991), comparable to the "Nernst-Bertholet" distribution of trace elements between mineral phases. Equation (III.2) accounts as well for the properties of the permeable polypropylene tubing and its impact on the transport of soil water vapor into its vicinity prior to sampling. Equation (III.2) gives similar, yet significantly different results as compared with the formulations of e.g. Majoube (1971), and Horita and Wesolowski (1994).

Water isotopic analyzer readings were drift-corrected using two different water standards (Std 1 and Std 2), that were measured for 30 min each five times per day. Standard water vapor was

generated by flushing a 1 m long piece of gas-permeable tubing, which was installed in airtight acrylic glass cylinders (diameter: 12.2 cm, height: 22 cm; for details see Rothfuss et al. (2013)) filled with medium sand (FH31) and saturated with water of known isotopic composition ($\delta^{18}O$ vs. VSMOW: –8.20 ‰ ± 0.10 ‰ for Std 1, and +8.15 ‰ ± 0.10 ‰ for Std 2, respectively; calibrated against the primary standards VSMOW, SLAP and GISP). The standards were placed in a temperature-controlled water bath at 18°C to ensure water vapor formation at constant temperature. To measure the isotopic composition of source water used to saturate the sand column, liquid water samples were injected into the vaporizer of the WS-CRDS using an autosampler (HTC-PAL, CTC Analytics, Zwingen, Switzerland). Each sample was measured at least six times consecutively, with the first two measurements being omitted to avoid memory effects. Precision and accuracy of $\delta^{18}O\text{-}H_2O$ measurements were smaller than 0.1 ‰.

III. 2.2.2 CO_2

To compensate for instrument drift and to calibrate CO_2 isotopic measurements using TDLAS, two reference gases (450 and 1000 ppmv CO_2 in synthetic air; Air Liquide, Düsseldorf, Germany, and Linde AG, Pullach, Germany; $\delta^{18}O\text{-}CO_2$ vs. VPDB-CO_2: –24.67 to –24.47 ± 0.20 ‰, and –7.59 to –5.11 ± 0.20 ‰, respectively) were measured for 30 s each in every measurement cycle. A datalogger (CR3000, Campbell Scientific, Inc.) was used to control the CO_2 measurement cycle, that was 6 min in total, including 30 s for each reference gas, 4 min for the sand column profile, and 1 min for CO_2 analysis of the atmospheric profile. The actual isotope ratios of the reference gases were measured with an isotope ratio mass spectrometer (IsoPrime100, Isoprime Ltd., Cheadle Hulme, UK). The precision of TDLAS measurements was 0.1 ‰ and was determined by the Allan Variance (Sturm et al., 2012; Werle, 2011) for an integration time of 10 s. To avoid high flow rates (~500 mL min^{-1}), that are normally required for measurements with the TDLAS, the sampled air from the sand column was connected to a

void reference gas inlet port of the sampling manifold where the sample flow could be adjusted to 50 mL min^{-1}.

The oxygen isotopic composition of soil CO_2 at full equilibrium with soil water ($\delta^{18}O_{eqs}$) was calculated according to Brenninkmeijer et al. (1983) (eq. III.3) and afterwards converted to the VPDB-CO_2 scale:

$$\delta^{18}O_{eqs} = \delta^{18}O_{sw} + 17.604/T_s - 0.01793 \quad \text{(III.3)}$$

where T_s represents the soil temperature.

III.2.3 Preliminary tests

The suitability of gas-permeable polypropylene tubing for $\delta^{18}O\text{-}H_2O$ and $\delta^{13}C\text{-}CO_2$ measurements in porous media has been shown in prior studies (Parent et al., 2013; Rothfuss et al., 2013). To test for potential fractionation against $CO^{18}O$, a closed polyacrylic test chamber (length: 0.84 m, width: 0.23 m, height: 0.48 m) was flushed continuously at 2 L min^{-1} with CO_2 reference gas to obtain a stable mixing ratio inside the chamber (Fig. III.1 b). The experiment was performed separately with two different CO_2 reference gases (1000.1 ± 1.0 ppmv CO_2 in synthetic air, $\delta^{18}O\text{-}CO_2$ vs. VPDB-CO_2 = –5.15 ± 0.19 ‰; and 386.4 ± 0.1 ppmv CO_2 in synthetic air, $\delta^{18}O\text{-}CO_2$ = –23.10 ± 0.27 ‰). A 2 m long piece of gas-permeable tubing was installed in the chamber, connected *via* an inlet and outlet port, operated with three-way magnetic valves (V1 and V3, respectively) and flushed with 75 mL min^{-1} of either dry or moist synthetic air. To supply the TDLAS with the required flow rate (~500 mL min^{-1}), the reference gas, that was used to flush the chamber at a rate of 700 mL min^{-1} (valve V2), was added to the air stream at the outlet of the chamber/gas-permeable tubing (valve V3) before measurement. The air composition at the outlet of the chamber and at the outlet of the gas-permeable tubing

was measured alternately for 30 s each over 4 hrs. In a first test, the reference gas was supplied dry, while in a second test it was passed through a dew point generator (LI-610, LI-COR, Lincoln, NE, USA) at 75 mL min^{-1} and 15 °C dew point temperature before entering the chamber to test whether moist conditions influence the sampling *via* the gas-permeable tubing. To test potential fractionation effects by the Nafion dryer used for drying the sample air from the outlets of the sand column, a CO_2 reference gas, that was passed first through a dew point generator at 75 mL min^{-1} and 20 °C and then through the Nafion dryer (counterflow 200 mL min^{-1} dry synthetic air), was compared with CO_2 reference gas that had not passed through the Nafion dryer.

III.2.4 Experiments

The sand column was saturated with deionized tap water ($\delta^{18}O$ = –8.08 ± 0.10 ‰) from the bottom upward *via* the connection port at the bottom side. As the column was open on top, the column dried out because of evaporation from the sand surface. In addition, liquid water could be withdrawn from the column by applying suction at the bottom *via* a diaphragm vacuum pump (Laboport N820.3FTP, KNF Neuberger, Germany). In a first experiment (dry column), we measured the oxygen isotope exchange in the sand column at $SWC < 0.1$. In a second experiment (irrigation), a precipitation event was simulated to test the ability of the new methodology to reliably monitor temporal dynamics in $\delta^{18}O_{sw}$ and $\delta^{18}O_{sc}$. For this, the sand column was watered from the top with 1.7 L of deionized tap water (corresponding to a precipitation amount of 8.7 mm) using a commercially available drip irrigation system (length: 12 m; Micro-Drip-System, Gardena, Ulm, Germany). The irrigation procedure lasted approx. 20 min. Finally, the oxygen isotope exchange was measured over the following 8 days. In a third experiment (irrigation+*CA*), we tested the effect of carbonic anhydrase on $\delta^{18}O_{sc}$ and isotopic CO_2–H_2O equilibrium. For this, 200 mg of enzyme (C3934 Carbonic Anhydrase,

Sigma Aldrich Chemie GmbH, Steinheim, Germany) were dissolved in 1.7 L of deionized tap water at room temperature (concentration of 0.12 mg mL^{-1}) and applied *via* the irrigation system to the soil. Note that the precipitation amount was the same as for experiment 2 (8.7 mm) and was chosen to confine the *CA* activity mostly to the top 15 cm of the soil column. This was supposed to resemble natural conditions because *CA* activity in natural soils and its effect on $\delta^{18}O_{sc}$ are often observed in the near-surface soil layers (Seibt et al., 2006b; Wingate et al., 2008).

III.2.5 Simulation of $\delta^{18}O_{sw}$ and $\delta^{18}O_{sc}$

The soil sub-module of the biophysical soil-vegetation-atmosphere model MuSICA (Ogee et al., 2003a) was used to simulate *SWC*, T_s, $\delta^{18}O_{sw}$ and $\delta^{18}O_{sc}$ at the different depths of the sand column. MuSICA is a multilayer–multileaf model, that was originally developed and validated for simulations of the exchange of energy, water and CO_2 in a coniferous forest (Ogee et al., 2003a), but has since been extended to reproduce $\delta^{18}O\text{-}CO_2$ and $\delta^{18}O\text{-}H_2O$ profiles at the canopy scale (Ogee et al., 2003b; Ogee et al., 2004). For this study, a reduced version of MuSICA, consisting solely of its soil compartment, was used. The model solves for the coupled heat and mass transfer inside the soil column in a very similar fashion as in Braud et al. (1995) or Saito et al. (2007), but following Patankar (1980) for the numerical scheme. The maximum soil depth was set to 0.6 m and the total number of soil layers to 80, with an increased spatial resolution at the soil surface. The model was forced with hourly data of air temperature (T_a), relative humidity (*rh*), CO_2 mixing ratio, $\delta^{18}O\text{-}CO_2$, and $\delta^{18}O$ of water vapor, that were measured at 1 m above the sand surface, and with atmospheric pressure at daily resolution from the meteorological station of the German Meteorological Service (Deutscher Wetterdienst, Offenbach, Germany) at Aachen-Orsbach, located about 30 km south-west of the laboratory. Global incoming radiation (R_g) and wind speed, that were further forcing variables, were

assumed constant at 1 W m^{-2} and 0.5 m s^{-1}, respectively, because of the sheltered conditions inside the PVC column. The bottom boundary water and heat fluxes were set to zero, as the column was closed at the bottom and well insulated, while soil water retention and conductivity curves were modeled according to the Van Genuchten-Mualem formulation (Van Genuchten, 1980). Output data was produced at an hourly time step (Table III.1). Soil parameters for the specific sand type were taken from Stingaciu et al. (2009; 2010) and were assumed homogeneous over the whole sand column (Table III.1). The isotope-related parameter file includes a soil *CA* activity factor (f_{CA}), that is commonly used to account for an increased reaction rate constant for the oxygen isotope exchange reaction caused by *CA* activity in soils, where f_{CA} = 1 means no *CA* activity. Here, f_{CA} was used to adapt the effective reaction rate constant of the isotopic CO_2–H_2O equilibrium reaction ($k_e = f_{CA} \cdot k_s$) and match simulated and measured $\delta^{18}O_{sc}$. The uncatalyzed temperature-dependent reaction rate constant (k_s) for the oxygen isotope exchange is firmly implemented in the model and corresponds to one third of the hydration rate constant (Skirrow, 1975), i.e., k_s = 0.012 s^{-1} at 25 °C.

Table III.1 Soil parameters used for simulations with the MuSICA soil sub-module where α and N are the shape parameters of the water retention curve, K_{sat} is the soil saturated hydraulic conductivity, M is the particle size distribution curve parameter, SWC_{sat} and SWC_{res} are the saturation and residual soil water content, respectively, R_{25} is the soil respiration rate at 25 °C, κ is the tortuosity factor, and f_{CA} represents the soil *CA* activity factor.

Parameter	**Value**
α [cm^{-1}]	0.033
K_{sat} [m d^{-1}]	45.0
M	0.5
N	5.4
SWC_{sat} [m^3 m^{-3}]	0.34
SWC_{res} [m^3 m^{-3}]	0.02
R_{25} [µmol m^{-2} s^{-1}]	0
κ [-]	0.67
f_{CA} [-]	0.01, 0.1, 1, 10

III.3 Results

III.3.1 Testing fractionation effects of gas-permeable tubing and Nafion dryer

Potential isotopic fractionation by the microporous polypropylene tubing was tested for dry and moist air with different CO_2 mixing ratios and $\delta^{18}O$ values, spanning the range of measured values. No significant differences in CO_2 mixing ratio and $\delta^{18}O$ between chamber air and air sampled *via* gas-permeable tubing were observed in dry and in moist air (Table III.2). The reference gas measured with (609.4 ± 4.6 ppmv, 5.47 ± 0.37 ‰) and without (610.1 ± 0.5 ppmv, 5.35 ± 0.07 ‰) the Nafion dryer was not significantly different in terms of mixing ratio or $\delta^{18}O$-CO_2, and confirmed the absence of $CO^{18}O$ isotope fractionation.

Table III.2 Comparison of average CO_2 mixing ratio and $\delta^{18}O$ measured (± standard deviation) at the outlet of test chamber and polypropylene tubing, respectively (all p-values > 0.05).

	CO_2 mixing ratio [ppmv]		***$\delta^{18}O$-CO_2* [‰ vs. VPDB-CO_2]**	
	chamber outlet	*PP tubing*	*chamber outlet*	*PP tubing*
Dry air	964.6 ± 1.1	964.9 ± 1.1	–5.26 ± 0.07	–5.28 ± 0.08
	384.7 ± 1.1	384.8 ± 1.1	–23.06 ± 0.24	–23.06 ± 0.30
Humidified air	1000.1 ± 0.4	1000.1 ± 0.6	–5.15 ± 0.09	–5.15 ± 0.09

III.3.2 Measured sand column profiles of $\delta^{18}O_{sw}$ and $\delta^{18}O_{sc}$ at soil water content < 0.1 (experiment 1, dry column)

During the 9 days of the first experiment, the column was open at the top to allow evaporation. Soil water content decreased slightly at all depths, except at the bottom of the column (–55 cm, Fig. III.2 e). Temperature was relatively stable at the different column depths within a range of approximately 0.5 °C, although the diurnal amplitude at –1 cm was approximately 1 °C higher (Fig. III.2 f). Values of $\delta^{18}O_{av}$ were similar at all heights in the air column and varied within and between individual days, with slightly higher values during daytime than at nighttime (Fig. III.2 c). Measured $\delta^{18}O_{sw}$ was equal to –7.54 ± 0.16 ‰ at the bottom of the column (–55 cm), i.e., about 0.5 ‰ higher than that of the deionized tap water used to saturate the sand (Fig. III.2 g), whereas it was slightly higher at –30 cm (i.e., –6.25 ±0.22 ‰), and highest at –7 cm (i.e., ranging from 4.76 ‰ to 8.41 ‰). The $\delta^{18}O_{sw}$ observed at the two topmost layers (–3 and –1 cm) was lower than that measured at –7 cm, with values around 4.42 ± 0.63 ‰ (–3 cm) and –3.38 ± 0.82 ‰ (–1 cm). While $\delta^{18}O_{sw}$ remained constant at the bottom of the column over the duration of the experiment, it varied much more at –1 cm (0.82 ‰ standard deviation), where the atmospheric influence was the strongest. During the experiment, the maximum value of $\delta^{18}O_{sw}$, observed at –7 cm, increased from approx. +5 ‰ to +8 ‰.

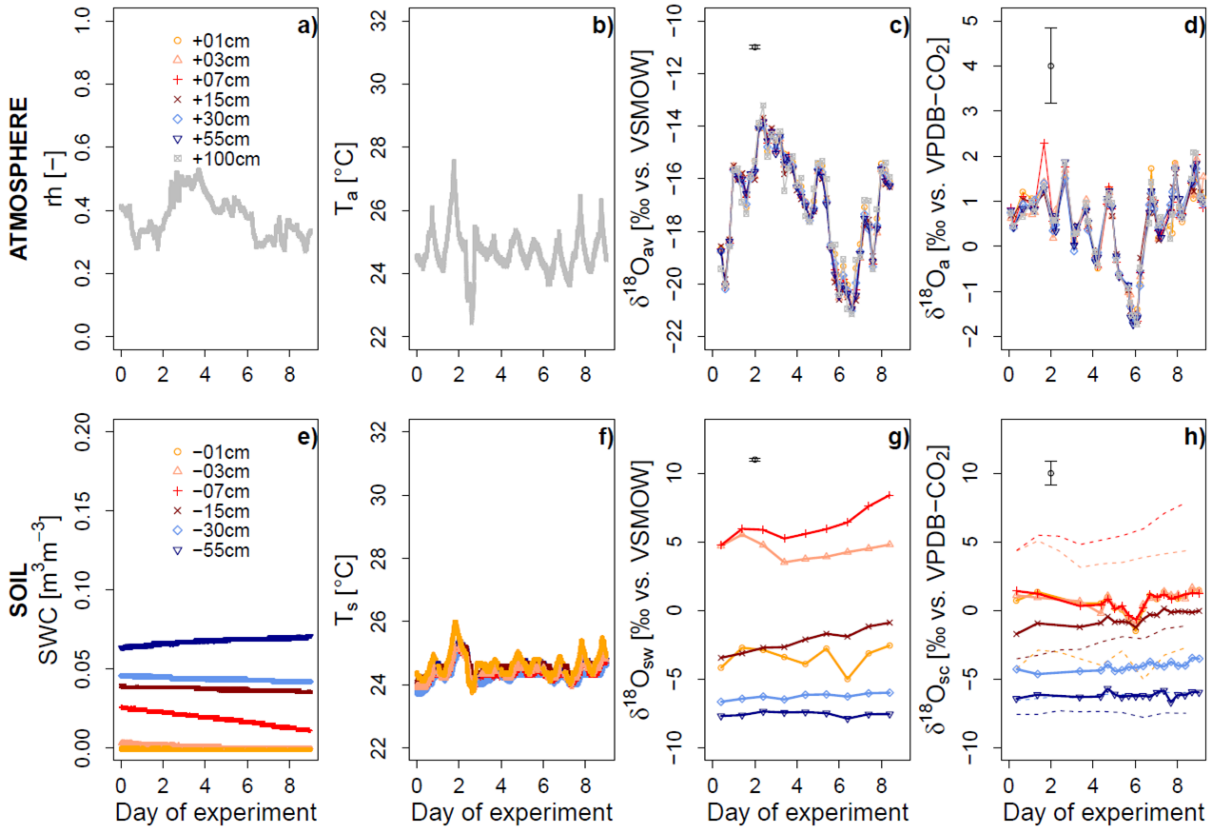

Figure III.2 Experiment 1, dry column: Relative humidity (a), air temperature (b), oxygen isotope signatures ($\delta^{18}O$) of water vapor (c) and CO_2 (d) in the atmosphere column, volumetric water content (e), temperature (f), $\delta^{18}O$ of liquid water (g) and CO_2 (h, dashed lines show values for $\delta^{18}O_{eqs}$ in the respective depths) in the sand column. The single data point with error bar represents average standard deviation over the experimental period.

The $\delta^{18}O_{sc}$ profile resembled the $\delta^{18}O_{sw}$ profile as CO_2 became increasingly ^{18}O-enriched from the bottom to the top of the column (Fig. III.2 h). Measured $\delta^{18}O_{sc}$ at –1, –3, and –7 cm was more variable in time than at greater depths and, although dampened, resembled the temporal dynamics of $\delta^{18}O_a$ with up to 1 ‰ higher values during daytime compared to nighttime. It even followed the strong $\delta^{18}O_a$ depletion at day 6 of the experiment (Fig. III.2 d and h). In contrast, $\delta^{18}O_{sc}$ at –15, –30 and –55 cm was less variable in time, and the diurnal pattern as observed for the upper sand layers was less pronounced or absent (Fig. III.2 h). Absolute $\delta^{18}O_{sc}$ values at these depths were about 1 to 2.5 ‰ higher than the theoretical values for $\delta^{18}O$-CO_2 ($\delta^{18}O_{eqs}$)

calculated from $\delta^{18}O_{sw}$, assuming full equilibrium and considering the temperature-dependent equilibrium fractionation during CO_2–H_2O isotopic equilibration.

III.3.3 Measured profiles of $\delta^{18}O_{sw}$ and $\delta^{18}O_{sc}$ after irrigation (experiment 2, irrigation)

Variations in $\delta^{18}O_{av}$ were similar to those observed during experiment 1 and ranged mostly from –18 to –14 ‰ (Fig. III.3 c). In the air column, $\delta^{18}O_a$ varied diurnally with minimum and maximum values of –1.5 ‰ and +2.9 ‰, respectively (Fig. III.3 d). Soil temperature at all column depths was around 24.7 °C before irrigation and dropped by approx. 1 °C or more (at –1 cm) after irrigation (Fig. III.3 f). Soil temperature increased again until day 5, followed by another drop with subsequent increase. One day after irrigation, $\delta^{18}O_{sw}$ at –1 cm increased by approx. 4 ‰, whereas it was 10 ‰ and 6 ‰ lower than before irrigation at –3 cm and –7 cm, respectively (Fig. III.3 g). At –1 cm, $\delta^{18}O_{sw}$ continued to increase for two more days before it decreased again. In contrast, at –3 cm and –7 cm $\delta^{18}O_{sw}$ started to increase again at day 1 and 5 after irrigation, respectively, and continued to rise until the end of the experiment. Eight days after irrigation, evaporative enrichment of water brought $\delta^{18}O_{sw}$ approximately back to pre-watering values at –3 cm and –7 cm. At the three lower depths, $\delta^{18}O_{sw}$ decreased from day 3 to day 5 of the experiment, concurrent with the delayed arrival of irrigation water at these depths, that was reflected by changes in *SWC* (i.e., at –30 and –55 cm, Fig. III.3 e and g).

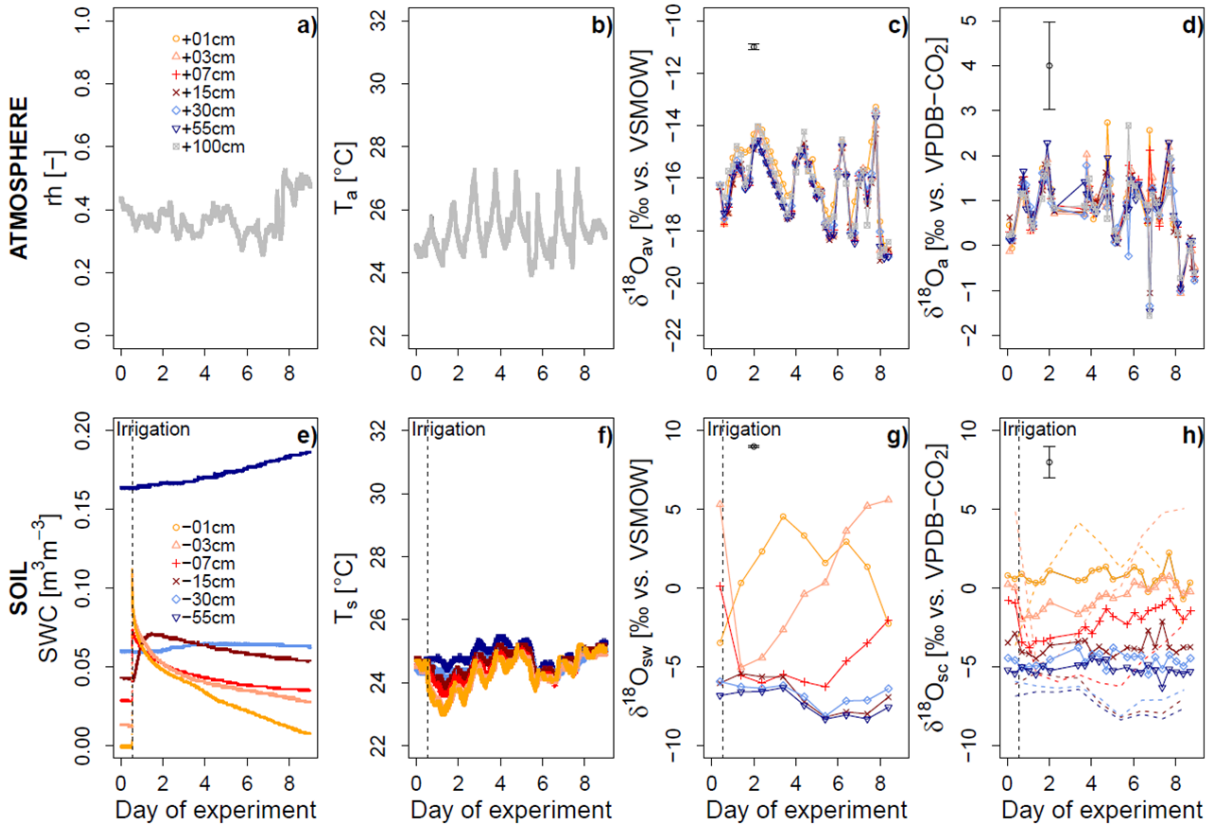

Figure III.3 Experiment 2, irrigation: Relative humidity (a), air temperature (b), oxygen isotope signatures ($\delta^{18}O$) of water vapor (c) and CO_2 (d) in the atmosphere column, volumetric water content (e), temperature (f), $\delta^{18}O$ of liquid water (g) and CO_2 (h, dashed lines show values for $\delta^{18}O_{eqs}$ in the respective depths) in the sand column. The single data point with error bar represents average standard deviation over the experimental period.

Prior to irrigation, CO_2 was enriched in ^{18}O at the top relative to the bottom of the column (Fig. III.3 h). In response to irrigation, $\delta^{18}O_{sc}$ decreased significantly by 1.7 to 3 ‰ at –3 cm, –7 cm, and –15 cm, but did not change significantly at the other depths. During the remaining days of the experiment, temporal dynamics and absolute values of $\delta^{18}O_{sc}$ at –1 cm and –3 cm were similar to $\delta^{18}O_a$ (Fig. III.3 d and h): a significant correlation was found between $\delta^{18}O_a$ at +1 cm and $\delta^{18}O_{sc}$ at –1 cm ($r^2 = 0.41$, n = 25) (data not shown). In contrast, $\delta^{18}O_{sc}$ at –30 and –55 cm did not show a clear temporal trend, but fluctuated around –5 ‰ with an amplitude of approximately 1.5 ‰ (Fig. III.3 h). At all depths, measured $\delta^{18}O_{sc}$ was markedly different from the corresponding calculated $\delta^{18}O_{eqs}$, values (Fig. III.3 h).

III.3.4 Measured profiles of $\delta^{18}O_{sw}$ and $\delta^{18}O_{sc}$ after irrigation with water containing *CA* (experiment 3, irrigation+*CA*)

Air temperature was similar to experiment 2 during the first 3 days, but increased markedly afterwards (Fig. III.4 b). Soil temperature at all column depths showed a similar response to irrigation as in experiment 2, but mirrored the increase in air temperature after day 3 (Fig. III.4 f).

Changes of $\delta^{18}O_{sw}$ (Fig. III.4 g) were similar to those observed during the irrigation experiment without *CA* (Fig. III.3 g). However, $\delta^{18}O_{sc}$ at –1 cm and –3 cm was strongly influenced by *CA* addition to irrigation water (Fig. III.4 h), i.e., the immediate $\delta^{18}O_{sc}$ drop after irrigation was this time also visible at –1 cm. After the irrigation-induced depletion, $\delta^{18}O_{sc}$ values mirrored the increase in $\delta^{18}O_{sw}$ with an offset of 3 to 6 ‰ (solid and dashed lines, respectively, in Fig. III.4 h), yielding an r^2 of 0.92 (n = 23) and 0.52 (n = 23) between $\delta^{18}O_{sc}$ and $\delta^{18}O_{eqs}$ at –1 cm and –3 cm, respectively. Furthermore, the depletion of $\delta^{18}O_{sc}$ at –3 cm and –7 cm in response to the watering was much more pronounced than in experiment 2, with values dropping from +2 ‰ and +1 ‰ down to –5 ‰ and –2 ‰, respectively. However, the *CA* effect was less pronounced at –7 cm, and similar to experiment 2, no effect of irrigation on $\delta^{18}O_{sc}$ in deeper layers was observed (Fig. III.4 h). Surprisingly, the $\delta^{18}O_{sc}$ was always far away from its equilibrated value with soil water, even in deep layers and before irrigation (Fig. III.4 h).

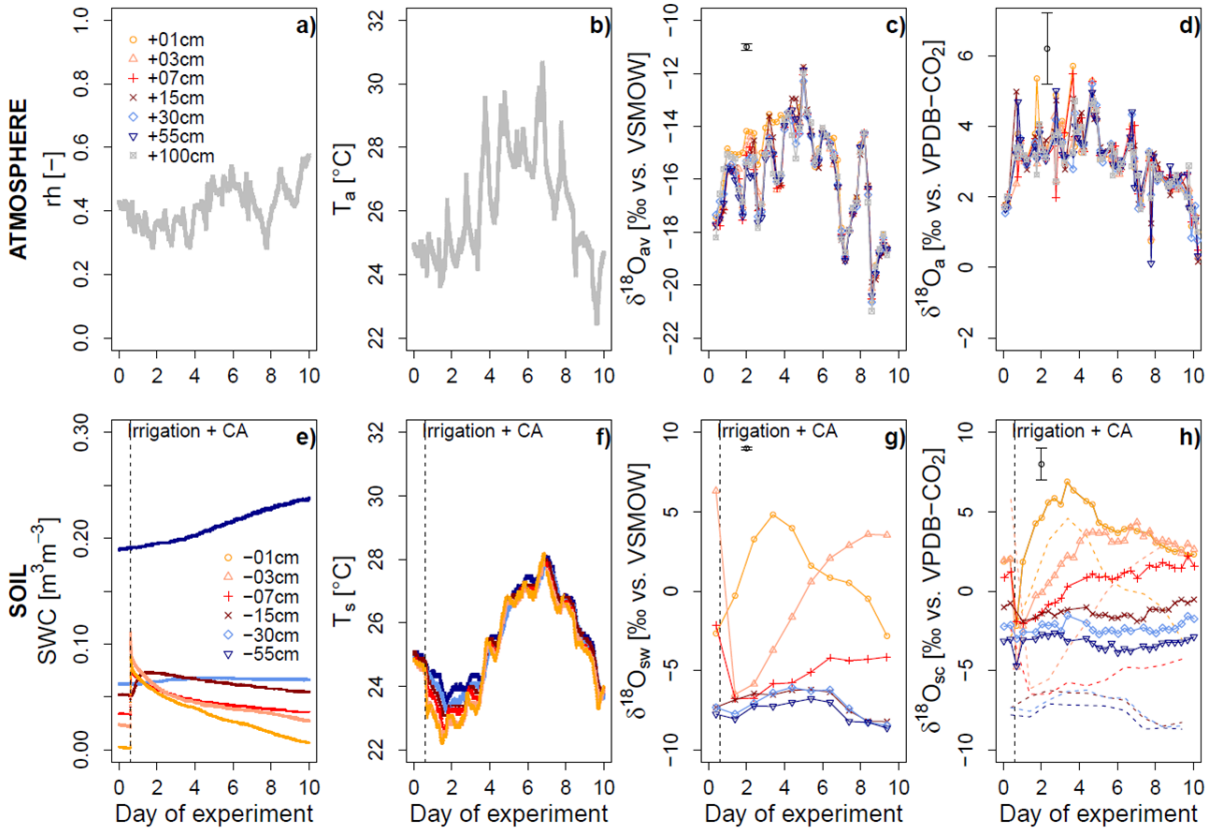

Figure III.4 Experiment 3, irrigation+*CA*: Relative humidity (a), air temperature (b), oxygen isotope signatures ($\delta^{18}O$) of water vapor (c) and CO_2 (d) in the atmosphere column, volumetric water content (e), temperature (f), $\delta^{18}O$ of liquid water (g) and CO_2 (h, dashed lines show values for $\delta^{18}O_{eqs}$ in the respective depths) in the sand column. The single data point with error bar represents average standard deviation over the experimental period.

III.3.5 Simulation of *SWC*, T_s, $\delta^{18}O_{sw}$ and $\delta^{18}O_{sc}$ profiles

The general pattern of increasing *SWC* with increasing depth was reproduced well by the model (Fig. III.5, Table III.3). Regarding all experiments, the RMSE for *SWC* simulations was lowest at –30 cm, with a maximum value around 0.01 m^3 m^{-3}, and was always smaller than the measurement precision of 0.03 m^3 m^{-3}. Modeled and measured data of T_s also matched well and yielded the lowest RMSE of 0.17 °C at –15 cm depth for experiment 1 (Fig. III.5, Table III.3).

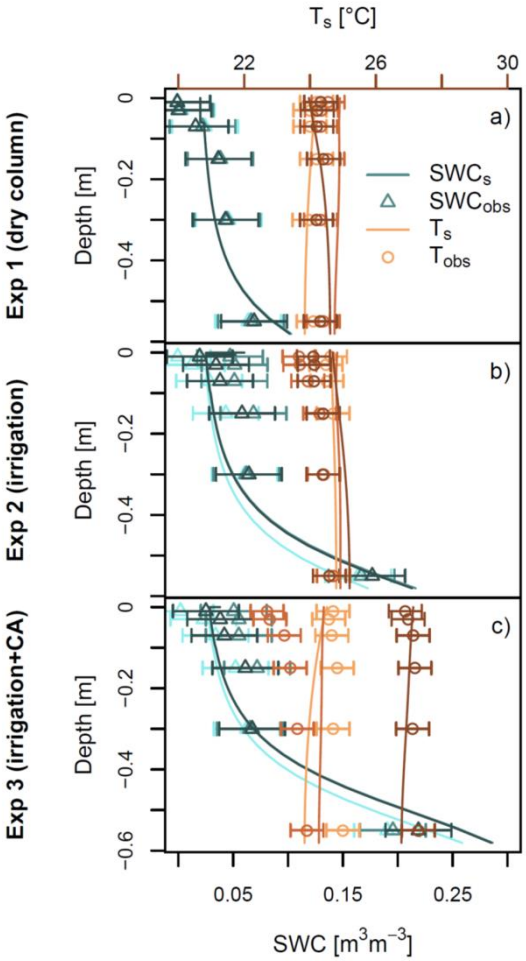

Figure III.5 Soil column profiles of measured and simulated volumetric soil water content (*SWC*) and soil temperature (T_s) for three individual days of experiment 1 (a), experiment 2 (b) and 3 (c). The three intensities of colors from light to dark refer to day 0 (day before irrigation for exp. 2 and 3), day 2 (day after irrigation for exp. 2 and 3), and day 6 of the experiment, respectively. Error bars show precision of *SWC* and T_s measurements.

Table III.3 Statistical results for model–data fit of $\delta^{18}O\text{-}H_2O$ and $\delta^{18}O\text{-}CO_2$, volumetric soil water content (*SWC*), and soil temperature (T_s). RMSE, $RMSE_u$ and $RMSE_s$ refer to the total, unsystematic and systematic root mean square error. Slope and intercept were obtained from ordinary least squares regression, and *n* is the number of data points.

		r^2	RMSE	$RMSE_u$	$RMSE_s$	Intercept	slope	*n*
$\delta^{18}O_{sw}$	Exp1	0.75	2.61	2.36	1.10	0.10	0.80	54
	Exp2	0.65	2.48	2.12	1.29	-1.27	0.69	54
	Exp3	0.61	2.55	1.97	1.61	-2.21	0.63	48
$\delta^{18}O_{sc}$	Exp1 (f_{CA} =0.01)	0.59	2.51	0.62	2.43	0.23	0.26	162
	Exp1 (f_{CA}=0.1)	0.95	0.77	0.52	0.57	-0.61	0.84	162
	Exp1 (f_{CA} =1)	0.98	1.16	0.45	1.07	-0.69	1.18	162
	Exp1 (f_{CA} =10)	0.96	1.49	0.79	1.26	0.31	1.44	162
	Exp2 (f_{CA} =0.01)	0.65	2.65	0.74	2.54	0.85	0.46	162
	Exp2 (f_{CA} =0.1)	0.75	1.41	1.33	0.47	0.62	1.07	162
	Exp2 (f_{CA} =1)	0.88	1.33	0.98	0.91	-0.18	1.22	162
	Exp2 (f_{CA} =10)	0.79	2.17	1.31	1.73	-1.31	1.15	162
	Exp3 (f_{CA} =0.01)	0.39	2.59	2.21	1.35	0.81	0.63	162
	Exp3 (f_{CA} =0.1)	0.64	2.64	2.32	1.25	-1.21	1.10	162
	Exp3 (f_{CA} =1)	0.79	3.29	1.70	2.81	-2.75	1.18	162
	Exp3 (f_{CA} =10)	0.79	4.43	1.50	4.16	-4.16	1.04	162
SWC	Exp1	0.70	0.01	0.01	0.01	0.01	0.76	54
	Exp2	0.94	0.02	0.01	0.01	-0.01	1.03	54
	Exp3	0.96	0.02	0.02	0.02	-0.02	1.30	48
T_s	Exp1	0.28	0.21	0.19	0.09	4.75	0.81	54
	Exp2	0.26	0.66	0.20	0.62	18.14	0.28	54
	Exp3	0.72	0.91	0.57	0.72	10.85	0.58	48

The $\delta^{18}O$ profiles of H_2O and CO_2 in the sand column were simulated for the three experiments with different parameterizations for the soil *CA* activity factor (f_{CA}). Three example days are shown for each experiment (Fig. III.6). For the two irrigation experiments (exp. 2 and exp. 3), day 0 refers to the day before irrigation, whereas day 2 refers to the day after irrigation. Overall, the general pattern of $\delta^{18}O_{sw}$, with increasing values towards the top of the sand column, was reproduced well by the model, with r^2 between 0.61 and 0.75 (Table III.3, Fig. III.6). The model

was also able to reproduce the inversion of $\delta^{18}O_{sw}$ profiles in the upper three sand layers after irrigation for both irrigation experiments, although at –30 cm modeled and measured data did not entirely match (Fig. III.6 e, f, h, i). The simulation of $\delta^{18}O_{sc}$ profiles was very sensitive to the parameterization of f_{CA}, especially at greater depth (Fig III.6), yielding considerably different RMSE and r^2 for the four f_{CA} parameterizations (Table III.3, Table B 1). For all three experiments, $\delta^{18}O_{sc}$ simulated with f_{CA} = 1 yielded the highest r^2 when taking into account all six depths. However, the RMSE for experiment 3 was more than twice as high as compared to experiment 1 and 2 (> 3 ‰) (Table III.3, Fig. III.6 a, b, c). At –55 cm and –30 cm, the simulated $\delta^{18}O_{sc}$ was closer to measured $\delta^{18}O_{sc}$ when f_{CA} was set to 0.1 (experiment 2, Fig. III.6 d, e, f) or even to 0.01 (experiment 3, Fig. III.6 g, h, i, Table B 1).

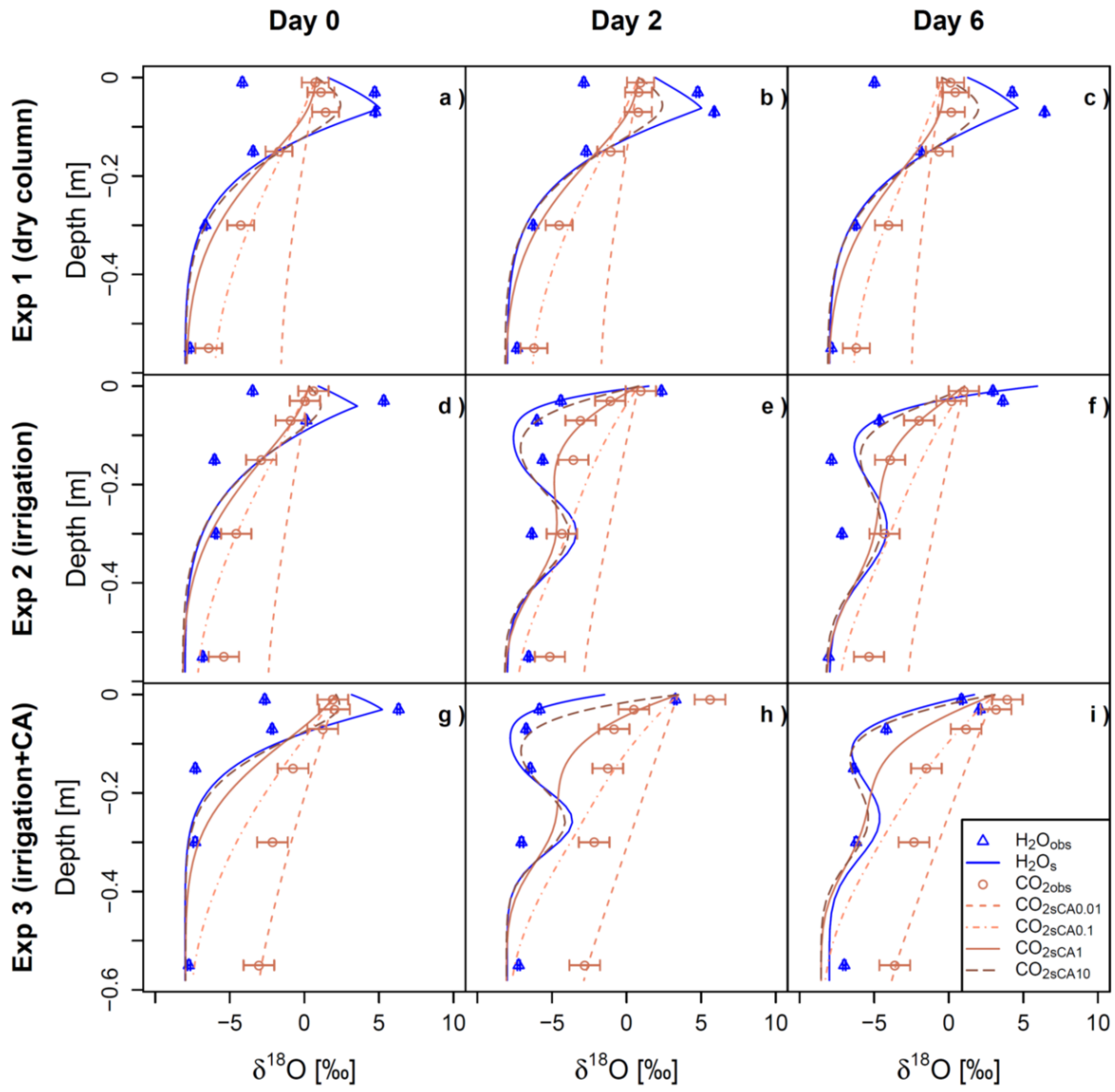

Figure III.6 Soil column profiles of measured and simulated oxygen isotope ratios of H_2O and CO_2 for three individual days of experiment 1 (a, b, c), experiment 2 (d, e, f) and experiment 3 (g, h, i), including different parameterizations for the *CA* activity factor. Error bars indicate average standard deviation over the experimental period.

III.4. Discussion

III.4.1 Suitability of tubing material to measure profiles of $\delta^{18}O_{sc}$

The use of microporous polypropylene tubing for trace gas and isotopic measurements has been described previously, for example for determination of $\delta^{13}C\text{-}CO_2$ and $\delta^{18}O_{sw}$ (Gut et al., 1998; Parent et al., 2013; Rothfuss et al., 2013). Here, we showed that the oxygen isotope ratio of CO_2

($\delta^{18}O_{sc}$) could also be reliably monitored in soils using this tubing material. The absence of any fractionation effects revealed that the tubing was suitable to measure temporal variations of $\delta^{18}O_{sc}$ in sand at varying *SWC*. The temporal resolution in this specific setup was limited because we had to minimize the flushing of the gas-permeable tubing to ensure the sand column was not depleted of CO_2. Since the measurement of $\delta^{18}O_{sw}$ took 30 min per depth, in contrast to 4 min per depth required for $\delta^{18}O_{sc}$, we could measure $\delta^{18}O_{sw}$ and $\delta^{18}O_{sc}$ profiles only once and three times per day, respectively. However, this limitation was related to the specific setup, as we used pure sand with negligible production of CO_2. Thus, CO_2 diffusion from the atmosphere into the sand was the only source of CO_2. Much higher temporal resolution could be realized during measurements in natural (CO_2 producing) soils.

The hydrophobic properties of the microporous polypropylene tubing make its use suitable for field applications, and its installation in natural soils has been described in previous studies (Goffin et al., 2014; Gut et al., 1998; Parent et al., 2013). The spatial resolution of this methodology is also promising for field applications, as it is only limited by the availability of sample gas in the sand gas phase, that puts a lower limit of a few centimeters distance between two sampling depths. The flow rate through the gas-permeable tubing should be kept as low as possible to minimize the disturbance of the sand gas phase, and to avoid potential artifacts by advection or air efflux into the sand. Gut et al. (1998) provide some information on the optimum permeation efficiency that can be obtained for the microporous tubing depending on the flow rate and tubing length.

III.4.2 Profiles of $\delta^{18}O_{sw}$ and $\delta^{18}O_{sc}$ before irrigation

The logarithmic profile of $\delta^{18}O_{sw}$ in unsaturated soils subject to evaporation, with higher values below the surface and lower values at the bottom of the column, observed in our study, is well established. It can be explained in first approximation by the conjugated effect of equilibrium

and kinetic isotope fractionation processes, leading to ^{18}O-enrichment in the evaporative zone on the one hand, and the capillary rise of ^{18}O-depleted source water from greater depths on the other. The latter water pool mixes with the ^{18}O-enriched water diffusing down the soil profile (Barnes and Allison, 1988; Mathieu and Bariac, 1996). The ^{18}O-depletion of liquid water at the very top of the sand column reflected the intrusion of isotopically depleted atmospheric water vapor into the sand. The maximum enrichment at –7 cm was corroborated by the decreasing trend of *SWC* at the same depth, showing that this depth was contributing for the most part to the evaporation from the sand column.

In the top 10 cm of the sand column, temporal variations of $\delta^{18}O_{sc}$ resembled those of $\delta^{18}O_a$, revealing the invasion of CO_2 from the air into the sand column facilitated by the very low *SWC* (< 0.1 m^3 m^{-3}) in the upper sand layers. The fact that the atmospheric CO_2 signal ($\delta^{18}O_a$) was still partially visible at all depths and that $\delta^{18}O_{sc}$ values deviated from $\delta^{18}O_{eqs}$ throughout the column indicated that the uncatalyzed reaction rate constant (k_s) of the CO_2–H_2O oxygen isotope exchange in the absence of carbonic anhydrase was too low to allow full oxygen isotope exchange between CO_2 and H_2O. The model simulations demonstrated that on average the $\delta^{18}O_{sc}$ profiles were described best with $f_{CA}=1$, i.e., the uncatalyzed reaction rate constant (k_s $=0.012$ s^{-1}), but also showed that for –30 cm and –55 cm the best model-data fit was obtained with f_{CA} values less than unity, i.e., by reducing k_e to a magnitude of 10^{-3}. This indicates that k_e may vary with depth, even within one soil or sand type, caused by inhomogeneous bulk density and *SWC*. Seibt et al. (2006b) also suggested that assuming a constant relationship between $\delta^{18}O_{sw}$ and $\delta^{18}O_{sc}$ over the soil depth is inappropriate for simulations. While their conclusion was derived from their observations of *CA* activity, here we show that also in the absence of *CA* activity a depth-resolved parameterization of k_e may be appropriate.

III.4.3 Profiles of $\delta^{18}O_{sw}$ and $\delta^{18}O_{sc}$ after irrigation

The irrigation caused an ^{18}O-depletion in H_2O at –3 and –7 cm in response to the addition of isotopically depleted irrigation water. The irrigation effect, as well as the general profiles of $\delta^{18}O_{sw}$, were captured well by the model. The fact that modeled and measured profiles in some cases did not match entirely (e.g., for $\delta^{18}O_{sw}$ at –30 cm), indicated that, although assumed in the simulation, the sand properties were not homogeneous over the column. The manual filling of the column with sand could have produced an inhomogeneous density that was not described by our parameterization of the model at these depths in the column. Consequently, if our parameterization at these lower depths was incorrect we would obtain a difference in simulated and measured profiles.

In contrast to observations at –3 and –7 cm, no temporary ^{18}O-depletion in soil water was observed at –1 cm directly after irrigation, although the topmost layer of the sand column was expected to be the most rapidly influenced because of its immediate contact with irrigation water. Most probably, the ^{18}O-depletion at this depth was missed because of an insufficient temporal resolution, as it lasted probably only for a very short time (i.e., less than a day) because of the strong evaporative enrichment close to the surface. The observation that ^{18}O-enrichment at –1 cm was rather transient and decreased again when ^{18}O-depleted water vapor progressively diffused into the drying sand, was consistent with this assumption.

The irrigation increased the influence of $\delta^{18}O_{sw}$ on $\delta^{18}O_{sc}$ at shallower depths, i.e., at –3 and –7 cm, where $\delta^{18}O_{sc}$ decreased significantly after irrigation. This is in agreement with studies which reported reduced $\delta^{18}O_{sc}$ related to changes in $\delta^{18}O_{sw}$ induced by relatively ^{18}O-depleted precipitation events (Sturm et al., 2012; Wingate et al., 2010). However, irrigation did not enhance the isotopic equilibrium between CO_2 and liquid water, as $\delta^{18}O_{sc}$ still deviated from $\delta^{18}O_{eqs}$, and the best model−data fit in the simulations was maintained with a k_e similar to that of the dry column simulations.

The strong decrease in $\delta^{18}O_{sc}$ at –1 cm directly after irrigation with *CA*, and the steeply rising $\delta^{18}O_{sc}$ values at –1 cm in the following days, reflecting the shape of $\delta^{18}O_{eqs}$, albeit with a positive offset of 2-3 ‰ caused by the temporal discrepancy between $\delta^{18}O_{sw}$ and $\delta^{18}O_{sc}$ measurements, clearly indicated an effect of *CA*, as these variations in $\delta^{18}O_{sc}$ were not observed after *CA*-free irrigation in experiment 2. A similar response of $\delta^{18}O_{sc}$ to irrigation was also observed at –3 cm and –7 cm, although this response was dampened with increasing depth. This likely reflected a reduction of *CA* content at greater depths because it was applied at the surface. The *CA* effect was not visible in the model simulations, which yielded the best fit between measured and modeled $\delta^{18}O_{sc}$ for all depths with f_{CA} = 1 or even lower rather than with an enhanced f_{CA}, both before and after irrigation. Furthermore, measured $\delta^{18}O_{sc}$ was higher than all modeled $\delta^{18}O_{sc}$ values at –1 cm on day 2 and at –1 cm and –3 cm on day 6 after irrigation with *CA* (Fig. III.5 h, i), although the deviation from the modeled values decreased with time.

To interpret the discrepancy between modeled and observed $\delta^{18}O_{sc}$ after irrigation with *CA*, it has to be mentioned that the model−data fit was already low at the beginning of experiment 3 (before irrigation with *CA*), i.e., CO_2 in the sand column in experiment 3 was on average approximately 3 ‰ more enriched compared with the other experiments, while $\delta^{18}O_{sw}$ was similar. This observation suggested a more general reason for the model−data disagreement in this experiment. The higher measured $\delta^{18}O_{sc}$ in this experiment was more likely caused by an enhanced invasion flux from the atmosphere above (compared to the two other experiments), rather than an inhibited CO_2 hydration rate as would be deduced from the higher model−data agreement with f_{CA} =0.01. Air temperature was higher in this last experiment that could have resulted in an enhanced turbulence at the surface soil column. However, simulations with increased wind speed (2.5 m s^{-1} instead of 0.5 m s^{-1}) did not yield a better agreement between simulated and measured $\delta^{18}O_{sc}$ (data not shown). Furthermore, advection, which is not

accounted for by the model, could have contributed to the different measured $\delta^{18}O_{sc}$ under these conditions.

Nevertheless, the experimental data of experiment 3 were indicative of a significant influence of *CA* activity in the uppermost sand layers, slowly moving from the surface into the sand profile, but at the same time diminishing due to degrading extracellular *CA* activity in the absence of *CA* producing microorganisms. To our knowledge, the impact of *CA* on the oxygen isotope exchange in soils has never been observed in experimental studies before, but was rather deduced by fitting modeled to measured $\delta^{18}O_{sc}$ (Santos et al., 2014; Seibt et al., 2006b; Wingate et al., 2008). In these studies, *CA* activity has simply been treated as a factor which enhances the uncatalyzed CO_2–H_2O oxygen isotope exchange rate constant ($k_e = f_{CA} \cdot k_s$) by 10-300 times. Here, we demonstrated that *CA* at a concentration of 0.12 mg mL^{-1} with a specific activity of 2500 W-A units mg^{-1}, applied in an irrigation event of 8.7 mm, was sufficient to considerably increase the oxygen isotope equilibrium between CO_2 and H_2O in the two uppermost sand layers, i.e., at 1 cm and 3 cm below the sand surface.

III.4.4 Conclusions

Laser absorption spectroscopy allows *in situ* measurements of soil water isotopes (Herbstritt et al., 2012; Rothfuss et al., 2013; Soderberg et al., 2012; Volkmann and Weiler, 2014) and near-continuous CO_2 isotope profiles (Goffin et al., 2014). However, until now no simultaneous measurements of $\delta^{18}O_{sw}$ and $\delta^{18}O_{sc}$ in soils have been reported. Our results show that by combining gas-permeable tubing and laser-based isotope analyzers, $\delta^{18}O_{sc}$ and $\delta^{18}O_{sw}$ profiles can be monitored on-line and simultaneously, and the oxygen isotope exchange between soil water and CO_2 can be calculated for different soil depths. This is especially promising for field measurements, where traditional sampling techniques have not been able to monitor temporal dynamics of $\delta^{18}O_{sc}$ and $\delta^{18}O_{sw}$ profiles, e.g., related to precipitation events (Santos et al., 2012;

Wingate et al., 2008), with a sufficient time resolution. High resolution $\delta^{18}O_{sw}$ and $\delta^{18}O_{sc}$ data obtained with the new methodology could also be used to improve analytical model simulations of $\delta^{18}O_{sc}$, as provided by Tans (1998), or complex numerical models. Also the high spatial resolution represents a major step forward because it allows monitoring $\delta^{18}O_{sc}$ close to the soil surface and, therefore, could help to constrain the effective diffusional fractionation of $CO^{18}O$, a crucial factor for calculations of $\delta^{18}O$ of soil CO_2 efflux. A further outcome of the present study is that the effective rate constant for the isotopic hydration reaction between CO_2 and H_2O (k_e) may be highly variable in time and space. More detailed experiments examining *CA* activity and k_e at varying environmental conditions and for different soil types are thus required.

IV. Simulation of soil and canopy $\delta^{18}O$-CO_2 in a temperate Norway spruce forest

On the basis of the manuscript

Laura Gangi, Jerome Ogee, Lisa Wingate, Harry Vereecken, Nicolas Brüggemann

manuscript in preparation

IV.1 Introduction

The stable isotopes of CO_2 offer the potential of partitioning net ecosystem CO_2 flux into net assimilation (F_a) and soil respiration (F_r), and therefore allow a process-based understanding of the terrestrial carbon budget. An absolute requirement for this methodology is a sufficient difference in the isotopic signature between the respective CO_2 component fluxes ($\delta^{18}O_A$ and $\delta^{18}O_r$), the so called isotopic disequilibrium (D_{eq}). Equation (IV.1) shows the isotopic mass balance equation which is generally used for isotope-based partitioning (Ogee et al., 2004).

$$\delta^{18}O_A \cdot F_a + \delta^{18}O_r \cdot F_r = F_t \cdot \delta^{18}O_t \quad \text{(IV.1)}$$

Here, $\delta^{18}O_A \cdot F_a$ and $\delta^{18}O_r \cdot F_r$ are the products of isotope ratio and flux (i.e., the isofluxes) of net assimilation and soil respiration, respectively, and $F_t \cdot \delta^{18}O_t$ is the isoflux related to the total net CO_2 exchange. The isotopic signature of assimilation is defined by

$$\delta^{18}O_A = \delta^{18}O_a - \Delta_A \quad \text{(IV.2)}$$

where $\delta^{18}O_a$ is the isotope ratio of atmospheric CO_2 and Δ_A is the isotopic discrimination associated with photosynthesis, calculated according to Gillon and Yakir (2001):

$$\Delta_A = a_d + \xi\,[\theta\,(\delta^{18}O_{eql} - \delta^{18}O_a) - (1 - \theta)\,a_d\,/(\xi + 1)] \quad \text{(IV.3)}$$

where a_d is the mean diffusional isotopic fractionation of $CO^{18}O$ from atmosphere to leaf, and $\xi = c_c/(c_c - c_a)$ with c_c and c_a representing the CO_2 mixing ratio in the chloroplast and atmosphere, respectively. The variable $\delta^{18}O_{eql}$ represents the $\delta^{18}O$ of CO_2 in full equilibrium with leaf water

and θ is the degree of CO_2–H_2O isotopic equilibrium inside the leaf ranging between 0 and 1 (full equilibrium).

Until now, mostly the carbon isotope signature of CO_2 has been used to disentangle gross fluxes of CO_2 for different ecosystems (Bowling et al., 2001; Lai et al., 2003; Zhang et al., 2006; Zobitz et al., 2008), whereas ^{18}O-based partitioning has been rarely applied (Langendörfer et al., 2002; Ogee et al., 2004; Yakir and Wang, 1996), even though the isotopic disequilibrium can be much larger for $\delta^{18}O\text{-}CO_2$ than for $\delta^{13}C\text{-}CO_2$. The reason for the scarcity of ^{18}O-based partitioning studies is that the $\delta^{18}O\text{-}CO_2$ signature is very variable in time due to the oxygen isotope exchange between CO_2 and the different water pools of the ecosystem. Ogee et al. (2004) analyzed the uncertainties related to ^{18}O-based partitioning and found that the error could be significantly reduced by increasing the accuracy of determining both $CO^{18}O$ isoflux and photosynthetic discrimination (Δ_A), as previously suggested by Langendörfer et al. (2002). Only since a few years, infrared laser spectroscopy allows the direct measurement of the ecosystem $CO^{18}O$ isofluxes. Before, they could only be determined by indirect methods, such as the hyperbolic relaxed eddy accumulation (HREA) and the EC/flask sampling method, which involved labor-intensive flask sampling and subsequent calculations relying on critical assumptions (Bowling et al., 1999). A comprehensive review about the various studies that have taken advantage of the new laser-based methodology using quantum cascade laser absorption spectrometers (QCLAS) or tunable diode laser (TDL) instruments to study ecosystem isofluxes with high temporal resolution was published by Griffis (2013). These studies also emphasized the uncertainties related to Δ_A, which are owed to the fact that Δ_A cannot be measured directly at the canopy scale and therefore has to be calculated with "big-leaf" models or multilayer models, such as MuSICA (Ogee et al., 2003a).

An important parameter required to calculate Δ_A is the degree of isotopic equilibrium between CO_2 and leaf water (θ), sometimes referred to as the CO_2 hydration efficiency (eq. IV.3). Griffis

et al. (2011) and Xiao et al. (2010) reported that θ was much lower at the canopy scale when compared to commonly accepted values, which were derived from laboratory experiments. Very recently, Santos et al. (2014) confirmed that the isotopic disequilibrium between the oxygen isotope ratio of assimilation ($\delta^{18}O_A$) and respiration ($\delta^{18}O_s$) was very sensitive to the parameterization of θ in the canopy, emphasizing the importance of this parameter. Although the impact on the partitioning results might be relatively small (Ogee et al., 2004), a reduction of the error related to the second term on the left side of eq. IV.1 could be achieved by increasing the accuracy of $\delta^{18}O_s$. The integration of the soil $C^{18}O$ isoflux ($CO^{18}O_s$) in process-based soil-plant-atmosphere models helps to better understand the isotopic exchange between the different ecosystem components and their relative contributions to atmospheric $\delta^{18}O$-CO_2. However, simulations of $CO^{18}O_s$ are still challenging, as they are highly sensitive to the depth-dependent prediction of soil water $\delta^{18}O$ ($\delta^{18}O_{sw}$), assumptions about the fractionation associated with diffusion, and especially, the potential activity of carbonic anhydrase which greatly enhances the CO_2 hydration rate (Seibt et al., 2006b; Wingate et al., 2009).

The aim of this study was to test whether implementation of a θ value, determined from gas exchange measurements with Norway spruce in the laboratory, could improve the simulation of Δ_A at the canopy scale. Therefore, we compared $\delta^{18}O$-CO_2 measured at different heights in a temperate Norway spruce stand with $\delta^{18}O$-CO_2 simulated with the multilayer, multileaf model MuSICA (Ogee et al., 2003a). For this purpose, a variable parameterization for θ was newly implemented in MuSICA, replacing the constant default value of $\theta = 1$. In addition, we tested the ability of MuSICA to reproduce the soil $C^{18}O$ isoflux ($CO^{18}O_s$), an output variable that had also been newly implemented for this study.

IV.2 Material and Methods

IV.2.1 Study site

The field measurements were conducted in the Höglwald forest, which is located in a hilly landscape 40 km north-west of Munich (48° 17' 20" N, 11° 4' 30" E; 560 m asl) and has been used for long-term monitoring of biosphere-atmosphere-hydrosphere exchange processes since 1993 (Butterbach-Bahl and Papen, 2002; Kreutzer and Weiss, 1998; Luo et al., 2012). The climate is sub-oceanic, with a mean annual precipitation around 932 mm and a mean annual temperature of 8.6 °C for the observation period from 2004-2010. The forest area covered approx. 370 ha, dominated by more than 100-year-old Norway spruce (*Picea abies*), and was surrounded by intensive agriculture with high nitrogen input. The stand density was approx. 620 trees ha^{-1}, with a mean stand height of 35.2 m, a leaf area index of 6.15 m^2 m^{-2}, and a mean breast height diameter of 42.4 cm. The minimum and maximum canopy height was 12.6 and 37 m, respectively. The soil at the experimental site is a Typic Hapludalf (FAO: dystric cambisol, for details see Kreutzer (1995)).

IV.2.2 Isotope measurements

From December 2007 to November 2008, CO_2 mixing ratios, $\delta^{18}O$-CO_2 and $\delta^{13}C$-CO_2 were measured at 2, 8, 15 and 50 m above the ground using a tunable diode laser absorption spectrometer (TDLAS, TGA100A, Campbell Scientific Instruments, Logan, UT, USA). The oxygen and carbon isotopic composition of total and heterotrophic soil respiration was measured with three soil respiration chambers each from April to November 2008. The custom-made chambers (diameter 10 cm, height 15 cm), which were located close to the measurement tower, were made of stainless steel and were equipped with an inlet, an outlet, and a vent to avoid pressure differences between inside and outside. Total and heterotrophic soil respiration chambers were placed on stainless steel rings of 2 and 30 cm depth, respectively, to include or

to exclude roots. Rainwater was collected with a funnel and led into the chambers through a small PTFE tube. Inlet air for the chambers was provided from a 50 L buffer tank that was continuously filled by a pump with ambient air taken at 1 m height. Each height and each soil respiration chamber was sampled once within 30 min for 100 sec, of which the last 45 sec were taken as averaging period. Two reference gases (325 and 552 ppmv CO_2 in air) were sampled every 15 min to monitor instrument drift.

Soil respiration rates (F_r) and $\delta^{18}O$-CO_2 of soil efflux ($\delta^{18}O_s$) were determined with mass balance equations based on measurements at the inlet and outlet of the chamber and considering the total flow rate through the chamber (0.5 L min^{-1}). The soil respiration rate was calculated according to eq. IV.4:

$$F_r = air \cdot ([CO_{2out}] - [CO_{2in}])/(S \cdot V_m) \cdot (p/p_0) \quad \text{(IV.4)}$$

where *air* is the air flow rate through the chamber, $[CO_{2in}]$ and $[CO_{2out}]$ are the CO_2 mixing ratio at the inlet and outlet of the chamber, respectively, S is the surface area covered by the respiration chamber, V_m is the molar volume of air at standard conditions, and p and p_o are ambient and standard pressure, respectively, whereas $\delta^{18}O_s$ was calculated as follows:

$$\delta^{18}O_s = (\delta^{18}O_{out} \cdot [CO_{2out}] - \delta^{18}O_{in} \cdot [CO_{2in}]) / ([CO_{2out}] - [CO_{2in}]) \quad \text{(IV.5)}$$

Here, $\delta^{18}O_{in}$ and $\delta^{18}O_{out}$ is the $\delta^{18}O$ of CO_2 measured at the inlet and at the outlet of the soil chamber, respectively. Soil $CO^{18}O$ isoflux ($CO^{18}O_s$) was calculated as the average product of F_r and $\delta^{18}O_s$ derived from the three soil respiration chambers:

$$CO^{18}O_s = \delta^{18}O_s \cdot F_r \quad \text{(IV.6)}$$

Isotopic compositions are reported in the δ-notation and referenced to VSMOW for H_2O, to VPDB-CO_2 for ^{18}O-CO_2, and to VPDB for ^{13}C-CO_2.

IV.2.3 Supporting measurements

The net ecosystem exchange of CO_2 as well as sensible and latent heat flux were quantified by eddy covariance flux measurements using an open-path infrared absorption analyzer (LI-7500, LI-COR Biosciences, Lincoln, NE, USA) and an ultrasonic anemometer (CSAT-3, Campbell Scientific, Inc., Logan, UT, USA), installed at 50 m height (approx. 10 m above the canopy). Details are given by Luo et al. (2012). Net radiation and global incoming radiation were measured at the same height with a pyrradiometer (BILANZ, UMS, München, Germany) and a star pyranometer (GLOBAL, UMS, München, Germany), respectively. Soil heat flux was measured with six soil heat flux plates (HFP01SC-L, Hukseflux, Delft, The Netherlands), which were installed at 10 cm depth.

IV.2.4 Simulations with MuSICA

The version 2.0.x, as described in Domec et al. (2012), of the biophysical soil-vegetation-atmosphere model MuSICA (**Mu**ltilayer **S**imulator of the **I**nteractions between a **C**oniferous stand and the **A**tmosphere) was used to simulate the ecosystem gas and energy exchange and ^{18}O-CO_2 discrimination associated with soil and vegetation CO_2 fluxes. A detailed description of the model and its validation in terms of energy, water, and CO_2 flux simulations can be found in previous studies (Ogee et al., 2003a; Ogee et al., 2003b; Ogee et al., 2004). The model distinguishes different vegetation and soil layers, and different leaf types based on their age, sun exposure and water status. The number of layers in air was set to 15 of which 10 layers were within the canopy, whereas the number of soil layers was set to 30 with an increased spatial resolution at the soil surface. The output data was obtained in a half-hourly time

resolution. The forcing height was set to 40 m, which is approx. 3 m above the canopy. Meteorological data for the forcing file was mostly obtained from on-site measurements and was provided in 30 min resolution. Air pressure (p) data was taken from the German meteorological station (Deutscher Wetterdienst, Offenbach, Germany) at Munich airport which is located about 40 km south-east of the study site. CO_2 mixing ratio, $\delta^{18}O$-CO_2 and $\delta^{13}C$-CO_2 were obtained from TDLAS measurements at 50 m height. Since there were no measurements available, $\delta^{18}O$ of water vapor and rainfall were derived in daily resolution from the Isotope-incorporated Global Spectral Model (IsoGSM; Yoshimura et al., (2008)), taking the nearest grid point to the study site (11° 25' E and 48°57' N). Most soil and plant parameters for the model were taken from Weis et al. (2007) and Huber et al. (2010) (Table IV.1). Since the understory at the study site was dominated by mosses (Huber et al., 2010), it was not considered in the simulation.

Previous versions of the model allowed the computation of $\delta^{18}O$-CO_2 profiles in the canopy (Ogee et al., 2004). The model calculates the concentration of the CO_2 isotopologues at any height making use of the Lagrangian turbulent transfer scheme (Raupach, 1989b) that includes the CO_2 flux from the soil, a source/sink term (S_j) of each vegetation layer j and a turbulent dispersion matrix, which relates the source/sink terms to the scalar concentrations and is calculated based on the localized near-field theory (Raupach, 1989a). Here, S_j is defined as:

$$S_j = F_{a\,j} * (\delta^{18}O_{a\,j} - \Delta_{A\,j}) / (1 + \delta^{18}O_{a\,j} / 1000) \quad \text{(IV.7)}$$

The respective equations have been described analogously for ^{13}C in more detail in the appendix of Ogee et al. (2003b). For this study, the degree of isotopic CO_2-H_2O equilibrium inside the leaf (θ) was implemented as an adjustable parameter. The parameter θ is used by the model to compute Δ_A according to eq. IV.3. To test whether simulations of canopy $\delta^{18}O$-CO_2 could be

improved by a suitable parameterization of θ, we ran the model simulations with different θ values. We used θ = 0.53, which was the average value derived from gas exchange measurements with Norway spruce in a plant chamber, as the default parameterization. Furthermore, the soil discrimination against $CO^{18}O$, i.e. $CO^{18}O_s$, was included as a new output variable. The model study was complemented by simulations of the carbon isotope ratio of canopy CO_2 ($\delta^{13}C$-CO_2), which were only used for interpretation of model output and not discussed specifically, as the focus of this study was on $\delta^{18}O$.

Table IV.1 Plant and (depth-dependent) soil parameters used for MuSICA simulations where α and N are the shape parameters of the water retention curve, κ is the tortuosity factor, K_{sat} is the soil saturated hydraulic conductivity, M is the particle size distribution curve parameter, SWC_{sat} and SWC_{res} are the saturation and residual soil water content, respectively, LAI is the leaf area index, ρ is the Péclet number, Q_{10s} is the temperature coefficient of the soil respiration rate, and R_{25} is the soil respiration rate at 25 °C.

Parameter	**Value**				
Soil depth [m]	**0.05**	**0.10**	**0.15**	**0.225**	**0.55**
α [cm^{-1}]	0.03	0.03	0.04	0.007	0.007
κ [-]	0.67	0.67	0.67	0.67	0.67
K_{sat} [m d^{-1}]	2.31	2.31	2.31	1.2	0.1
M	0.5	0.5	0.5	0.5	0.5
N	1.37	1.67	1.43	1.23	1.56
SWC_{sat} [m^3 m^{-3}]	0.37	0.37	0.37	0.37	0.38
SWC_{res} [m^3 m^{-3}]	0.16	0.16	0.16	0.0	0.1
Canopy height top [m]	37				
Canopy height bottom [m]	12.6				
LAI [-]	7.56				
ρ [-]	0.15				
Q_{10s} [-]	2.7				
R_{25} [mol m^{-2} s^{-1}]	6e-6				
water volume per LAI [mol m^{-2}]	12				

For the validation of the model simulations, the root mean square error (RMSE), its systematic and unsystematic components ($RMSE_s$, $RMSE_u$), the coefficient of determination (r^2), the slope and intercept of an ordinary least-squares regression between the simulated and observed

variable, and an index of agreement (d) according to Willmott (1981) were calculated. The RMSE and its components have the units of the respective variable, whereas d varies between 0 and 1, with a value of 1 indicating a perfect model−data fit.

IV.3 Results

IV.3.1 Boundary conditions of climate and atmospheric CO_2

Daily mean values for total incoming short-wave radiation (R_g) for the Norway spruce stand showed a clear seasonal pattern with maximum values of up to 300 W m^{-2} s^{-1} in summer and lowest values around 50 W m^{-2} s^{-1} during winter (Fig. IV.1). Periods with no rain and precipitation events were evenly distributed throughout the year, while the highest precipitation events with up to 30 mm per day occurred during summer. The oxygen isotope ratio in precipitation ($\delta^{18}O_{Prec}$) varied between –2 and –10 ‰ from April to October but was considerably lower before and after that period, with the lowest values of –40 ‰ in December 2007. Similar to R_g, air temperature (T_{air}) was highest during summer, with values up to 25 °C, and lowest in winter, ranging between –5 and +5 °C. Daily means of atmospheric pressure and air relative humidity (*rh*) did not show a strong seasonal pattern, but a clear day-to-day variability. The seasonal variation of CO_2 mixing ratio [CO_2] above the canopy was complementary to R_g and T_{air}, as daily means of [CO_2] were lowest in summer, with a minimum at 370 ppmv, and higher during winter, with values up to 420 ppmv. From March to May 2008, the day-to-day variability of [CO_2] was reduced compared to the rest of the year. Carbon and oxygen isotope ratios of atmospheric CO_2 above the canopy increased from March onward and were highest during summer, before they decreased again in late summer/autumn. The range of $\delta^{13}C$-CO_2 and $\delta^{18}O$-CO_2 daily means over the year was –11 to –6 ‰ and –4 to +4 ‰, respectively. A striking increase of [CO_2] up to 480 ppmv within several days was observed in

December 2007. At the same time the ^{13}C and ^{18}O content of atmospheric CO_2 decreased remarkably, whereas P was high and T_{air} and wind speed (U) were relatively low (Fig. IV.1).

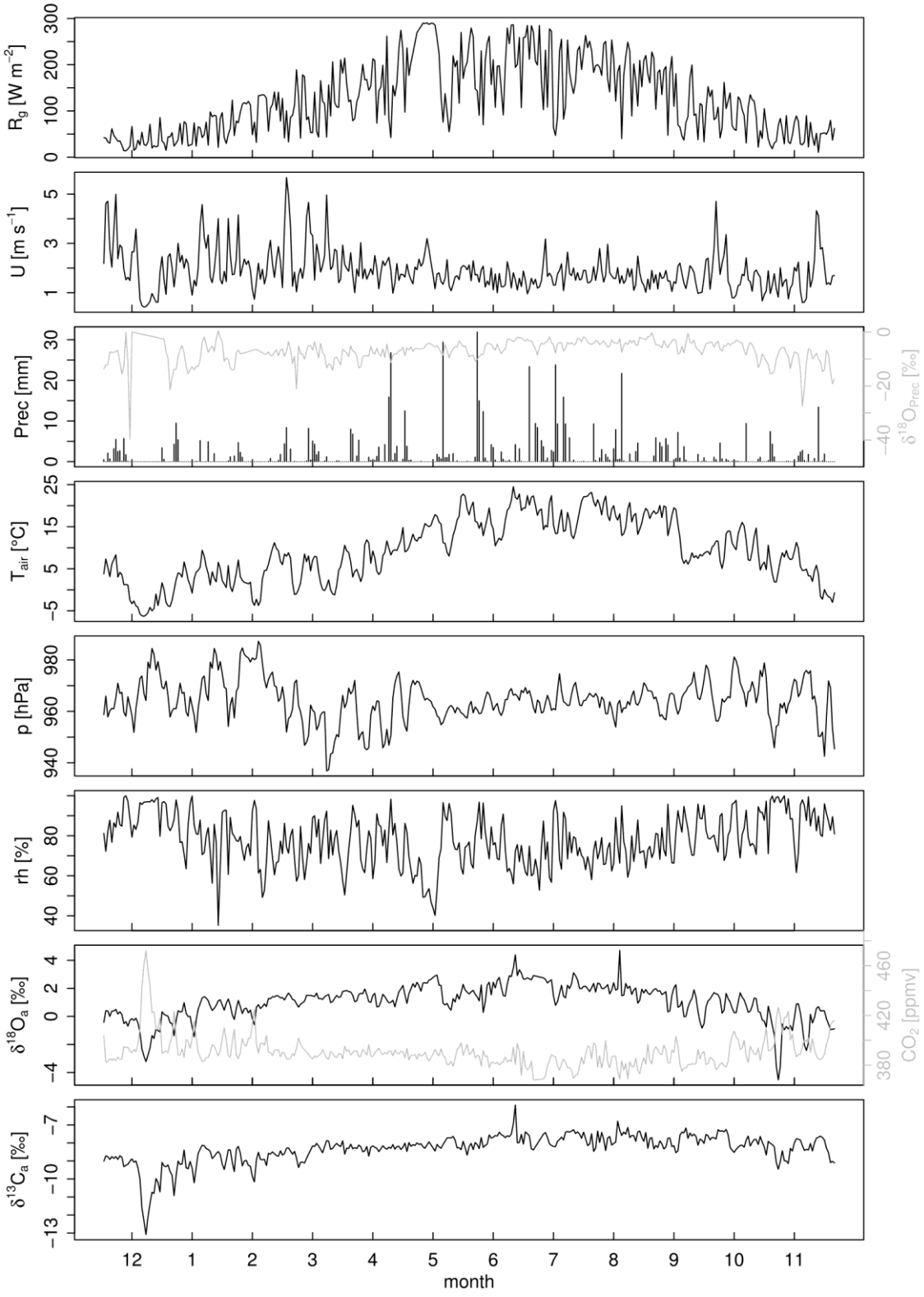

Figure IV.1 Global incoming radiation (R_g), wind speed (U), precipitation ($Prec$), $\delta^{18}O$ of $Prec$, air temperature (T_{air}), atmospheric pressure, relative humidity, CO_2 mixing ratio, $\delta^{13}C$ and $\delta^{18}O$ of CO_2 at forcing height + 40 m above the ground.

IV.3.2 Model validation

IV.3.2.1 Non-isotope variables

Since we did not use any EC flux data to force the model simulation, we could validate the model by comparing the simulated with the measured fluxes of energy and CO_2 at the Norway spruce site. The model–data agreement for net radiation (R_{net}) was high, with an r^2 of 0.9 and RMSE of 54.82 W m^{-2}, which was dominated by the unsystematic error component $RMSE_u$, and an index of agreement close of d=0.97 (Table IV.2). For the scalar flux data, the model–data agreement varied for the different months and was generally lower than for R_{net} (Table IV.2, Table C 1).

Table IV.2 Statistical results for the linear regression between simulated and measured net radiation (R_{net}), sensible, latent, and soil heat flux (H, LE, G), net ecosystem exchange (NEE), soil temperature (T_s) and soil water content (SWC) based on 30 min data of the whole data set. N is the number of data points.

	Intercept	**Slope**	**r^2**	**RMSE**	**$RMSE_u$**	**$RMSE_s$**	**d**	***n***
***R_{net}* [W m^{-2}]**	10.06	0.99	0.90	54.82	53.98	9.53	0.97	17568
***H* [W m^{-2}]**	2.58	0.87	0.44	52.90	108.20	15.31	0.78	17568
***LE* [W m^{-2}]**	27.86	0.48	0.46	80.67	56.19	57.89	0.78	17568
***G* [W m^{-2}]**	0.84	1.12	0.14	15.33	15.28	1.20	0.37	17568
***NEE* [mol m^{-2} s^{-1}]**	1.6e−05	0.45	0.24	1.1−04	8.0e-5	7.2e-5	0.57	17568
***T_s* [°C]**								
-5 cm	-1.62	1.32	0.93	2.50	1.79	1.75	0.95	17568
-10 cm	-1.53	1.37	0.90	2.92	2.06	2.07	0.93	17568
-15 cm	-1.02	1.35	0.86	3.18	2.36	2.14	0.91	17568
-20 cm	-1.87	1.40	0.88	3.01	2.21	2.05	0.92	17568
***SWC* [-]**								
-5 cm	10.36	0.48	0.78	1.54	0.67	1.39	0.85	17568
-10 cm	14.25	0.20	0.68	2.40	0.37	2.37	0.46	17568
-15 cm	10.21	0.46	0.69	1.61	0.66	1.47	0.74	17568
-20 cm	-2.77	1.14	0.76	1.54	1.45	0.51	0.9	17568

Figure IV.2 shows exemplarily a time series of the measured and simulated fluxes for May 2008. The figure reveals that the measured data for *LE* and *NEE* still contained some outliers,

although the data had run through the standard EC data processing, which could explain the relatively low r^2 for these variables. Furthermore, modeled daytime *NEE* was lower than measured *NEE* during several days in May 2008, which was also the general trend for the whole data set (Fig. IV.2, Table IV.2). The temporal dynamics and amplitudes of the soil heat flux (*G*) were lower in the simulated than in the measured data (Fig. IV.2), which is also reflected in the low r^2 (Table IV.2). Soil temperature (T_s) was reproduced well by the model, with an r^2 of up to 0.93, slightly decreasing with depth. Soil temperature at the different depths was slightly higher in the simulated than in the measured data during summer and lower in December 2007 (Fig. IV.3). The temporal dynamics of the volumetric soil water content (*SWC*) were simulated reasonably well with an overall r^2 between 0.68 (at –10 cm) and 0.78 (–5 cm) for the different depths, but *SWC* was overestimated at 5 cm, 10 cm and 15 cm depth in autumn 2008 (Fig. IV.3).

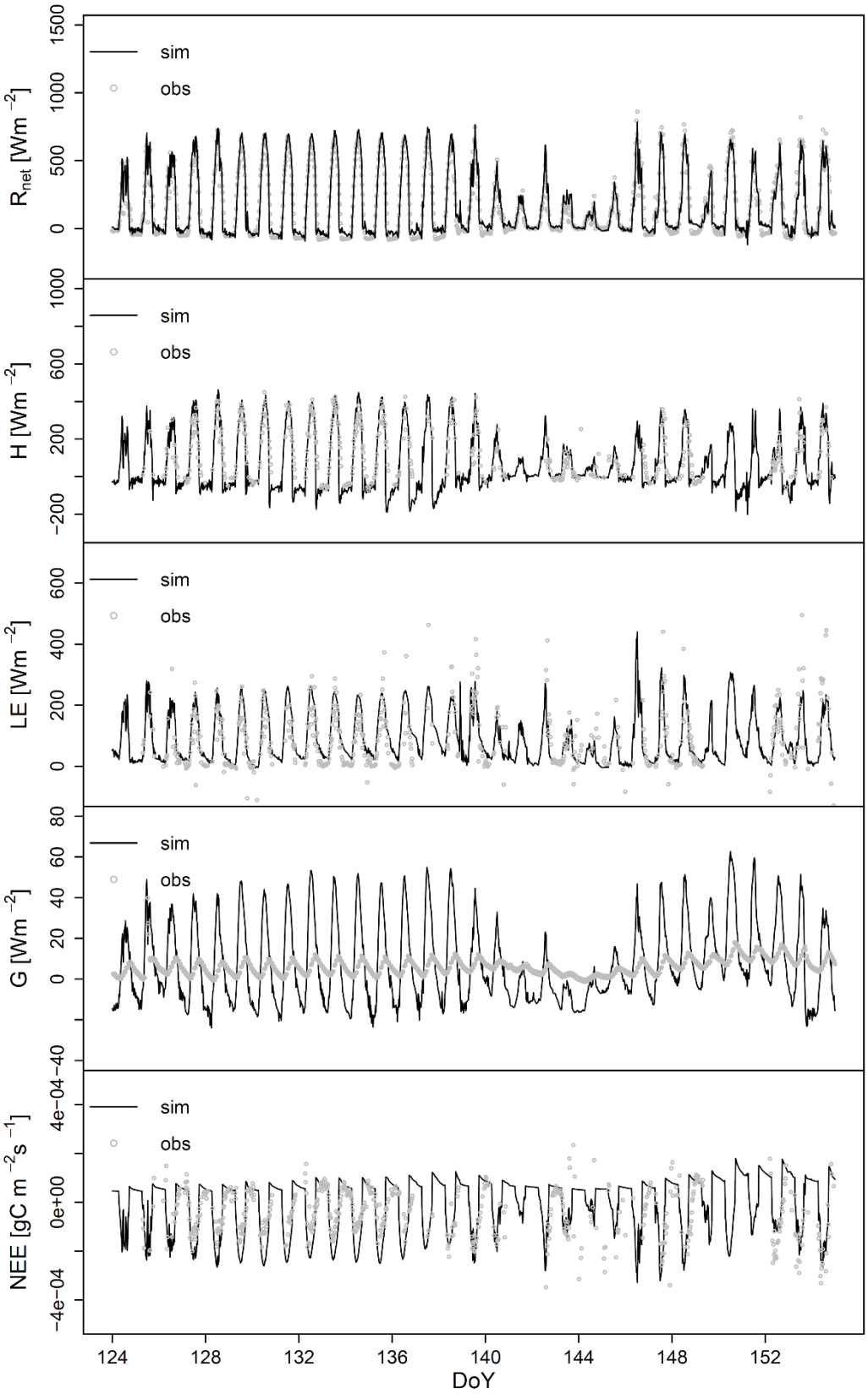

Figure IV.2 Simulated and measured net radiation (R_{net}), sensible and latent heat flux (*H*, *LE*), soil heat flux (*G*), and net ecosystem exchange (*NEE*) in May 2008.

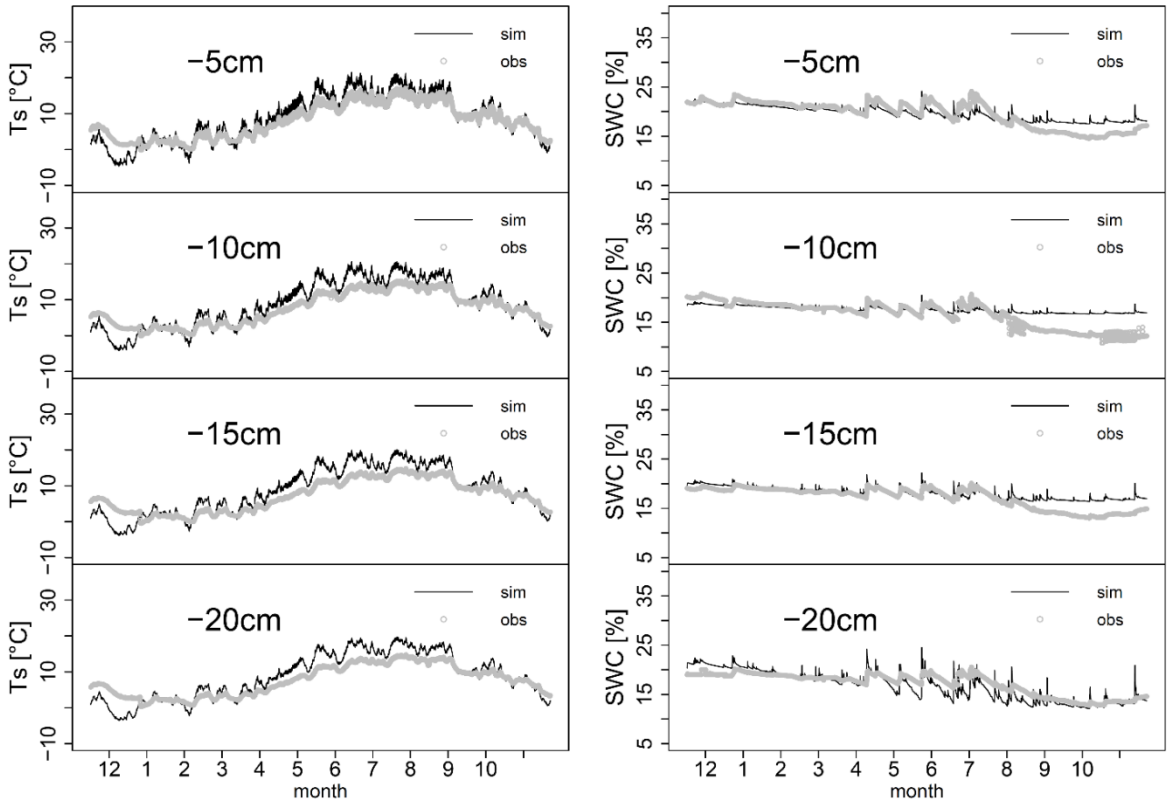

Figure IV.3 Simulated and measured soil temperature (left panel) and volumetric soil water content (right panel) at different depths.

IV.3.2.2 [CO_2] and CO_2 isotope air profiles

The highest r^2 between measured and simulated [CO_2] at 2 m, 8 m and 15 m height was 0.5 (Table IV.3). The RMSE for these heights was between 19 and 29 ppmv, and was mainly composed of an unsystematic error with an $RMSE_u$ between 17 and 27 ppmv. However, simulations and measurements agreed almost completely ($r^2 = 1$) at 50 m, which is 10 m above the forcing height of the simulations. Measured and simulated $\delta^{18}O$-CO_2 agreed well at all four heights, with a maximum r^2 of 1 at 50 m and a minimum r^2 of 0.66 at 2 m (Table IV.3).

Table IV.3 Statistical results for the linear regression between simulated and measured values of CO_2 mixing ratio, $\delta^{18}O$-CO_2, and $\delta^{13}C$-CO_2 at different heights based on 30 min data for 12 months. *N* is the number of data points.

Height above ground	**Intercept**	**Slope**	**r^2**	**RMSE**	**$RMSE_u$**	**$RMSE_s$**	**d**	***n***
2 m								
[CO_2] [ppmv]	54.65	0.88	0.36	28.60	27.56	7.63	0.70	17566
$\delta^{18}O$-CO_2 [‰]	0.20	0.79	0.66	0.89	0.84	0.31	0.89	17566
$\delta^{13}C$-CO_2 [‰]	-1.81	0.80	0.46	1.04	1.01	0.24	0.8	17566
8 m								
[CO_2] [ppmv]	59.48	0.87	0.36	24.89	23.1	9.28	0.67	17566
$\delta^{18}O$-CO_2 [‰]	0.05	0.84	0.77	0.71	0.67	0.24	0.93	17566
$\delta^{13}C$-CO_2 [‰]	-2.01	0.79	0.51	0.94	0.87	0.34	0.82	17566
15 m								
[CO_2] [ppmv]	49.47	0.89	0.48	18.39	16.91	7.22	0.77	17566
$\delta^{18}O$-CO_2 [‰]	0.03	0.88	0.87	0.53	0.50	0.18	0.96	17566
$\delta^{13}C$-CO_2 [‰]	-1.52	0.85	0.66	0.72	0.67	0.28	0.89	17566
50 m								
[CO_2] [ppmv]	-1.95	1.0	1.0	1.13	1.04	0.43	1	17566
$\delta^{18}O$-CO_2 [‰]	0.00	1.0	1.0	0.03	0.03	0.01	1	17566
$\delta^{13}C$-CO_2 [‰]	0.06	1.00	1.00	0.04	0.04	0.02	1	17566

The daily averages shown in Fig. IV.4 underline the good fit for $\delta^{18}O$-CO_2 and the lower model−data agreement for [CO_2], which is most obvious for the summer months of 2008, when [CO_2] was higher in the model than in the measured data at 2 m, 8 m and 15 m, both during day- and nighttime. However, the model–data agreement was higher during winter months at the beginning of the time series, when even the striking [CO_2] peak in December 2007 was reproduced (Fig. IV.4). The peak in [CO_2] was accompanied by a depression in $\delta^{18}O$-CO_2, which was also represented well in the simulated values. Overall, the seasonal trend with higher $\delta^{18}O$-CO_2 in summer and lower $\delta^{18}O$-CO_2 in winter was reproduced adequately by the model

(Fig. IV.4). The model–data agreement for $\delta^{13}C\text{-}CO_2$ increased with canopy height and was slightly lower than for $\delta^{18}O\text{-}CO_2$ (Table IV.3).

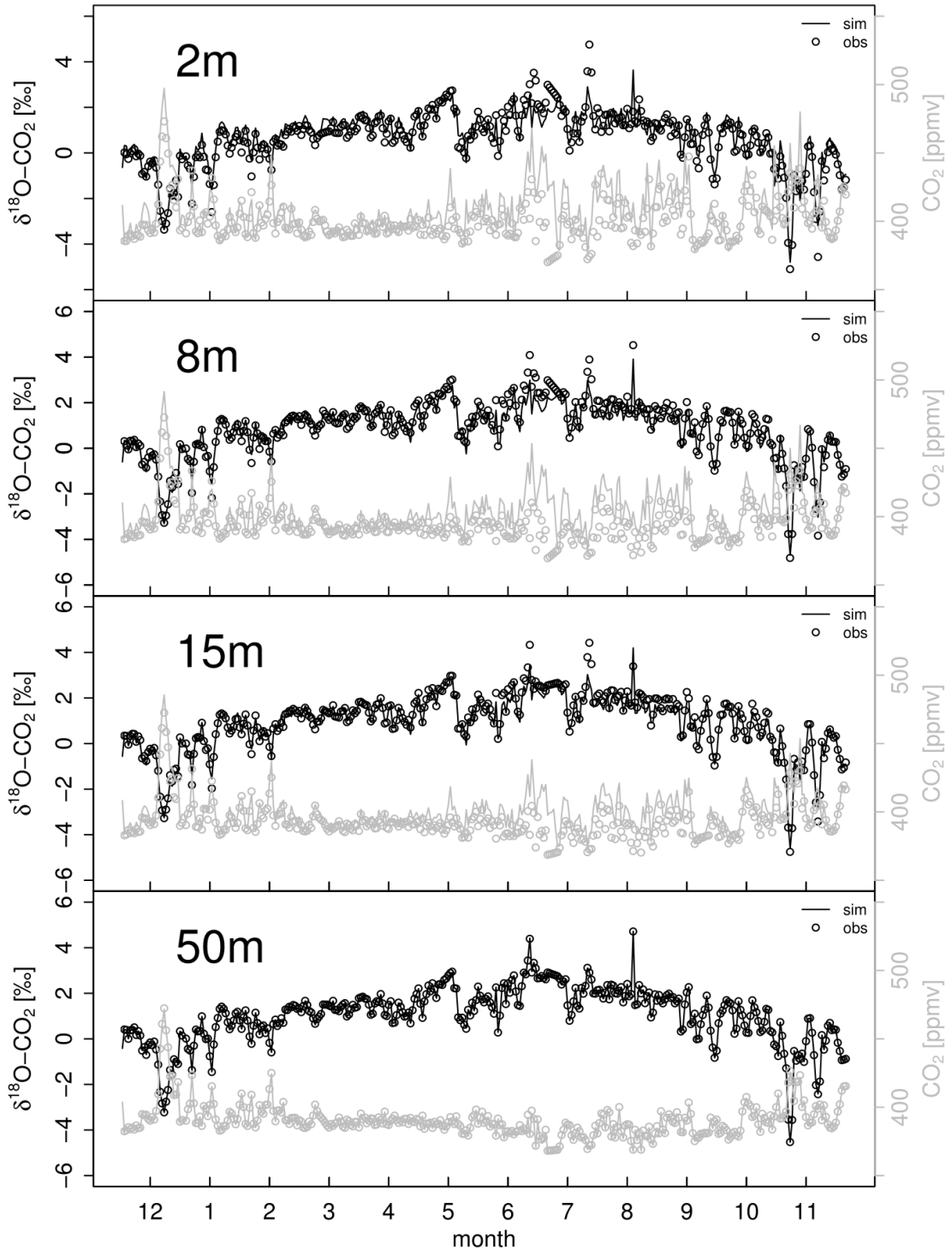

Figure IV.4 Daily averages of simulated and measured $\delta^{18}O$-CO_2 (in black color, left axis) and CO_2 mixing ratio (in grey color, right axis) at different heights.

The model−data fit related to $\delta^{18}O$-CO_2 inside the canopy was influenced by the different parameterizations of θ (Table IV.4). When the 30-min raw data of one year were considered, the r^2 was highest and the RMSE smallest for θ = 0.53, which was the θ obtained for Norway spruce from gas exchange measurements in plant chambers in a previous study, and was used as default value in this study. Taking into account a measurement precision of 0.1 ‰ for $\delta^{18}O$-CO_2, the RMSE resulting from parameterization with θ =0.53 was therefore significantly lower than the RMSE obtained from simulations with θ =1 (Table IV.4).

Table IV.4 Statistical results for model-data fit of $\delta^{18}O$-CO_2 at +15 m height for model runs with different parameterizations of the degree of leaf isotopic CO_2−H_2O equilibrium (θ). Default parameterization is shown in bold numbers. *N* is the number of data points.

θ	Intercept	Slope	r^2	RMSE	$RMSE_u$	$RMSE_s$	d	*n*
0.53	**0.03**	**0.88**	**0.87**	**0.53**	**0.50**	**0.18**	**0.96**	17566
0.6	0.03	0.89	0.85	0.57	0.54	0.17	0.96	17566
0.7	0.05	0.90	0.85	0.55	0.53	0.15	0.96	17566
0.8	0.06	0.91	0.86	0.55	0.53	0.14	0.96	17566
1	0.08	0.93	0.80	0.67	0.66	0.11	0.95	17566

When the summary statistics were calculated for individual months of the study period, the optimum θ parameterization varied considerably (Table IV.5). Assuming a full isotopic equilibrium (θ = 1) yielded the best results in June, August, and September 2008, whereas for other months parameterizations with θ < 1 resulted in a better model−data agreement (Table IV.5). The parameterization of θ = 0.53 yielded the best fit in December, January, and March.

Table IV.5 Best parameterization (highest r^2, lowest RMSE) of the degree of leaf isotopic CO_2–H_2O equilibrium (θ) for model-data fit of $\delta^{18}O$-CO_2 at +15 m height for individual months. *N* is the number of data points.

Month	**best θ**	**r^2**	**RMSE**	***n***
12	0.53	0.90	0.38	1440
1	0.53	0.81	0.43	1440
2	0.7	0.66	0.43	1441
3	0.53	0.52	0.29	1441
4	0.8	0.76	0.35	1441
5	0.7	0.83	0.43	1441
6	1	0.67	0.71	1441
7	0.8	0.62	0.65	1441
8	1	0.57	0.69	1441
9	1	0.78	0.57	1441
10	0.8	0.83	0.36	1441
11	0.7	0.92	0.45	1441

IV.3.2.3 F_r and soil $CO^{18}O$ isoflux

The soil respiration rate (F_r) showed a clear seasonal pattern, with maximum values up to 4 µmol m^{-2} s^{-1} during summer 2008, and was reproduced well by the model (Fig. IV.5 a). However, daily averages of F_r were approximately 0.7 µmol m^{-2} s^{-1} higher in the simulated than in the measured data in autumn 2008 (Fig. IV.5 a). Like F_r, the soil $CO^{18}O$ isoflux ($CO^{18}O_s$) varied seasonally, with the most negative values around –50 µmol m^{-2} s^{-1} ‰, occurring in summer 2008 (Fig. IV.5 b). The seasonal pattern of $CO^{18}O_s$ was captured well by the model, whereas for the sub-seasonal day-to-day variability the model–data agreement was lower leading to a lower r^2 than for F_r (Fig. IV.5 b). The modeled $CO^{18}O_s$ was on average approximately 15 µmol m^{-2} s^{-1} ‰ lower (less negative) than the measured $CO^{18}O_s$ with the highest model−data offset in the summer months.

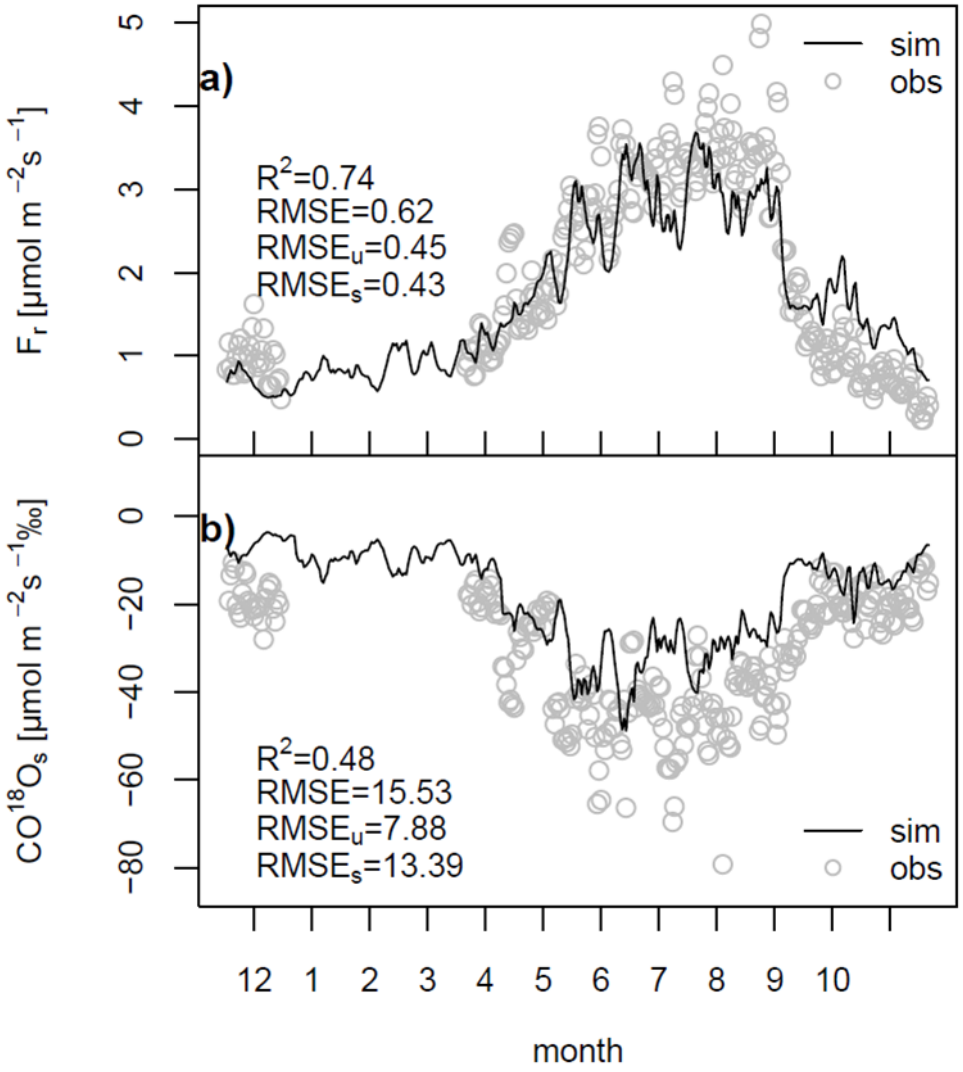

Figure IV.5 Daily averages of simulated and measured soil respiration rate (a), and soil $CO^{18}O$ isoflux (b). Statistical results for the linear regression between simulated and measured data are based on 30 min data.

IV.4 Discussion

IV.4.1 Simulation of $\delta^{18}O$-CO_2 in air profile

The model–data agreement was good for $\delta^{18}O$-CO_2 at the four different heights available for validation, with the agreement increasing with height. The very good agreement at 50 m is not surprising, as the model was forced with atmospheric $\delta^{18}O$-CO_2 at 40 m height and the maximum canopy height was 37 m. MuSICA was also able to reproduce the depression in $\delta^{18}O$-CO_2 and the concurrent peak in [CO_2] in December 2007. Since this phenomenon went along

with a depression in $\delta^{13}C$-CO_2, it can be explained by the advection of fossil CO_2 favored by an atmospheric inversion, which was indicated by the meteorological boundary conditions, such as low U and T_{air} as well as high p (Fig. IV.1). The performance of MuSICA with regard to the simulation of $\delta^{18}O$-CO_2 profiles in air was already reported previously (Ogee et al., 2004). In the former study, a full isotopic equilibrium between CO_2 and leaf water at the evaporation sites was firmly implemented, whereas in the present study the value for θ could be adapted in the parameter file for each simulation. The parameterization with θ = 0.53, which was the value obtained from laboratory experiments with Norway spruce, yielded a significantly better model−data agreement for $\delta^{18}O$-CO_2 than θ = 1, which is a commonly used default value for conifers (Gillon and Yakir, 2001). This demonstrates that θ values derived from isotopic gas exchange measurements provide useful estimates for the species-specific parameterization of ecosystem $\delta^{18}O$-CO_2 models and highlights once more that θ determined from leaf-level *CA* activity, as the above mentioned average θ for conifers, might be unrealistic at the canopy level (Griffis et al., 2011; Xiao et al., 2010).

The fact that different parameterizations of θ were required for individual months to achieve the best model−data fit for canopy $\delta^{18}O$-CO_2, suggested that θ might be variable throughout the year, e.g., related to seasonal variations in environmental conditions. Previous indications of a temporally variable θ were given by Cousins et al. (2006), who showed that θ varied with light intensity, and Gangi et al. (2015), who demonstrated a drought-induced decrease of θ for several plant species. Reported variations in leaf *CA* activity determining the hydration reaction and therefore θ, in dependence of soil water availability, osmotic stress, and light exposure (Durand et al., 2011; Tiwari et al., 2006; Yu et al., 2007) are supportive of a dynamic θ over time. However, we cannot completely exclude that other factors, apart from the parameterization of θ, influenced our simulation results for $\delta^{18}O$-CO_2. For example, the simulation of the $\delta^{18}O$ of

leaf water at the evaporation site, which caused errors in $\delta^{18}O$-CO_2 simulations in a previous study (Ogee et al., 2004), could not be validated due to unavailable measurement data.

IV.4.2 Simulation of soil-atmosphere ^{18}O exchange

For this study, the soil $CO^{18}O$ isoflux ($CO^{18}O_s$) was newly implemented in MuSICA. We could validate the model's performance of simulating $CO^{18}O_s$ by comparing it with $CO^{18}O_s$ calculated from F_r and $\delta^{18}O_s$ obtained from soil chamber measurements. The observed and simulated $CO^{18}O_s$ for the spruce forest floor was in the same range (between –10 and –100 µmol m^{-2} s^{-1} ‰) as previously reported for a grassland (Riley et al., 2003) and a corn-soybean rotation (Griffis et al., 2011). The one-year dataset revealed seasonal variations in $CO^{18}O_s$, with less negative values in winter and the most negative $CO^{18}O_s$ in summer, which corresponded to $\delta^{18}O_s$ values of approximately –12 ‰. The seasonal variations in $CO^{18}O_s$ were represented well by the model. However, the model−data agreement was lower at shorter time scales (day-to-day or diurnal) and simulated $CO^{18}O_s$ was on average less negative than measured $CO^{18}O_s$. The offset between modeled and observed $CO^{18}O_s$ can be explained as follows: The observed $CO^{18}O_s$ was calculated as a product of F_r and $\delta^{18}O_s$. The measured $\delta^{18}O_s$ was derived from a mass balance (eq. IV.5), based on measurements of $\delta^{18}O$-CO_2 and [CO_2] at the inlet and outlet of the soil chamber. This approach, therefore, yielded an "apparent" $\delta^{18}O$-CO_2 of the net CO_2 flux, resulting in very large $\delta^{18}O_s$ values due to the effect of atmospheric CO_2 invasion and back-diffusion, which considerably influences $\delta^{18}O$-CO_2, but not the net CO_2 flux (Kapiluto et al., 2007; Miller et al., 1999; Tans, 1998). In contrast to this, MuSICA computes $CO^{18}O_s$ directly by numerically solving the mass balance for $CO^{18}O$ in the soil and without considering the atmospheric CO_2 invasion and back-diffusion, and the enhancement of this process by catalytic activity of *CA*. Seibt et al. (2006b) observed a similar discrepancy between more negative measured and less negative modeled $\delta^{18}O$ of soil CO_2 fluxes. They only achieved a

good model−data agreement, when the hydration rate in the model was increased by a factor of 140, i.e., when substantial soil *CA* activity was assumed. In addition, Santos et al. (2012) discussed that soil *CA* activity might be temporally variable, and suggested the use of a temporally variable *CA* factor. The fact that the discrepancy between simulated and measured $CO^{18}O_s$ was highest in summer 2008, when the highest T_s of the measurement period occurred, i.e., soil *CA* activity was likely highest (Stern et al., 2001), was consistent with the theory that non-consideration of *CA* activity by MuSICA contributed to the discrepancy between model and data. Apart from the hydration rate, the $\delta^{18}O$ of the CO_2 soil efflux is largely determined by the $\delta^{18}O$ of soil water (Stern et al., 1999). Taking $\delta^{18}O$ of water vapor and rainfall for the model´s forcing file from IsoGSM could have biased the simulated $\delta^{18}O_{sw}$, i.e. $\delta^{18}O$-CO_2. Since no measured data of $\delta^{18}O_{sw}$ was available, though, we could not examine the contribution of a potential mismatch between modeled and measured $\delta^{18}O_{sw}$ on $CO^{18}O_s$.

A more mathematical explanation for the model−data disagreement of $CO^{18}O_s$ in winter 2007 can be found in the very small difference between [CO_2] at the inlet and outlet of the soil chambers due to low F_r, minimizing the denominator in the mass balance used to calculate $\delta^{18}O_s$ and thus leading to very negative $\delta^{18}O_s$, i.e. $CO^{18}O_s$, derived from measurements. To obtain reliable estimates of $\delta^{18}O_s$ from measurements in the field at low F_r, e.g., in winter, $\delta^{18}O_s$ could be estimated *via* methodologies, which are independent of a chamber mass-balance, like, for example, mini-tower $\delta^{18}O$ Keeling plots (Mortazavi et al., 2004). Alternatively, direct measurements of $\delta^{18}O$ of soil CO_2 could be conducted by installing gas-permeable tubing in soils and continuously monitoring soil $\delta^{18}O$-CO_2 *via* laser-based spectroscopy.

As Ogee et al. (2004) pointed out, the magnitude of the isotopic ^{18}O disequilibrium, which is a requirement for ^{18}O-based carbon flux partitioning, depends on the ecosystem. Overall, the combination of the depleted $\delta^{18}O$ signal from the soil and the enriched $\delta^{18}O$-CO_2 signal within the canopy indicates that, especially in summer time, D_{eq} within the Norway spruce forest would

be sufficiently high to allow for ^{18}O-based carbon flux partitioning. In this respect, eddy covariance measurements of CO_2 isotopologues using a QCLAS could be conducted at a position close to the canopy that yields a high signal-to-noise ratio, as recently suggested by Sturm (2012).

IV.4.3 Conclusions

As Welp et al. (2011) demonstrated, not only ecosystem F_r/F_a partitioning, but also global GPP derived from $\delta^{18}O\text{-}CO_2$, strongly depend on the underlying assumptions related to θ and the soil invasion flux. In this study, we showed that estimates of θ derived from isotopic gas exchange experiments can improve predictions of canopy $\delta^{18}O\text{-}CO_2$ and that different parameterizations of θ were required over time to further improve the model–data fit of canopy $\delta^{18}O\text{-}CO_2$, although the effect was only small. This finding indicates that the implementation of a (temporally) variable parameterization of θ could increase the accuracy of simulated photosynthetic ^{18}O discrimination. This approach could therefore help reducing the uncertainties related to global CO_2 fluxes between the terrestrial biosphere and the atmosphere, but also highlights the need for further experimental studies examining temporal variations of θ.

Our study also revealed that simulations of the newly implemented $CO^{18}O_s$ did not match $CO^{18}O_s$ derived from measurements with soil respiration chambers and mass balance calculations, with the largest offset in summer. We assume the reason is that atmospheric CO_2 invasion and back-diffusion was insufficiently accounted for in the model simulations, which implied zero *CA* activity. The implementation of soil *CA* activity into MuSICA and other similar soil models should therefore be addressed in the future.

V. Synopsis

V.1 Summary

The overall aim of the present study was to identify and quantify the processes and factors that influence the oxygen isotope exchange between atmospheric CO_2 and the water pools in leaves and soil. This is important for the quantitative use of $\delta^{18}O\text{-}CO_2$ measurements, i.e., to derive independent estimates of gross primary productivity (GPP) based on atmospheric $\delta^{18}O_a$.

The research was based on highly innovative, simultaneous measurements of oxygen isotope ratios of H_2O and CO_2 in the gas phase with infrared laser-based spectroscopy and included the development of a novel methodology for isotope-specific, simultaneous soil gas profile measurements of H_2O and CO_2. The work was complemented by simulation studies using a process-based numerical model. The main results of this study and their relevance for future research are summarized in the following sections. Furthermore, the hypotheses which were formulated in the general introduction (I.4) are taken up below.

i) Short-term variations of environmental conditions significantly influence $CO^{18}O$ isoforcing, i.e. the plants' impact on atmospheric $\delta^{18}O\text{-}CO_2$, *via* induced changes in the respective drivers (θ, g_s, A_r, $\delta^{18}O_{ev}$) of the oxygen isotope exchange, which vary between plant species.

The impact of short-term variations of environmental conditions on the ^{18}O-exchange between CO_2 and leaf water and the underlying processes and factors had not been sufficiently characterized for different plant functional types prior to this study. To address this research gap, $\delta^{18}O$ of CO_2 and water vapor were measured *online* in chamber-based experiments using infrared laser analyzers. Poplar, maize, spruce, and wheat plants were exposed to elevated air temperature (35°C) and cessation of water supply in individual experiments. $CO^{18}O$ isoforcing ($CO^{18}O\text{-}Iso$) was reduced at 35°C compared to 25°C due to the reduction of stomatal conductance (g_s) in all plant species except for

maize, and at decreasing water availability in all four plant species due to a reduction of the degree of isotopic CO_2−H_2O equilibrium (θ), assimilation rate (A_r) and g_s, while leaf water at the evaporation site ($\delta^{18}O_{ev}$) became progressively ^{18}O-enriched. The θ, g_s, A_r and $\delta^{18}O_{ev}$ all together were important determinants of $CO^{18}O$-*Iso*, with the contribution of the individual factors depending on the plant species. The degree of isotopic CO_2–H_2O equilibrium calculated from isotopic gas exchange (θ) also differed between the plant species, reaching maximum values of 0.51 and 0.53 in maize and spruce, and 0.67 and 0.74 in wheat and poplar, respectively, and decreased in response to decreasing soil water availability.

ii) The $\delta^{18}O_{sc}$ signal over the soil profile is influenced by variations in $\delta^{18}O_{sw}$, $\delta^{18}O_a$, soil water content, and *CA* activity.

The oxygen isotope exchange in soils is very complex due to the different factors and processes that influence the respective reaction rate, such as soil water content (*SWC*), soil texture and tortuosity, and the catalytic activity of the enzyme carbonic anhydrase (*CA*) in different soil layers. The relevant processes have been addressed by modeling studies, but experimental data has been scarce. A new methodology to monitor the $\delta^{18}O$ of soil CO_2 ($\delta^{18}O_{sc}$) and soil water ($\delta^{18}O_{sw}$) nearly simultaneously at varying *SWC* was developed. Infrared laser spectroscopy was combined with gas-permeable polypropylene tubing installed at different depths in a sand column filled with medium sand. Profiles of $\delta^{18}O_{sw}$ showed the expected logarithmic pattern, with soil water becoming gradually ^{18}O-enriched from the top of the soil over several days. Measured $\delta^{18}O_{sc}$ indicated incomplete CO_2–H_2O isotopic equilibrium at low *SWC* (<0.1 m^3 m^{-3}) and followed temporal dynamics of $\delta^{18}O_a$ in the top 10 cm. Model simulations revealed that the effective rate constant of the oxygen isotope exchange (k_e) was around 0.012 s^{-1} and that k_e decreased

with depth. Irrigation of the sand column with tap water resulted in a temporary reset of $\delta^{18}O_{sw}$ in the drenched soil depths, while $\delta^{18}O_{sc}$ was only slightly affected. However, the addition of *CA* to the irrigation water demonstrated that *CA* activity significantly influenced $\delta^{18}O_{sc}$.

iii) Estimates of θ obtained from gas exchange measurements with single Norway spruce plants can be up-scaled and help to improve simulations of canopy $\delta^{18}O$-CO_2.

Several studies have indicated that the up-scaling of laboratory-based θ estimates to the canopy scale might be difficult. A biophysical soil–vegetation–atmosphere model, MuSICA, was parameterized with different values for θ, which included $\theta = 0.53$ obtained from gas exchange measurements with Norway spruce in this study. The model−data agreement for $\delta^{18}O$-CO_2 was significantly improved when using $\theta = 0.53$ instead of $\theta = 1$, the approximate average value for Norway spruce from a former study. Model simulations also revealed that the implementation of a temporally variable θ should be addressed in the future to account for dynamics in oxygen isotope exchange between CO_2 and H_2O at the leaf level in response to varying environmental conditions.

V.2 Synthesis

V.2.1 The oxygen isotope exchange between leaf and atmosphere

The degree of CO_2−H_2O isotopic equilibrium inside the leaf (θ) is an important factor for the parameterization of mechanistic $\delta^{18}O$-CO_2 models. Estimates of θ vary largely in the literature, and the only comprehensive survey on the variability of θ between different plant groups yielded θ as low as 0.4 for C_4 grasses and up to unity for C_3 trees (Gillon and Yakir, 2001). However, more current studies indicated much lower values for θ at the canopy scale (Griffis et al., 2011; Xiao et al., 2010). In the present study (chapter II), θ values of 0.51 and 0.53 in

maize and spruce, and 0.67 and 0.74 in wheat and poplar, respectively, were determined, being also lower than the θ estimates for the respective plant groups reported in the study by Gillon and Yakir (2001) and consistent with the previously reported lower canopy-based estimates of θ (Griffis et al., 2011; Xiao et al., 2010). With regard to the global atmospheric $\delta^{18}O\text{-}CO_2$ budget, a lower θ would be equivalent to an increase in GPP, which indeed would be in agreement with the higher GPP estimates reported in a previous ^{18}O-isotope-based study (Welp et al., 2011). The present study also showed that i) the magnitude of θ was correlated with the specific leaf *CA* activity of the plant species (chapter II), but also that ii) as discussed by Cousins et al. (2006), absolute θ values derived from leaf *CA* activity analysis were inappropriate to accurately reflect the actual θ. In fact, θ obtained from gas exchange measurements even allowed the observation of temporal variations in θ, induced, e.g., by limited water availability, a phenomenon which had been completely ignored in previous studies, where θ was usually assumed constant. In addition, the requirement of simultaneously measuring mesophyll conductance to derive precise θ estimates from gas exchange measurements was shown (chapter II) and is strongly recommended for future applications of this methodology.

The up-scaling of θ from measurements at the laboratory to the canopy scale is a crucial but not straightforward step, as previous studies indicated (Griffis et al., 2011; Santos et al., 2014). Hence, it was tested whether θ = 0.53, obtained for Norway spruce from gas exchange measurements at the single plant scale, yielded a suitable input parameter for simulations of $\delta^{18}O\text{-}CO_2$ in a Norway spruce forest with the ecosystem model MuSICA (chapter IV). A new version of MuSICA, which allowed the free parameterization of θ, replacing the previously constant default value of θ = 1, was applied, and the simulation results for canopy $\delta^{18}O\text{-}CO_2$ were validated with measured (isotope) data from a Norway spruce forest. The simulation study showed that a parameterization with θ = 0.53 reduced the RMSE for the $\delta^{18}O\text{-}CO_2$ model output significantly compared with θ = 1. A further outcome was that different values for θ between

0.5 and 1 yielded the best model−data fit for $\delta^{18}O\text{-}CO_2$ in different months (chapter IV). This finding was consistent with the temporal variability of θ observed in the first study (chapter II). A strong correlation between canopy $\delta^{18}O\text{-}CO_2$ and $\delta^{18}O_{ev}$ and the importance of considering isotopic non steady-state of leaf water enrichment for photosynthetic ^{18}O discrimination was emphasized in several studies (Griffis et al., 2011; Xiao et al., 2010). Owing to the laser-based technology applied in this study, the temporal dynamics of $\delta^{18}O_{ev}$ and their effect on $\delta^{18}O\text{-}CO_2$ could be monitored online (chapter II), i.e., free from the assumption of isotopic steady-state or information on the isotopic composition of source water (Simonin et al., 2013; Wang et al., 2012). Real-time measurements at the plant-scale allowed to monitor temporal variations in $\delta^{18}O_{ev}$, such as its drought-induced increase, and in the relationship between $\delta^{18}O\text{-}CO_2$ and $\delta^{18}O_{ev}$. The small θ and the specific *VPD* conditions inside the plant chamber, which resulted in unusual diurnal patterns of $\delta^{18}O_{ev}$, might have contributed to the weak relationship between $\delta^{18}O\text{-}CO_2$ and $\delta^{18}O_{ev}$ observed in this study (chapter II). To minimize potential artifacts introduced by unnatural temporal variations of $\delta^{18}O_{ev}$ and to obtain more physiological conditions in future experiments, the $\delta^{18}O$ of water vapor at the chamber inlet should be kept constant, e.g., by using a vaporization module (Simonin et al., 2013), and the diurnal *VPD* pattern should be adjusted with an alternative method.

In the present study (chapter II), the isoforcing concept of Lee (2009), in which the $CO^{18}O$-isoforcing ($CO^{18}O\text{-}Iso$) is defined as the EC flux of $CO^{18}O$, was adapted to the single plant level to quantify the plants' impact on ambient $\delta^{18}O\text{-}CO_2$ and to examine the drivers of $CO^{18}O\text{-}Iso$ for the four different plant species poplar, maize, spruce, and wheat. The combination of θ, g_s, A_r and $\delta^{18}O_{ev}$ explained up to 98% of the variations in $CO^{18}O\text{-}Iso$, while the relationship between the individual variables and $CO^{18}O\text{-}Iso$ was weaker. Chamber-based $CO^{18}O\text{-}Iso$ from gas exchange measurements and $CO^{18}O\text{-}Iso_{sim}$ derived from a mechanistic model (Lee et al., 2009) agreed well and showed that i) plant chamber measurements are an efficient methodology

to examine $CO^{18}O$-*Iso* for different plant species, and ii) provide a good alternative to labor-intensive field measurements and mechanistic models, which rely on some critical assumptions, e.g., related to θ (θ is time-invariant) and the calculation of $\delta^{18}O_{ev}$ (chapter II).

V.2.2 The oxygen isotope exchange between soil and atmosphere

Besides the ^{18}O discrimination by plants, the $\delta^{18}O$-CO_2 of soil efflux is a large contributor to temporal patterns in $\delta^{18}O_a$. The $\delta^{18}O$-CO_2 emitted from soils is not only determined by respired soil CO_2, but also by CO_2 that invades the soil, equilibrates with soil water and diffuses back to the atmosphere, the so-called soil invasion flux (Miller et al., 1999). As discussed by Welp et al. (2011), it is the soil invasion flux which adds large uncertainty to global GPP estimates derived from $\delta^{18}O_a$ budgets. In the past, the experimental examination of the ^{18}O-exchange in soils was limited in time and space due to discrete soil sampling procedures (Allison et al., 1987; Amundson et al., 1996), and studies were often based on analytical or numerical models (Amundson et al., 1998; Tans, 1998). Advances in optical isotope analyzers (Griffis, 2013) and gas-permeable tubing techniques (Gut et al., 1998) have opened up new possibilities in this respect (Goffin et al., 2014; Parent et al., 2013). In the present study (chapter III), a novel methodology, involving the aforementioned techniques, was successfully tested to monitor $\delta^{18}O_{sw}$ and $\delta^{18}O_s$ quasi simultaneously at different depths of a sand column at varying *SWC*. This is promising for future applications in the field because the temporal and spatial resolution of isotope measurements in natural soils could be considerably increased. The experiments conducted with the new setup (chapter III) revealed on the one hand the well-known logarithmic pattern in $\delta^{18}O_{sw}$, with soil water becoming gradually enriched from the top of the soil over several days, and on the other hand an incomplete CO_2–H_2O isotopic equilibrium at any depth of the sand column. Hence, the effective rate constant of the isotopic equilibration reaction (k_e) around 0.012 s^{-1}, as determined by confronting simulated with measured $\delta^{18}O_{sc}$, was too low to

allow full isotopic equilibrium at low *SWC* (< 0.1 m^3 m^{-3}) in the sand column. A rate constant of 0.012 s^{-1} corresponds to the reaction rate constant for the oxygen isotope exchange in pure water (k_s) (Skirrow, 1975). However, the model simulations also indicated that k_e was one to two orders of magnitude smaller at depths below 30 cm. Reaction rate constants smaller than 0.012 s^{-1} have already been suggested before and were explained with the interference of physical processes, such as the diffusion of CO_2 across the air/water interface in the soil (Stern et al., 1999). In spite of that, many studies still use simply the value of k_s as the rate constant of the oxygen isotope exchange between CO_2 and H_2O in soils (Riley et al., 2002; Seibt et al., 2006b; Wingate et al., 2009). The magnitude of k_e for different soil types and varying *SWC* and also the spatiotemporal variability of this factor, that was indicated by the model simulations of the present study (chapter III), should be examined in further experimental studies. This is of importance because a more thorough parameterization of k_e would improve simulations of $\delta^{18}O_{sc}$ and $\delta^{18}O_{sw}$ in soils, and therefore also reduce the uncertainties related to the modeled $\delta^{18}O$-CO_2 of soil efflux.

In the present study (chapter III) it was also shown that *CA* applied in an irrigation event enhanced the oxygen isotope equilibrium between CO_2 and H_2O in the top few cm of a sand column. Hence, for the first time, the effect of *CA* activity in soils was demonstrated in experiments, whereas it was rather deduced from model simulations before (Santos et al., 2014; Seibt et al., 2006b; Wingate et al., 2008). This is an important finding for the global ^{18}O budget of atmospheric CO_2, considering the fact that *CA* activity influences the $\delta^{18}O$ of the CO_2 gross fluxes from soils. In this respect, the present study (chapter III) also provides a promising methodology for clarifying the role of *CA* in natural soils. The importance of considering *CA* activity in soils was further highlighted in a simulation study related to the ecosystem exchange of a Norway spruce forest (chapter IV). The non-consideration of *CA* activity by MuSICA was a likely reason for the offset between simulated and measured soil $CO^{18}O$ isoflux.

V.3 Outlook

In this study, the oxygen isotope exchange in the soil–plant–atmosphere continuum was examined at the laboratory scale using a plant chamber and a sand column. The experiments contributed to a deeper knowledge about the processes and factors that influence the oxygen isotope composition of atmospheric CO_2 and yielded results that are relevant for future research. Estimates of θ for further plant species should be determined from gas exchange experiments, including measurements of g_m, rather than by analysis of leaf *CA* activity, to obtain unbiased results and capture temporal dynamics in θ. In this respect, a major outcome of this study was that current $\delta^{18}O\text{-}CO_2$ models should be extended by including a time-variable θ and a depth-dependent parameterization of soil *CA* activity and k_e. If in addition to more precise and species-specific θ estimates, the future distribution of plant functional types (C_3 and C_4 photosynthesis) is known, changes in the global carbon budget, e.g., related to climate change, could be predicted more reliably.

The novel methodology developed in this study, i.e., combining laser-based, simultaneous isotope measurements of H_2O and CO_2 in the soil with gas-permeable tubing, yielded promising results in sand column experiments. Its transfer to natural soils in the field offers the potential to bring forward research on the oxygen isotope exchange between soil water and CO_2, and thus, to minimize the uncertainties related to the soil component of the global $\delta^{18}O_a$ budget.

VI. References

Affek, H.P., Krisch, M.J.,Yakir, D., 2006. Effects of intraleaf variations in carbonic anhydrase activity and gas exchange on leaf $C^{18}OO$ isoflux in Zea mays. New Phytol. 169, 321-329.

Ainsworth, E.A.,Rogers, A., 2007. The response of photosynthesis and stomatal conductance to rising [CO_2]: mechanisms and environmental interactions. Plant Cell Environ. 30, 258-270.

Allison, G.B., Colinkaczala, C., Filly, A.,Fontes, J.C., 1987. Measurement of isotopic equilibrium between water, water vapor and soil CO_2 in arid zone soils. J. Hydrol. 95, 131-141.

Amundson, R., Wang, Y.,Int Atom Energy, A., 1996. Relationship between the oxygen isotopic composition of soil CO_2 and water, Isotopes in Water Resources Management, Vol 1. Proceeding Series of the International Atomic Energy Agency, pp. 315-332.

Amundson, R., Stern, L., Baisden, T.,Wang, Y., 1998. The isotopic composition of soil and soil-respired CO_2. Geoderma 82, 83-114.

Barbour, M.M., Fischer, R.A., Sayre, K.D.,Farquhar, G.D., 2000. Oxygen isotope ratio of leaf and grain material correlates with stomatal conductance and grain yield in irrigated wheat. Aust. J. Plant Physiol. 27, 625-637.

Barbour, M.M., Farquhar, G.D., Hanson, D.T., Bickford, C.P., Powers, H.,McDowell, N.G., 2007. A new measurement technique reveals temporal variation in delta O-18 of leaf-respired CO_2. Plant Cell Environ. 30, 456-468.

Barnes, C.J.,Allison, G.B., 1983. The distribution of deuterium and ^{18}O in dry soils: 1. Theory. J. Hydrol. 60, 141-156.

Barnes, C.J.,Allison, G.B., 1988. Tracing of water movement in the unsaturated zone using stable isotopes of hydrogen and oxygen. J. Hydrol. 100, 143-176.

Bazargani, M.M., Sarhadi, E., Bushehri, A.-A.S., Matros, A., Mock, H.-P., Naghavi, M.-R. et al., 2011. A proteomics view on the role of drought-induced senescence and oxidative stress defense in enhanced stem reserves remobilization in wheat. J. Proteomics 74, 1959-1973.

Behnke, K., Ehlting, B., Teuber, M., Bauerfeind, M., Louis, S., Hasch, R. et al., 2007. Transgenic, non-isoprene emitting poplars don't like it hot. Plant J. 51, 485-499.

Bottinga, Y.,Craig, H., 1968. Oxygen isotope fractionation between CO_2 and water, and the isotopic composition of marine atmospheric CO_2. Earth Planet. Sci. Lett. 5, 285-295.

Bowling, D.R., Baldocchi, D.D.,Monson, R.K., 1999. Dynamics of isotopic exchange of carbon dioxide in a Tennessee deciduous forest. Glob. Biogeochem. Cycles 13, 903-922.

Bowling, D.R., Tans, P.P.,Monson, R.K., 2001. Partitioning net ecosystem carbon exchange with isotopic fluxes of CO_2. Global Change Biol. 7, 127-145.

Braud, I., Dantas-Antonino, A.C., Vauclin, M., Thony, J.L.,Ruelle, P., 1995. A simple soil-plant-atmosphere transfer model (SiSPAT) development and field verification. J. Hydrol. 166, 213-250.

Brenninkmeijer, C.A.M., Kraft, P.,Mook, W.G., 1983. Oxygen isotope fractionation between CO_2 and H_2O. Isot. Geosci. 1, 181-190.

Buenning, N., Noone, D.C., Riley, W.J., Still, C.J.,White, J.W.C., 2011. Influences of the hydrological cycle on observed interannual variations in atmospheric $CO^{18}O$. J. Geophys. Res. Biogeosc. 116, G04001, doi:10.1029/2010jg001576.

Buenning, N., Noone, D.C., Randerson, J.T., Riley, W.J.,Still, C.J., 2014. The response of the $^{18}O/^{16}O$ composition of atmospheric CO_2 to changes in environmental conditions. J. Geophys. Res. Biogeosc. 119, 55-79.

Butterbach-Bahl, K.,Papen, H., 2002. Four years continuous record of CH(4)-exchange between the atmosphere and untreated and limed soil of a N-saturated spruce and beech forest ecosystem in Germany. Plant Soil 240, 77-90.

Cernusak, L.A., Farquhar, G.D., Wong, S.C.,Stuart-Williams, H., 2004. Measurement and interpretation of the oxygen isotope composition of carbon dioxide respired by leaves in the dark. Plant Physiol. 136, 3350-3363.

Ciais, P., Denning, A.S., Tans, P.P., Berry, J.A., Randall, D.A., Collatz, G.J. et al., 1997. A three-dimensional synthesis study of delta O-18 in atmospheric CO_2. 1. Surface fluxes. J. Geophys. Res. Atmos. 102, 5857-5872.

Cousins, A.B., Badger, M.R.,von Caemmerer, S., 2006. A transgenic approach to understanding the influence of carbonic anhydrase on (COO)-O-18 discrimination during C-4 photosynthesis. Plant Physiol. 142, 662-672.

Craig, H.,Gordon, L., 1965. Deuterium and oxygen-18 variations in the ocean and marine atmosphere. In:Tongiorgi, ed. Proceedings of a conference non stable isotopes in oceanographic studies and paleaotemperatures, Spoleto, Italy.

Cuntz, M., Ciais, P., Hoffmann, G.,Knorr, W., 2003. A comprehensive global three-dimensional model of delta O-18 in atmospheric CO_2. 1. Validation of surface processes. J. Geophys. Res. Atmos. 108, 4527, doi:10.1029/2002JD003153.

Cuntz, M., Ogee, J., Farquhar, G.D., Peylin, P.,Cernusak, L.A., 2007. Modelling advection and diffusion of water isotopologues in leaves. Plant Cell Environ. 30, 892-909.

Demir, N., Nadaroglu, H.,Demir, Y., 2009. Carbonic Anhydrase from Potato (Solanum tuberosum) Roots and Leaves. Asian J. Chem. 21, 5104-5116.

Domec, J.C., Ogee, J., Noormets, A., Jouangy, J., Gavazzi, M., Treasure, E. et al., 2012. Interactive effects of nocturnal transpiration and climate change on the root hydraulic redistribution and carbon and water budgets of southern United States pine plantations. Tree Physiol. 32, 707-723.

Dongmann, G., Nürnberg, H.W., Förstel, H.,Wagener, K., 1974. On the enrichment of $H_2{}^{18}O$ in the leaves of transpiring plants. Radiat. Environ. Biophys. 11, 41-52.

Durand, T.C., Sergeant, K., Renaut, J., Planchon, S., Hoffmann, L., Carpin, S. et al., 2011. Poplar under drought: Comparison of leaf and cambial proteomic responses. J. Proteomics 74, 1396-1410.

Evans, J.R.,Von Caemmerer, S., 2013. Temperature response of carbon isotope discrimination and mesophyll conductance in tobacco. Plant Cell Environ. 36, 745-756.

Farquhar, G.D.,Lloyd, J., 1993. Carbon and Oxygen Isotope Effects in the Exchange of Carbon Dioxide between Terrestrial Plants and the Atmosphere. In: J.R. Ehleringer, A.E. Hall and G.D. Farquhar (Editors), Stable Isotopes and Plant Carbon-Water Relations Academic Press, San Diego, CA, USA, pp. 47-70.

Farquhar, G.D., Lloyd, J., Taylor, J.A., Flanagan, L.B., Syvertsen, J.P., Hubick, K.T. et al., 1993. Vegetation effects on the isotope composition of oxygen in atmospheric CO_2. Nature 363, 439-443.

Farquhar, G.D.,Cernusak, L.A., 2005. On the isotopic composition of leaf water in the non-steady state. Funct. Plant Biol. 32, 293-303.

Farquhar, G.D.,Cernusak, L.A., 2012. Ternary effects on the gas exchange of isotopologues of carbon dioxide. Plant Cell Environ. 35, 1221-1231.

Ferrio, J.P., Pou, A., Florez-Sarasa, I., Gessler, A., Kodama, N., Flexas, J. et al., 2012. The Péclet effect on leaf water enrichment correlates with leaf hydraulic conductance and mesophyll conductance for CO_2. Plant Cell Environ. 35, 611-625.

Flanagan, L.B., Kubien, D.S.,Ehleringer, J.R., 1999. Spatial and temporal variation in the carbon and oxygen stable isotope ratio of respired CO_2 in a boreal forest ecosystem. Tellus Series B-Chemical and Physical Meteorology 51, 367-384.

Flexas, J., Bota, J., Loreto, F., Cornic, G.,Sharkey, T.D., 2004. Diffusive and Metabolic Limitations to Photosynthesis under Drought and Salinity in C_3 Plants. Plant Biol. 6, 269-279.

Flexas, J., Ribas-Carbo, M., Diaz-Espejo, A., Galmes, J.,Medrano, H., 2008. Mesophyll conductance to CO_2: current knowledge and future prospects. Plant Cell Environ. 31, 602-621.

Flexas, J., Barbour, M.M., Brendel, O., Cabrera, H.M., Carriquí, M., Díaz-Espejo, A. et al., 2012. Mesophyll diffusion conductance to CO_2: An unappreciated central player in photosynthesis. Plant Sci. 193–194, 70-84.

Francey, R.J.,Tans, P.P., 1987. Latitudinal variation in oxygen-18 of atmospheric CO_2. Nature 327, 495-497.

Friedli, H., Siegenthaler, U., Rauber, D.,Oeschger, H., 1987. Measurements of concentration, $^{13}C/^{12}C$ and $^{18}O/^{16}O$ ratios of tropospheric carbon dioxide over Switzerland. Tellus B 39B, 80-88.

Gangi, L., Tappe, W., Vereecken, H.,Brüggemann, N., 2015. Effect of short-term variations of environmental conditions on atmospheric $CO^{18}O$ isoforcing of different plant species. Agric. For. Meteorol. 201, 128-140.

Gat, J.R.,Bowser, C., 1991. The heavy isotope enrichment of water in coupled evaporative systems. Stable Isotopes in Geochemistry 3, 159-168.

Gillon, J.S.,Yakir, D., 2000. Naturally low carbonic anhydrase activity in C_4 and C_3 plants limits discrimination against $C^{18}OO$ during photosynthesis. Plant Cell Environ. 23, 903-915.

Gillon, J.S.,Yakir, D., 2001. Influence of carbonic anhydrase activity in terrestrial vegetation on the O-18 content of atmospheric CO_2. Science 291, 2584-2587.

Goffin, S., Aubinet, M., Maier, M., Plain, C., Schack-Kirchner, H.,Longdoz, B., 2014. Characterization of the soil CO_2 production and its carbon isotope composition in forest soil layers using the flux-gradient approach. Agric. For. Meteorol. 188, 45-57.

Gonfiantini, R., 1978. Standards for stable isotope measurements in natural compounds. Nature 271, 534-536.

Griffis, T.J., Baker, J.M., Sargent, S.D., Tanner, B.D.,Zhang, J., 2004. Measuring field-scale isotopic CO_2 fluxes with tunable diode laser absorption spectroscopy and micrometeorological techniques. Agric. For. Meteorol. 124, 15-29.

Griffis, T.J., Sargent, S.D., Baker, J.M., Lee, X., Tanner, B.D., Greene, J. et al., 2008. Direct measurement of biosphereatmosphere isotopic CO_2 exchange using the eddy covariance technique. J. Geophys. Res. 113, doi: 10.1029/2007JD009297.

Griffis, T.J., Lee, X., Baker, J.M., Billmark, K., Schultz, N., Erickson, M. et al., 2011. Oxygen isotope composition of evapotranspiration and its relation to C-4 photosynthetic discrimination. J. Geophys. Res. Biogeosc. 116, G01035, doi: 10.1029/2010jg001514.

Griffis, T.J., 2013. Tracing the flow of carbon dioxide and water vapor between the biosphere and atmosphere: A review of optical isotope techniques and their application. Agric. For. Meteorol. 174–175, 85-109.

Gut, A., Blatter, A., Fahrni, M., Lehmann, B.E., Neftel, A.,Staffelbach, T., 1998. A new membrane tube technique (METT) for continuous gas measurements in soils. Plant Soil 198, 79-88.

Harwood, K.G., Gillon, J.S., Roberts, A.,Griffiths, H., 1999. Determinants of isotopic coupling of CO_2 and water vapour within a Quercus petraea forest canopy. Oecologia 119, 109-119.

Hatch, M.D.,Burnell, J.N., 1990. Carbonic Anhydrase Activity in Leaves and Its Role in the First Step of C_4 Photosynthesis. Plant Physiol. 93, 825-828.

Hatch, M.D., 1991. Carbonic anhydrase assay: Strong inhibition of the leaf enzyme by CO_2 in certain buffers. Anal. Biochem. 192, 85-89.

Herbstritt, B., Gralher, B.,Weiler, M., 2012. Continuous *in situ* measurements of stable isotopes in liquid water. Water Resour. Res. 48, doi:10.1029/2011wr011369.

Hesterberg, R.,Siegenthaler, U., 1991. Production and stable isotopic composition of CO_2 in a soil near Bern, Switzerland. Tellus B 43, 197-205.

Horita, J.,Wesolowski, D.J., 1994. Liquid-vapor fractionation of oxygen and hydrogen isotopes of water from the freezing to the critical temperature. Geochim. Cosmochim. Acta 58, 3425-3437.

Huber, C., Aherne, J., Weis, W., Farrell, E.P., Gottlein, A.,Cummins, T., 2010. Ion concentrations and fluxes of seepage water before and after clear cutting of Norway spruce stands at Ballyhooly, Ireland, and Hoglwald, Germany. Biogeochemistry 101, 7-26.

Kammer, A., Tuzson, B., Emmenegger, L., Knohl, A., Mohn, J.,Hagedorn, F., 2011. Application of a quantum cascade laser-based spectrometer in a closed chamber system for real-time $\delta^{13}C$ and $\delta^{18}O$ measurements of soil-respired CO_2. Agric. For. Meteorol. 151, 39-48.

Kapiluto, Y., Yakir, D., Tans, P.,Berkowitz, B., 2007. Experimental and numerical studies of the O-18 exchange between CO_2 and water in the atmosphere-soil invasion flux. Geochim. Cosmochim. Acta 71, 2657-2671.

Kaul, T., Reddy, P.S., Mahanty, S., Thirulogachandar, V., Reddy, R.A., Kumar, B. et al., 2011. Biochemical and molecular characterization of stress-induced beta-carbonic anhydrase from a C_4 plant, Pennisetum glaucum. J. Plant Physiol. 168, 601-610.

Khomik, M., Arain, M.A., Brodeur, J.J., Peichl, M., Restrepo-Coupe, N.,McLaren, J.D., 2010. Relative contributions of soil, foliar, and woody tissue respiration to total ecosystem respiration in four pine forests of different ages. J. Geophys. Res. Biogeosc. 115, G03024, doi:10.1029/2009JG001089.

Kodama, N., Cousins, A., Tu, K.P.,Barbour, M.M., 2011. Spatial variation in photosynthetic CO_2 carbon and oxygen isotope discrimination along leaves of the monocot triticale (Triticum x Secale) relates to mesophyll conductance and the Peclet effect. Plant Cell Environ. 34, 1548-1562.

Kreutzer, K., 1995. Effects of forest liming on soil processes. Plant Soil 168, 447-470.

Kreutzer, K.,Weiss, T., 1998. The Höglwald field experiments – aims, concept and basic data. Plant Soil 199, 1-10.

Lai, C.T., Schauer, A.J., Owensby, C., Ham, J.M.,Ehleringer, J.R., 2003. Isotopic air sampling in a tallgrass prairie to partition net ecosystem CO_2 exchange. J. Geophys. Res. Atmos. 108, 4566, doi: 10.1029/2002jd003369.

Lai, C.T., Riley, W., Owensby, C., Ham, J., Schauer, A.,Ehleringer, J.R., 2006. Seasonal and interannual variations of carbon and oxygen isotopes of respired CO_2 in a tallgrass prairie: Measurements and modeling results from 3 years with contrasting water availability. J. Geophys. Res. Atmos. 111, D08S06, doi:10.1029/2005JD006436.

Langendörfer, U., Cuntz, M., Ciais, P., Peylin, P., Bariac, T., Milyukova, I. et al., 2002. Modelling of biospheric CO_2 gross fluxes via oxygen isotopes in a spruce forest canopy: a ^{222}Rn calibrated box model approach. Tellus B 54, 476-496.

Lazova, G., Ignatova, L.,Baydanova, V., 2012. Drought and Salinity stress: Changes in Hydratase and Dehydratase Activities of Thylakoid-associated Carbonic Anhydrase in Pea Seedlings. Int. J. Plant Sci. 173, 7-15.

Lee, X.H., Griffis, T.J., Baker, J.M., Billmark, K.A., Kim, K.,Welp, L.R., 2009. Canopy-scale kinetic fractionation of atmospheric carbon dioxide and water vapor isotopes. Glob. Biogeochem. Cycles 23, GB1002, doi:10.1029/2008GB003331.

Loreto, F., Dimarco, G., Tricoli, D.,Sharkey, T.D., 1994. Measurements of mesophyll conductance, photosynthetic electron-transport and alternative electron sinks of field-grown wheat leaves. Photosynth. Res. 41, 397-403.

Luo, G.J., Bruggemann, N., Wolf, B., Gasche, R., Grote, R.,Butterbach-Bahl, K., 2012. Decadal variability of soil CO_2, NO, N_2O, and CH_4 fluxes at the Hoglwald Forest, Germany. Biogeosciences 9, 1741-1763.

Majoube, M., 1971. Oxygen-18 and Deuterium fractionation between water and steam J. Chim. Phys. Phys.-Chim. Biol. 68, 1423-1436.

Mathieu, R.,Bariac, T., 1996. An Isotopic Study (^2H and ^{18}O) of Water Movements in Clayey Soils Under a Semiarid Climate. Water Resour. Res. 32, 779-789.

Michener, R.,Lajtha, K., 2008. Stable Isotopes in Ecology and Environmental Science, Second Edition, 10.1002/9780470691854.fmatter. Blackwell Publishing Ltd, 1-594 pp.

Miller, J.B., Yakir, D., White, J.W.C.,Tans, P.P., 1999. Measurement of $^{18}O/^{16}O$ in the soil-atmosphere CO_2 flux. Global Biogeochem. Cycles 13, 761-774.

Mills, G.A.,Urey, H.C., 1940. The kinetics of isotopic exchange between carbon dioxide, bicarbonate ion, carbonate ion and water. J. Am. Chem. Soc. 62, 1019-1026.

Mortazavi, B., Prater, J.L.,Chanton, J.P., 2004. A field-based method for simultaneous measurements of the delta O-18 and delta C-13 of soil CO_2 efflux. Biogeosciences 1, 1-9.

Ogee, J., Brunet, Y., Loustau, D., Berbigier, P.,Delzon, S., 2003a. MuSICA, a CO_2, water and energy multilayer, multileaf pine forest model: evaluation from hourly to yearly time scales and sensitivity analysis. Global Change Biol. 9, 697-717.

Ogee, J., Peylin, P., Ciais, P., Bariac, T., Brunet, Y., Berbigier, P. et al., 2003b. Partitioning net ecosystem carbon exchange into net assimilation and respiration using $^{13}CO_2$ measurements: A cost-effective sampling strategy. Glob. Biogeochem. Cycles 17, 1070, doi:10.1029/2002GB001995.

Ogee, J., Peylin, P., Cuntz, M., Bariac, T., Brunet, Y., Berbigier, P. et al., 2004. Partitioning net ecosystem carbon exchange into net assimilation and respiration with canopy-scale isotopic measurements: An error propagation analysis with (CO_2)-C-13 and (COO)-O-18 data. Glob. Biogeochem. Cycles 18, GB2019, doi:10.1029/2003gb002166.

Oliver, R.J., Taylor, G.,Finch, J.W., 2012. Assessing the impact of internal conductance to CO_2 in a land-surface scheme: Measurement and modelling of photosynthesis in Populus nigra. Agric. For. Meteorol. 152, 240-251.

Parent, F., Plain, C., Epron, D., Maier, M.,Longdoz, B., 2013. A new method for continuously measuring the C-13 of soil CO_2 concentrations at different depths by laser spectrometry. European Journal of Soil Science 64, 516-525.

Patankar, S.V., 1980. Numerical heat transfer and fluid flow: Computational methods in mechanics and thermal science, citeulike-article-id:6355181. Hemisphere Publishing Corp., 210 pp.

Peylin, P., Ciais, P., Denning, A.S., Tans, P.P., Berry, J.A.,White, J.W.C., 1999. A 3-dimensional study of δ18O in atmospheric CO_2: contribution of different land ecosystems. Tellus B 51, 642-667.

Pfeffer, M.,Peisker, M., 1995. *In vivo* K_m for CO_2 (K_p) of phosphoenolpyruvate carboxylase (PEPC) and mesophyll CO_2 transport resistance (r_m) in leaves of Zea mays L. In: P. Mathis (Editor), Photosynthesis: From Light to Biosphere. Kluwer Academic Publishers, Dordrecht, The Netherlands, pp. 547-550.

Pons, T.L., Flexas, J., von Caemmerer, S., Evans, J.R., Genty, B., Ribas-Carbo, M. et al., 2009. Estimating mesophyll conductance to CO_2: methodology, potential errors, and recommendations. J. Exp. Bot. 60, 2217-2234.

Powers, H.H., Hunt, J.E., Hanson, D.T.,McDowell, N.G., 2010. A dynamic soil chamber system coupled with a tunable diode laser for online measurements of delta C-13, delta O-18, and efflux rate of soil-respired CO_2. Rapid Commun. Mass Spectrom. 24, 243-253.

Prakash, K.R.,Rao, V.S., 1996. The altered activities of carbonic anhydrase, phosphoenol pyruvate carboxylase and ribulose bisphosphate carboxylase due to water stress and after its relief. J. Environ. Biol. 17, 39-42.

Raupach, M.R., 1989a. A practical Lagrangian method for relating scalar concentrations to source distributions in vegetation canopies Q. J. R. Meteorol. Soc. 115, 609-632.

Raupach, M.R., 1989b. Applying Lagrangian fluid mechanics to infer scalar source distributions from concentration profiles in plant canopies. Agric. For. Meteorol. 47, 85-108.

Reddy, A.R., Chaitanya, K.V.,Vivekanandan, M., 2004. Drought-induced responses of photosynthesis and antioxidant metabolism in higher plants. J. Plant Physiol. 161, 1189-1202.

Riley, W.J., Still, C.J., Torn, M.S.,Berry, J.A., 2002. A mechanistic model of (H_2O)-O-18 and (COO)-O-18 fluxes between ecosystems and the atmosphere: Model description and sensitivity analyses. Glob. Biogeochem. Cycles 16, 1095, doi:10.1029/2002gb001878.

Riley, W.J., Still, C.J., Helliker, B.R., Ribas-Carbo, M.,Berry, J.A., 2003. ^{18}O composition of CO_2 and H_2O ecosystem pools and fluxes in a tallgrass prairie: Simulations and comparisons to measurements. Global Change Biol. 9, 1567-1581.

Riley, W.J., 2005. A modeling study of the impact of the delta O-18 value of near-surface soil water on the delta O-18 value of the soil-surface CO_2 flux. Geochim. Cosmochim. Acta 69, 1939-1946.

Rothfuss, Y., Vereecken, H.,Bruggemann, N., 2013. Monitoring water stable isotopic composition in soils using gas-permeable tubing and infrared laser absorption spectroscopy. Water Resour. Res. 49, 3747-3755.

Saito, H., Šimůnek, J., Hopmans, J.W.,Tuli, A., 2007. Numerical evaluation of alternative heat pulse probe designs and analyses. Water Resour. Res. 43, W07408, doi:10.1029/2006WR005320.

Santos, E., Wagner-Riddle, C., Lee, X., Warland, J., Brown, S., Staebler, R. et al., 2012. Use of the isotope flux ratio approach to investigate the (COO)-O-18-O-16 and (CO_2)-C-13 exchange near the floor of a temperate deciduous forest. Biogeosciences 9, 2385-2399.

Santos, E., Wagner-Riddle, C., Lee, X., Warland, J., Brown, S., Staebler, R. et al., 2014. Temporal dynamics of oxygen isotope compositions of soil and canopy CO_2 fluxes in a temperate deciduous forest. J. Geophys. Res. Biogeosc. 119, 996–1013.

Saveyn, A., Steppe, K.,Lemeur, R., 2007. Daytime depression in tree stem CO_2 efflux rates: is it caused by low stem turgor pressure? Ann. Bot. 99, 477-485.

Seibt, U., Wingate, L., Berry, J.A.,Lloyd, J., 2006a. Non-steady state effects in diurnal ^{18}O discrimination by Picea sitchensis branches in the field. Plant Cell Environ. 29, 928-939.

Seibt, U., Wingate, L., Lloyd, J.,Berry, J.A., 2006b. Diurnally variable delta ^{18}O signatures of soil CO_2 fluxes indicate carbonic anhydrase activity in a forest soil. J. Geophys. Res. Biogeosc. 111, G04005, doi:10.1029/2006JG000177.

Simonin, K.A., Roddy, A.B., Link, P., Apodaca, R., Tu, K.P., Hu, J. et al., 2013. Isotopic composition of transpiration and rates of change in leaf water isotopologue storage in response to environmental variables. Plant Cell Environ. 36, 2190-2206.

Skirrow, G., 1975. The dissolved gases-carbon dioxide. In: J.P. Riley and G. Skirrow (Editors), Chemical Oceanography. Academic Press, San Diego, CA, pp. 1-92.

Soderberg, K., Good, S.P., Wang, L.X.,Caylor, K., 2012. Stable Isotopes of Water Vapor in the Vadose Zone: A Review of Measurement and Modeling Techniques. Vadose Zone J. 11, doi:10.2136/vzj2011.0165.

Song, X., Barbour, M.M., Farquhar, G.D., Vann, D.R.,Helliker, B.R., 2013. Transpiration rate relates to within- and across-species variations in effective path length in a leaf water model of oxygen isotope enrichment. Plant Cell Environ. 36, 1338-1351.

Stern, L., Baisden, W.T.,Amundson, R., 1999. Processes controlling the oxygen isotope ratio of soil CO_2: Analytic and numerical modeling. Geochim. Cosmochim. Acta 63, 799-814.

Stern, L., Amundson, R.,Baisden, W.T., 2001. Influence of soils on oxygen isotope ratio of atmospheric CO_2. Glob. Biogeochem. Cycles 15, 753-759.

Stingaciu, L.R., Pohlmeier, A., Bluemler, P., Weihermueller, L., van Dusschoten, D., Stapf, S. et al., 2009. Characterization of unsaturated porous media by high-field and low-field NMR relaxometry. Water Resour. Res. 45, doi:10.1029/2008WR007459.

Stingaciu, L.R., Weihermueller, L., Haber-Pohlmeier, S., Stapf, S., Vereecken, H.,Pohlmeier, A., 2010. Determination of pore size distribution and hydraulic properties using nuclear magnetic resonance relaxometry: A comparative study of laboratory methods. Water Resour. Res. 46.

Sturm, P., Eugster, W.,Knohl, A., 2012. Eddy covariance measurements of CO_2 isotopologues with a quantum cascade laser absorption spectrometer. Agric. For. Meteorol. 152, 73-82.

Sültemeyer, D., Schmidt, C.,Fock, H.P., 1993. Carbonic anhydrases in higher plants and aquatic microorganisms. Physiologia Plantarum 88, 179-190.

Tans, P.P., 1998. Oxygen isotopic equilibrium between carbon dioxide and water in soils. Tellus Series B-Chemical and Physical Meteorology 50, 163-178.

Tazoe, Y., Von Caemmerer, S., Estavillo, G.M.,Evans, J.R., 2011. Using tunable diode laser spectroscopy to measure carbon isotope discrimination and mesophyll conductance to CO_2 diffusion dynamically at different CO_2 concentrations. Plant Cell Environ. 34, 580-591.

Tiwari, A., Kumar, P., Chawhaan, P.H., Singh, S.,Ansari, S.A., 2006. Carbonic anhydrase in Tectona grandis: kinetics, stability, isozyme analysis and relationship with photosynthesis. Tree Physiol. 26, 1067-1073.

Van Genuchten, M.T., 1980. A closed-form equation for predicting the hydraulic conductivity of unsaturated soils. Soil Sci. Soc. Am. J. 44, 892-898.

Volkmann, T.H.M.,Weiler, M., 2014. Continual *in situ* monitoring of pore water stable isotopes in the subsurface. Hydrol. Earth Syst. Sci. 18, 1819-1833.

Von Caemmerer, S.,Farquhar, G.D., 1981. Some relationships between the biochemistry of photosynthesis and gas-exchange of leaves. Planta 153, 376-387.

Vose, J.M.,Ryan, M.G., 2002. Seasonal respiration of foliage, fine roots, and woody tissues in relation to growth, tissue N, and photosynthesis. Glob. Chang. Biol. 8, 182-193.

Wang, L., Good, S.P., Caylor, K.K.,Cernusak, L.A., 2012. Direct quantification of leaf transpiration isotopic composition. Agric. For. Meteorol. 154–155, 127-135.

Wang, X.F.,Yakir, D., 1995. Temporal and spatial variations in the oxygen-18 content of leaf water in different plant species. Plant Cell Environ. 18, 1377-1385.

Wehr, R., Munger, J.W., Nelson, D.D., McManus, J.B., Zahniser, M.S., Wofsy, S.C. et al., 2013. Long-term eddy covariance measurements of the isotopic composition of the ecosystem–atmosphere exchange of CO_2 in a temperate forest. Agric. For. Meteorol. 181, 69-84.

Weis, W., Baier, R., Huber, C.,Göttlein, A., 2007. Long Term Effects of Acid Irrigation at the Höglwald on Seepage Water Chemistry and Nutrient Cycling. Water Air Soil Pollut: Focus 7, 211-223.

Welp, L.R., Keeling, R.F., Meijer, H.A.J., Bollenbacher, A.F., Piper, S.C., Yoshimura, K. et al., 2011. Interannual variability in the oxygen isotopes of atmospheric CO_2 driven by El Nino. Nature 477, 579-582.

Werle, P., 2011. Accuracy and precision of laser spectrometers for trace gas sensing in the presence of optical fringes and atmospheric turbulence. Appl. Phys. B-Lasers Opt. 102, 313-329.

Werner, C., Schnyder, H., Cuntz, M., Keitel, C., Zeeman, M.J., Dawson, T.E. et al., 2012. Progress and challenges in using stable isotopes to trace plant carbon and water relations across scales. Biogeosciences 9, 3083-3111.

Werner, R.A.,Brand, W.A., 2001. Referencing strategies and techniques in stable isotope ratio analysis. Rapid Commun. Mass Spectrom. 15, 501-519.

Wildt, J., Kley, D., Rockel, A., Rockel, P.,Segschneider, H.J., 1997. Emission of NO from several higher plant species. J. Geophys. Res. Atmos. 102, 5919-5927.

Williams, T.G., Flanagan, L.B.,Coleman, J.R., 1996. Photosynthetic gas exchange and discrimination against (CO_2)-C-13 and (COO)-O-18-O-16 in tobacco plants modified by an antisense construct to have low chloroplastic carbonic anhydrase. Plant Physiol. 112, 319-326.

Willmott, C.J., 1981. On the validation of models. Physical Geography 2, 184-194.

Wilson, C.C., 1948. The effect of some environmental factors on the movements of guard cells. Plant Physiol. 23, 5-37.

Wingate, L., Seibt, U., Moncrieff, J.B., Jarvis, P.G.,Lloyd, J.O.N., 2007. Variations in ^{13}C discrimination during CO_2 exchange by Picea sitchensis branches in the field. Plant Cell Environ. 30, 600-616.

Wingate, L., Seibt, U., Maseyk, K., Ogee, J., Almeida, P., Yakir, D. et al., 2008. Evaporation and carbonic anhydrase activity recorded in oxygen isotope signatures of net CO_2 fluxes from a Mediterranean soil. Global Change Biol. 14, 2178-2193.

Wingate, L., Ogee, J., Cuntz, M., Genty, B., Reiter, I., Seibt, U. et al., 2009. The impact of soil microorganisms on the global budget of delta O-18 in atmospheric CO_2. Proc. Natl. Acad. Sci. U. S. A. 106, 22411-22415.

Wingate, L., Ogee, J., Burlett, R.,Bosc, A., 2010. Strong seasonal disequilibrium measured between the oxygen isotope signals of leaf and soil CO_2 exchange. Global Change Biol. 16, 3048-3064.

Xiao, W., Xuhui, L., Griffis, T.J., Kyounghee, K., Welp, L.R.,Yu, Q., 2010. A modeling investigation of canopy-air oxygen isotopic exchange of water vapor and carbon dioxide in a soybean field. J. Geophys. Res. Biogeosc. 115, G01004, doi:10.1029/2009JG001163.

Xiao, W., Lee, X.H., Wen, X.F., Sun, X.M.,Zhang, S.C., 2012. Modeling biophysical controls on canopy foliage water ^{18}O enrichment in wheat and corn. Global Change Biol. 18, 1769-1780.

Yakir, D.,Wang, X.F., 1996. Fluxes of CO_2 and water between terrestrial vegetation and the atmosphere estimated from isotope measurements. Nature 380, 515-517.

Yakir, D.,Sternberg, L.D.L., 2000. The use of stable isotopes to study ecosystem gas exchange. Oecologia 123, 297-311.

Yakir, D., 2003. The stable isotopic composition of CO_2. In: H.D. Holland and K.K. Turekian (Editors), The Atmosphere, Treatise on Geochemistry. Elsevier-Pergamon, Oxford, pp. 175-212.

Yepez, E.A., Huxman, T.E., Ignace, D.D., English, N.B., Weltzin, J.F., Castellanos, A.E. et al., 2005. Dynamics of transpiration and evaporation following a moisture pulse in semiarid grassland: A chamber-based isotope method for partitioning flux components. Agric. For. Meteorol. 132, 359-376.

Yoshimura, K., Kanamitsu, M., Noone, D.,Oki, T., 2008. Historical isotope simulation using Reanalysis atmospheric data. J. Geophys. Res. Atmos. 113, D19108, doi:10.1029/2008JD010074.

Yu, S., Zhang, X.X., Guan, Q.J., Takano, T.,Liu, S.K., 2007. Expression of a carbonic anhydrase gene is induced by environmental stresses in Rice (Oryza sativa L.). Biotechnol. Lett. 29, 89-94.

Zhang, J., Griffis, T.J.,Baker, J.M., 2006. Using continuous stable isotope measurements to partition net ecosystem CO_2 exchange. Plant Cell Environ. 29, 483-496.

Zobitz, J.M., Burns, S.P., Reichstein, M.,Bowling, D.R., 2008. Partitioning net ecosystem carbon exchange and the carbon isotopic disequilibrium in a subalpine forest. Global Change Biol. 14, 1785-1800.

VII. Appendix

Appendix A

Table A 1 Mathematical functions fitted to transpiration rate (T_r), assimilation rate (A_r), stomatal conductance to CO_2 (g_{s_CO2}), $CO^{18}O$ isoforcing ($CO^{18}O$-*Iso*), $\delta^{18}O$-H_2O at evaporation site ($\delta^{18}O_{ev}$), and the degree of leaf isotopic CO_2–H_2O exchange (θ) to soil water potential. Only relationships with $p < 0.05$ are presented.

		Poplar	**Maize**	**Spruce**	**Wheat**
T_r	**f(x)**	39.6 exp(-x/-128.9)+66.2	83.3 exp(-x/-113.8) + 40.1	1.0E7exp(-x/-1.3E8) -1.0E7	107.2 + 0.08x
	r^2	1	0.64	0.74	0.81
A_r	**f(x)**	50.8 exp(-x/-145.1)+55.9	109.9 + 0.2x	5.1E6 exp(-x/-8.8E7) -5E6	-7.4 exp(-x/427.3) + 108.6
	r^2	0.99	0.55	0.62	0.67
$g_{s\_CO_2}$	**f(x)**	64.2 exp(-x/-204.1) + 43.7	118.1 exp(-x/-155) + 18.0	119.5 + 0.1x	-24 exp(-x/593.4) + 127
	r^2	0.99	0.81	0.84	0.83
$CO^{18}O$ -*Iso*	**f(x)**	71.0 exp(-x/-108.1) + 42.0	138.9 exp(-x/-60.2) + 30.9	113.2 + 0.1x	-26.1 exp(-x/718.5) + 130.7
	r^2	0.99	0.71	0.74	0.86
$\delta^{18}O_{ev}$	**f(x)**	95.1 + (-0.1)x	86.9 + (-0.1)x	98 + (-0.1)x	88.9 + (-0.22)x
	r^2	0.93	0.44	0.81	0.65
θ	**f(x)**	98.8 +(-0.11)x	145 exp(-x/-40.5) + 46.8		103 + (-0.03)x
	r^2	0.98	0.72		0.49

Appendix B

Table B 1 Statistical results for model–data fit of $\delta^{18}O\text{-}CO_2$ at different depths. RMSE, $RMSE_u$ and $RMSE_s$ refer to the total, unsystematic and systematic root mean square error. Slope and intercept were obtained from ordinary least squares regression, and *n* is the number of data points.

Experiment	f_{CA}	depth [cm]	r^2	RMSE	$RMSE_u$	$RMSE_s$	Intercept	slope	*n*
Exp 1	0.01	1	0.74	0.43	0.38	0.20	-0.20	1.00	27
		3	0.69	0.49	0.41	0.27	-0.30	1.04	27
		7	0.64	0.65	0.42	0.49	-0.54	1.08	27
		15	0.02	1.02	0.66	0.78	0.05	0.18	27
		30	0.00	3.57	0.60	3.52	-0.61	0.02	27
		55	0.03	4.81	0.54	4.78	1.61	0.49	27
	0.1	1	0.74	0.47	0.37	0.29	-0.28	0.98	27
		3	0.70	0.66	0.38	0.54	-0.53	0.99	27
		7	0.67	1.19	0.35	1.14	-1.11	0.96	27
		15	0.04	1.05	0.47	0.94	-1.47	0.19	27
		30	0.02	0.60	0.30	0.51	-3.22	0.13	27
		55	0.01	0.28	0.17	0.22	-5.37	0.11	27
	1	1	0.74	0.40	0.35	0.20	-0.15	0.93	27
		3	0.71	0.43	0.32	0.29	-0.17	0.84	27
		7	0.68	0.83	0.23	0.80	-0.52	0.66	27
		15	0.29	1.29	0.17	1.27	-1.80	0.23	27
		30	0.68	1.50	0.06	1.50	-4.53	0.27	27
		55	0.02	1.78	0.04	1.78	-8.13	-0.03	27
	10	1	0.73	0.47	0.31	0.36	0.48	0.80	27
		3	0.67	1.18	0.22	1.16	1.45	0.54	27
		7	0.73	1.43	0.09	1.43	1.92	0.27	27
		15	0.74	0.80	0.08	0.80	-1.26	0.28	27
		30	0.76	2.31	0.06	2.31	-5.06	0.34	27
		55	0.02	1.90	0.04	1.90	-8.30	-0.04	27
Exp 2	0.01	1	0.65	0.33	0.31	0.12	0.21	0.80	27
		3	0.01	1.58	0.50	1.49	0.70	0.07	27
		7	0.00	2.78	0.48	2.74	0.40	0.02	27
		15	0.01	3.58	0.43	3.55	-0.51	-0.09	27
		30	0.01	3.45	0.37	3.43	-0.80	0.07	27
		55	0.05	2.64	0.32	2.62	-1.42	0.21	27
	0.1	1	0.66	0.33	0.29	0.14	0.07	0.78	27
		3	0.05	1.19	0.45	1.10	0.29	0.13	27
		7	0.04	1.84	0.39	1.80	-0.44	0.09	27
		15	0.00	1.75	0.29	1.72	-2.01	0.01	27
		30	0.03	0.67	0.22	0.64	-3.68	0.08	27
		55	0.00	1.90	0.07	1.89	-6.96	0.00	27
	1	1	0.65	0.50	0.28	0.41	-0.18	0.72	27

		3	0.56	0.52	0.32	0.41	-0.35	0.47	27
		7	0.70	0.54	0.32	0.44	-1.20	0.55	27
		15	0.14	0.81	0.39	0.71	-3.18	0.30	27
		30	0.02	0.72	0.38	0.61	-4.46	0.12	27
		55	0.08	2.94	0.03	2.94	-8.19	-0.03	27
	10	1	0.17	1.08	0.68	0.84	-0.49	0.57	27
		3	0.76	1.54	0.66	1.39	-0.98	1.53	27
		7	0.68	2.79	0.86	2.65	-1.63	1.44	27
		15	0.07	2.66	0.98	2.47	-4.27	0.51	27
		30	0.02	0.81	0.73	0.34	-3.42	0.24	27
		55	0.16	3.05	0.03	3.05	-8.32	-0.03	27
Exp 3	0.01	1	0.32	1.69	0.66	1.56	2.33	0.25	24
		3	0.00	2.65	0.78	2.53	3.12	-0.01	24
		7	0.04	2.82	0.74	2.72	2.60	-0.13	24
		15	0.03	3.10	0.70	3.03	2.23	0.45	24
		30	0.15	2.35	0.61	2.27	1.73	0.77	24
		55	0.17	0.79	0.59	0.53	-0.84	0.60	24
	0.1	1	0.33	1.80	0.64	1.69	2.11	0.25	24
		3	0.00	2.40	0.71	2.29	2.45	0.00	24
		7	0.04	1.70	0.60	1.59	1.14	-0.11	24
		15	0.08	0.63	0.49	0.39	-0.36	0.49	24
		30	0.21	1.81	0.40	1.77	-2.68	0.61	24
		55	0.21	4.45	0.29	4.44	-6.64	0.33	24
	1	1	0.41	2.13	0.53	2.06	1.58	0.24	24
		3	0.07	2.38	0.51	2.33	0.81	0.06	24
		7	0.04	2.23	0.41	2.19	-1.71	0.07	24
		15	0.31	2.96	0.29	2.95	-3.42	0.66	24
		30	0.13	3.52	0.50	3.48	-4.46	0.58	24
		55	0.23	4.99	0.22	4.98	-7.38	0.27	24
	10	1	0.48	3.11	0.52	3.06	0.20	0.28	24
		3	0.47	4.16	0.89	4.07	-2.60	0.38	24
		7	0.27	5.72	1.14	5.61	-5.51	0.59	24
		15	0.11	5.02	0.82	4.95	-4.98	0.98	24
		30	0.11	3.27	0.79	3.17	-3.60	0.82	24
		55	0.23	5.00	0.22	4.99	-7.39	0.27	24

Appendix C

Table C 1 Statistical results for the linear regression between simulated and measured net radiation (R_{net}), sensible, latent, and soil heat flux (H, LE, G), net ecosystem exchange (NEE), soil temperature (T_s) and soil water content for individual months (SWC) based on 30 min data of the whole data set or individual months. No statistics could be calculated for some months as measurements were unavailable. N is the number of data points.

	Intercept	**Slope**	**r^2**	**RMSE**	**$RMSE_u$**	**$RMSE_s$**	**d**	***n***
R_{net} **[W m^{-2}]**								
all	10.06	0.99	0.90	54.82	53.98	9.53	0.97	17568
12/2007	-42.18	1.87	0.83	64.56	37.87	52.28	0.76	1441
01/2008	14.36	1.06	0.73	44.58	41.91	15.19	0.90	1441
02/2008	17.08	1.03	0.91	42.29	38.34	18.31	0.97	1441
03/2008	21.06	1.03	0.94	42.30	35.05	23.68	0.98	1441
04/2008	18.45	1.04	0.93	54.74	49.33	23.71	0.98	1441
05/2008	12.25	0.98	0.92	66.86	66.08	10.22	0.98	1441
06/2008	14.39	0.91	0.89	84.83	81.59	22.89	0.97	1441
07/2008	6.39	0.96	0.91	64.03	63.60	7.42	0.98	1441
08/2008	22.91	0.94	0.90	66.99	64.12	19.4	0.97	1441
09/2008	21.20	0.96	0.90	53.33	49.81	19.05	0.97	1441
10/2008	12.29	0.97	0.87	43.96	42.45	11.42	0.96	1441
11/2008	9.42	0.96	0.72	38.20	37.10	9.09	0.91	1441
H **[W m^{-2}]**								
all	2.58	0.87	0.44	52.90	108.20	15.31	0.78	17568
12/2007	-36.02	0.54	0.16	78.59	67.25	40.66	0.47	1441
01/2008	2.40	0.95	0.54	50.79	50.69	3.16	0.84	1441
02/2008	29.38	0.02	0.00	134.74	103.11	86.73	0.01	1441
03/2008	30.03	0.76	0.41	91.18	87.17	26.73	0.78	1441
04/2008	40.75	0.77	0.40	119.96	115.75	31.54	0.78	1441
05/2008	-15.88	0.98	0.61	113.26	112.54	12.75	0.87	1441
06/2008	12.59	0.98	0.56	96.44	95.88	10.46	0.85	1441
07/2008	-21.43	1.02	0.51	107.41	105.60	19.61	0.81	1441
08/2008	44.57	0.31	0.03	172.92	158.69	68.69	0.25	1441
09/2008	46.96	1.05	0.38	107.47	95.49	49.33	0.65	1441
10/2008	53.39	1.05	0.54	95.09	76.07	57.06	0.79	1441
11/2008	-	-	-	-	-	-	-	-
LE **[W m^{-2}]**								
all	27.86	0.48	0.46	80.67	56.19	57.89	0.78	17568
12/2007	6.85	0.16	0.12	50.89	22.59	46.6	0.4	1441
01/2008	17.24	0.23	0.12	41.80	26.41	32.41	0.49	1441
02/2008	20.50	0.25	0.11	46.05	31.3	33.79	0.48	1441
03/2008	31.33	0.20	0.17	77.16	34.28	69.12	0.41	1441

04/2008	42.80	0.36	0.25	78.92	53.47	58.05	0.64	1441
05/2008	46.05	0.65	0.52	68.53	57.94	36.60	0.83	1441
06/2008	57.59	0.50	0.49	96.99	66.23	70.86	0.79	1441
07/2008	75.18	0.42	0.44	116.76	71.74	92.12	0.75	1441
08/2008	90.03	0.16	0.11	151.97	68.35	135.37	0.34	1441
09/2008	27.55	0.38	0.43	51.49	28.65	42.78	0.71	1441
10/2008	31.0	0.19	0.31	79.99	23.66	76.41	0.4	1441
11/2008	-	-	-	-	-	-	-	-
G								
[W m^{-2}]								
all	0.84	1.12	0.14	15.33	15.28	1.20	0.37	17568
12/2007	7.42	1.61	0.28	10.64	9.81	4.138	0.42	1441
01/2008	6.25	1.26	0.11	12.41	11.04	5.65	0.10	1441
02/2008	5.54	1.78	0.22	15.33	14.29	5.55	0.33	1441
03/2008	1.82	1.90	0.26	14.39	13.79	4.12	0.40	1441
04/2008	-1.06	1.93	0.15	17.25	16.84	3.75	0.25	1441
05/2008	-6.93	2.34	0.20	18.35	17.57	5.23	0.28	1441
06/2008	-9.14	2.02	0.19	16.09	15.43	4.56	0.29	1441
07/2008	-8.00	2.21	0.2.	16.27	15.42	5.17	0.30	1441
08/2008	-7.56	2.21	0.17	15.82	14.95	5.17	0.21	1441
09/2008	-	-	-	-	-	-	-	-
10/2008	-	-	-	-	-	-	-	-
11/2008	-	-	-	-	-	-	-	-
NEE								
[mol m^{-2} s^{-1}]								
all	1.6e−05	0.45	0.24	1.1−04	8.0e-5	7.2e-5	0.57	17568
12/2007	1.5e−05	0.03	0.01	8.0e−05	1.7e-5	7.8e-5	-0.05	1441
01/2008	9.9e-5	0.17	0.13	7.6e−05	2.9e-5	7.0e-5	0.18	1441
02/2008	9.9e-7	-0.06	0.01	9.6e−05	4.0e-5	8.8e-5	-0.52	1441
03/2008	1.2e−05	0.45	0.34	7.5e−05	4.4e-5	6.0e-5	0.55	1441
04/2008	3.7e-6	0.51	0.29	9.1e−05	7.0e-5	5.8e-5	0.64	1441
05/2008	-2.4e-6	0.79	0.35	1.0e-4	9.9e-5	2.1e-5	0.73	1441
06/2008	2.6e-5	0.72	0.42	1.2e-4	1.0e-4	6.5e-5	0.74	1441
07/2008	5.5e-5	0.85	0.44	1.3e-4	1.1e-4	7.5e-5	0.71	1441
08/2008	7.0e-5	0.35	0.12	1.9e-4	1.1e-4	1.6e-4	-0.08	1441
09/2008	2.7e-5	0.60	0.41	9.0e−05	6.7e-5	6.0e-5	0.71	1441
10/2008	2.3e-5	0.52	0.63	9.3e−05	3.8e-5	8.5e-5	0.66	1441
11/2008	-	-	-	-	-	-	-	-
T_s								
[°C]								
-5 cm	-1.62	1.32	0.93	2.50	1.79	1.75	0.95	17568
-10 cm	-1.53	1.37	0.90	2.92	2.06	2.07	0.93	17568
-15 cm	-1.02	1.35	0.86	3.18	2.36	2.14	0.91	17568
-20 cm	-1.87	1.40	0.88	3.01	2.21	2.05	0.92	17568

SWC **[m^3 m^{-3}]**								
-5 cm	10.36	0.48	0.78	1.54	0.67	1.39	0.85	17568
-10 cm	14.25	0.20	0.68	2.40	0.37	2.37	0.46	17568
-15 cm	10.21	0.46	0.69	1.61	0.66	1.47	0.74	17568
-20 cm	-2.77	1.14	0.76	1.54	1.45	0.51	0.9	17568

Danksagung

An dieser Stelle möchte ich mich ganz herzlich bei Nicolas Brüggemann für die Formulierung des Themas und die gute Betreuung der Doktorarbeit bedanken.

Harry Vereecken möchte ich für die Halbjahresgespräche danken. Wulf Amelung danke ich für die Übernahme des Korreferates.

Ein besonderer Dank geht an Youri Rothfuss für die erfolgreiche Zusammenarbeit in der Halle, bei der ich sehr viel gelernt habe und die sehr motivierend für mich war- auch wenn die Bodensäule uns oft vor Herausforderungen gestellt hat.

Für die Unterstützung im Labor und die aufmunternden Gespräche, die so manchen Frust aufgefangen haben, möchte ich mich ganz besonders bei Normen Hermes, Bernd Schilling, Sirgit Kummer, Wolfgang Tappe, Holger Wissel und Ansgar Weuthen bedanken.

Für die Instituts-übergreifende Zusammenarbeit in der Technikumshalle, die mir die Nutzung der Pflanzenkammern und der dazugehörigen Infrastruktur ermöglichte, möchte ich mich bei Jürgen Wildt und Einhard Kleist bedanken. Außerdem ein herzliches Dankeschön an Marcel Schneider und Beate Uhlig, die mich bei der Pflanzenaufzucht unterstützt haben.

I would also like to thank Jerome Ogée and Lisa Wingate for hosting me at INRA, Bordeaux.

Ein großer Dank geht an die 11:15 Uhr Mittagessengruppe (Anja, Markus, Sebastian, Hanna, Nils, Michael, Anne(s), Luise, Wei, Roland, Dorina). Die Pause mit anschließendem Kaffeeritual am Löschteich war immer ein Highlight des Tages. Auch bei Inge, Christian und Jutta möchte ich mich ganz herzlich für die schöne gemeinsame Zeit im Büro bedanken.

Ganz besonders möchte ich mich bei Kadti und Charlotte bedanken, die sogar das Wohnen in Düren zu einer großartigen Zeit gemacht haben.

Von ganzem Herzen danke ich meinen Eltern, die mich immer unterstützt haben, und meinem Freund Oliver, der immer an mich geglaubt hat.